Aspects of Quantum Field Theory with Boundary Conditions

by

Erickson Tjoa

A thesis
presented to the University of Waterloo
in fulfillment of the
thesis requirement for the degree of
Master of Science
in
Physics (Quantum Information)

Waterloo, Ontario, Canada, 2019

This thesis consists of material all of which I authored or co-authored: see Statement of Contributions included in the thesis. This is a true copy of the thesis, including any required final revisions, as accepted by my examiners.

I understand that my thesis may be made electronically available to the public.

Statement of Contribution

This thesis is based on the following works:

- **Chapter 3:** Erickson Tjoa, Robert B. Mann, Eduardo Martín-Martínez. *Particle detectors, cavities, and the weak equivalence principle.* Phys. Rev. D **98**, 085004. (1807.07628)
- **Chapter 4:** Erickson Tjoa, Eduardo Martín-Martínez. *Zero mode suppression of superluminal signals in light-matter interactions.* Phys. Rev. D **99**, 065005. (1811.02036)
- **Chapter 5:** Wan Cong, Erickson Tjoa, Robert B. Mann. *Entanglement Harvesting with Moving Mirrors.* J. High Energ. Phys. **06** (2019) 021 (1810.07359)
- **Chapter 6**: unpublished work motivated by investigations in Chapter 5, documenting some important aspects of numerical integration methods used there.

Abstract

This thesis has two modest goals. The primary goal is to deliver three results involving particle detectors interacting with a quantum field in presence of non-trivial boundary conditions (Dirichlet, Neumann, periodic; dynamical or otherwise). The secondary goal is to cover some technical, less "interesting" aspects of numerical integration performed in one of the works discussed in this thesis.

For the primary goal, we will first discuss how particle detector models known as Unruh-DeWitt model, which mimics essential aspects of light-matter interaction in quantum field theory (QFT) in general curved spacetimes, can be used to reanalyse the Weak Equivalence Principle (WEP) involving uniformly accelerating cavity (Dirichlet boundaries). This complements past literature, in particular the relatively recent solid work in [1], expands past results to cover highly non-diagonal field states and clarifies a minor disagreement with another old result in [2]. We will then move on to the problem of zero mode of a bosonic quantum field in presence of periodic and Neumann boundary conditions and show that relativistic considerations require careful treatment of zero mode in order to respect (micro)causality of QFT. We will quantify the amount of causality violation when the zero mode is ignored. Finally, we will discuss entanglement dynamics between two detectors coupled to a bosonic field in presence of non-uniformly accelerating mirror (moving Dirichlet boundary) for several non-trivial mirror trajectories.

For the secondary goal, we aim to briefly summarize some technical difficulties regarding symbolic and numerical integration encountered in these works. While this is not directly relevant for the physical results of the papers, explicit discussion seems appropriate and useful even if concise. In particular, we will discuss, in the context of Unruh-DeWitt model, a particular way involving *Mathematica*'s symbolic integration which prove superior in many settings than simply "plug-in-and-integrate" from textbooks like [3] or the literature, as one might naturally do in the absence of closed-form expressions. This will prove useful as an explicit reference for future UDW-related studies when more complicated integrals of similar nature are encountered.

Notation and Convention

In this thesis, we will adopt the natural units $c = \hbar = 1$. For convenience, we mention explicitly that in this implies that we have the following dimensional relationships between energy, mass, length and wavevector (momentum): $[E] = [m] = [L]^{-1} = [k]$.

Let (M, g) be our Lorentzian manifold and let X be a timelike vector. In this thesis we will use the following convention that if $X \in T_pM$ is a timelike vector, then the norm with respect to the metric is negative $g(X, X) < 0$. This is equivalent to the "mostly plus" or "East coast convention" (e.g. as is used in [4]) when $\dim M = D > 2$. Since in this thesis most of the work is carried out in $(1 + 1)$ model spacetimes, the signature is exactly zero and hence the usual terminology is ambiguous.

Finally, we will almost always refer to metric tensor using its components $g_{\mu\nu}$ since g will be used, following many texts, to denote the metric determinant, i.e. $g := \det[g_{\mu\nu}]$, where $[g_{\mu\nu}]$ is the matrix representation of the metric. Context will make this clear.

Acknowledgements

In general, I would like to acknowledge two groups of people partitioned largely by their geographical locations: Singapore and Canada.

In Canada, my first thanks go to both my supervisors Robert B. Mann and Eduardo Martín-Martínez. I first met them in Spring 2016 during my "Overseas Final Year Project", a pilot initiative by CN Yang Programme from Nanyang Technological University (NTU) in Singapore, which supported me financially to write my Bachelor's thesis overseas. With Robert Mann and his then PhD student Robie Hennigar, I had great fortune to learn much general relativity from them and to me a huge bonus came in the form of two publications [5, 6] which contained parts of my efforts during the eight-month visit. As far as work is concerned, it was easily "the greatest period of my life". During this same period, Eduardo who co-supervised many of Robb's students arranged a reading course on group theory for mathematical physics, covering Lie algebra and Lie groups. I timidly followed Robie who was taking the course for credit, and certainly never imagined that Eduardo would eventually become my co-supervisor for my MSc. Parts of me still thought that his impression of me was somewhat too high, but in that little class I learnt a lot. The biggest effect they have on me was that they both care a lot about their own students in their own ways (and perhaps quirks). To have them as my co-supervisors for the past two years (and for the coming four years) have been (and will be) very much a blessing.

Many thanks to (ex-)colleagues who have shaped me in many ways when it comes to work and fun, through conversations and jokes, physics and otherwise: Robie Hennigar, Dan Grimmer, Laura Henderson, Fiona McCarthy, Jack Davis, Alex Smith, Saoussen Mbarek, Allison Sachs, Keith Ng, Keith Copsey, Meenu Kumari, Wan Cong[1], Haomiao Jiang, Matthew Robbins, Finnian Gray, Brayden Hull, Aida Ahmadzadegan, Natacha Altamirano, Wilson Brenna, Paulina Corona-Ugalde, Michael Meiers, Hannah Dykaar, Zhiwei Gu, Xiaoran Li, Masoumeh Takavoli, Niloofar Abbasvandi; Maria Papageorgiou, José de Ramon, Richard Lopp, Petar Simidjiza, Nayeli Rodriguez-Briones, Irene Melgarejo Leimas, Nicholas Funai, Alvaro Ortega, Jose M. Sánchez Velázquez. This gratitude is especially important for someone like me who is naturally (or perhaps by years of development) somewhat unsociable, almost anti-social. Special thanks to Robie, from whom I learnt the most — including sense of humour and other things — and great friendship; Alex, Dan, Laura, for dragging me around for food or drinks several times; Wan, for being a patient collaborator and friend — I never thought I would ever have a colleague from Singapore; Matthew for being awesome office mate (along with Andrew Reeves); Allison,

[1] I adopt the given name-surname convention even for the Chinese names for simplicity.

another patient and uniquely free-spirited one during our collaboration; José (aka Pipo) and Maria, from whom I learnt much (algebraic) QFT and fun; Petar, for great friendship and keeping me from dropping AdS/CFT class.

Somewhat separately, I would like to thank Achim Kempf for being a very supportive professor; whom despite his busy schedule had provided me numerous advice on physics and career, and even being in my committee member and wrote recommendation letters for my PhD applications. This support has been tremendously helpful and inspiring.

Special thanks to Matthew Robbins for reading parts of the first draft of this thesis.

To the host family whose basement room I am renting — Timothy Trisnadhama Iman, Vicky Huang and their children; Yao-Yi Huang, his mother and family who now stay here; thank you for treating me as part of a big family instead of a mere tenant, through various help, sharing food and other things. You have effectively given me a kind of second home half a globe away which I cherish more than you might think.

In Singapore, my thanks go to enough people to fill this page but I would like to at least explicitly thank the following: Chyi Huey Ng, Benjamin Yap, Lim Min[2], Duong Nghiep Khoan, Szechi Lim, Sihui Pang, Shuqi Luar, Xinyi Lin, Jinchang Peh, Jiaying Seng, Huifang Tan, Huimin Ong, Yeeching Goh, Siding Wang, Nicolette Chia, Kashmira Jirafe, Jana Lim. These people, in particular, despite their busy schedules, went their way to still check-up on me 13 hours difference away even when sometimes I did not do the same, electronically or physically by means of postcards. I would like to also specially thank my "godmother" Adibah Abbas who was both my English teacher in secondary school and often supported me as if I were her own son when I had personal issues with my own family. Her support has no doubt shaped my success (if any) and any shortcoming on my part can be cleanly decoupled from her.

Finally, to my two siblings Erico Tjoa and Evimarisa Tjoa — our relationships from my frame have been somewhat different from many siblings, but over the years I have come to enjoy this style of interaction. To my parents, above thanks, perhaps a proper apology is more appropriate — I do not think our relationships will ever be the same again, but I will strive to 'atone' for lack of better words. This is perhaps the only explicit gratitude I could ever give without sounding too worthless — gratitude for giving this unfilial son a chance of living a (thus far) blessed life.

I certainly have missed some people worth equal (if not more) gratitude, however for my odd "obsession" with confining acknowledgment to two pages maximum, I will have to thank you in silence. I seek your understanding.

[2]She is the only one which goes by convention surname-given name as it sounds more natural.

Dedication

For my parents who had to bear with my ungratefulness for the past 13 years;

For my teacher Adibah Abbas who, despite knowing the above, chose to stand in as a "godmother" for the same period and kept me from going astray.

Quote

旅に出て、初めて知ることがある;
この景色が掛けがえのないものだと言う事;
自分が見ていなくても、人も世界も変わって行く事;
何もない一日なんて存在しないのだと言う事。
On a journey, there are things you learn for the first time;
That this scenery is indispensable;
That even if you are not looking, the people and the world change;
That there is no such thing as an uneventful day.

「宇宙より遠い場所」
「A Place Further than the Universe」

それを諦めていないのなら、きっと、大丈夫だ。
So long as you do not give up, I am sure, you will be fine.

「ひまわりさん」
「Miss Sunflower」

Contents

List of Figures

Chapter 1

Introduction

In this chapter we will carry out two things: (1) to motivate the subject matter of *relativistic quantum information* which this thesis is a small subset of, and (2) to give an overview of the content of this thesis. We do not attempt to provide an exhaustive list of literature references in this chapter.

1.1 Relativistic quantum information

The overall subject matter covered in this thesis can be considered a small subset of an intersection of two large fields: quantum field theory (QFT) in curved spacetimes and quantum information (QI). This intersection can be considered a subfield in itself, now known by its practitioners as *relativistic quantum information* (RQI).

One can survey standard resources such as the famous reference by Nielsen and Chuang [7] to know the generic scope of QI: they can be broadly categorised into information theory and quantum computation. It is not an oversimplification to say that QI as it is normally understood excludes special relativity (SR) and general relativity (GR) *a priori*, since the regime of the problems of interest — such as the highly desired implementation of quantum computers — is expected to be highly non-relativistic.

One strong motivation may come from the desire of the practitioners of fundamental physics to unify two most successful theories at two extreme scales: quantum field theory which describes non-gravitational interactions at small scales, and general relativity which describes gravitational interaction at large scales. While proposals abound, ranging from efforts in string theory to loop quantum gravity to asymptotic safety to causal sets, none

are satisfactory enough theoretically. The lack of experimental data in the regime where quantum-gravitational effects are important certainly does not help. The first surprise came from the 1970s, when Hawking discovered in the framework of Euclidean quantum gravity that semi-classical black holes must radiate and hence black holes are thermodynamic objects [8]. This in turn leads to the (in)famous black hole information paradox whose resolution is to this day not universally agreed (see e.g. [9, 10] for more recent arguments).

Without going too far into quantum gravity, it is not difficult to see that entanglement in QFT must play a crucial role. It was shown that QFT vacuum is itself entangled in a way that saturates a properly formulated Bell inequality [11–13]. Furthermore, from the perspective of algebraic quantum field theory, entanglement seems to be not a sole property of the field but also on the algebra of observables [14]. This development also influences Anti-de Sitter/Conformal Field Theory (AdS/CFT) correspondence, where entanglement entropy of a state in CFT living in the boundary of asymptotically AdS bulk spacetime is computed using extremal surfaces in the gravitational bulk [15]. Entanglement has thus been conjectured to be fundamentally related to gravitational degrees of freedom, leading to the picture that one can build spacetime using entanglement (see e.g. [16–18]). All these however have an obvious, though arguably less "fundamental" drawback: as stated, none of these entanglement measures are operational, i.e. they cannot be reasonably measured by observers carrying (finite) laboratory with them. This state of affair was worsened by the observation that QFT does not carry with it an intrinsic local measurement theory, unlike quantum mechanics [19].

The above limitation partially motivated the Unruh-DeWitt particle detector model [20,21], which was able to demonstrate both Unruh effect and Hawking effect in operational language. This particle detector model, as we will review in Chapter 2, essentially transfers the burden of measurement to a non-relativistic quantum system such as an atom coupled to a quantum field. The idea that one can study classical and quantum correlations in the field using detector models was first explicitly demonstrated in e.g. [22, 23]. Away from quantum-gravitational context, it turns out that relativistic considerations also appear in seemingly harmless, flat space settings in which entanglement again plays a central role. One of the most remarkable results involves the demonstration that spin-spin entanglement is not Lorentz covariant [24]. It was also shown that entanglement is affected by relative motion, especially in presence of acceleration [25–27]. In these scenarios, the use of particle detector models is also extremely useful in making the physics transparent. In certain cases, non-perturbative methods are available and fundamental concepts such as channel capacity can be made for arbitrary curved spacetimes [28].

There are many other results in RQI which merit mention, however we do not do it here for brevity and we will mention them in subsequent chapters if they are relevant. In this

thesis we will explore a small corner of RQI, as described in what follows.

1.2 Overview of the thesis

The main goal of this thesis is to present a modest sets of results, spread over three chapters, done in the context of particle detector models (known more commonly as Unruh-DeWitt model) in quantum field theory. It is fortunate that 'boundary conditions' turn out to be a common theme among these works, though it was not intended when they were first studied. With this in mind, 'boundary conditions' will be used to partition this thesis into several coherent and relatively independent chapters. This thesis also contains secondary goal, namely to illustrate (in the last chapter) in somewhat detailed manner a numerical integration problem faced in one of the works presented in this thesis.

Chapter 2 reviews the basics of quantum field theory in curved spacetime and the Unruh-DeWitt model, a class of particle detector models that are commonly employed in the context of relativistic quantum information. This chapter will be kept as general as possible in order to provide common ground for setting up the problems in the next three chapters. Actual details unique to each problem (such as the number of detectors or actual initial state of the detector and the field) will be addressed specifically in each chapter.

Chapter 3 studies the old problem of the *weak equivalence principle* (WEP) in the context of particle detector models in relative motion with a cavity (i.e. Dirichlet boundary conditions along the direction of motion). We review the classical WEP and its generalization to a semiclassical setting when there is a quantum field present in the compact region in which the WEP is usually cast (imagine the prototypical free-falling lift or rocket). We will show that in principle, a detector can locally detect the difference between a free-falling cavity crossing a static detector and a free-falling detector in a static cavity and in the 'non-relativistic' regime, whose meaning we will clarify, the weak equivalence principle holds in semiclassical setting. This result holds largely independently of the quantum state of the field. One takeaway from this is that there seems to be a disagreement between what we found here — namely that WEP holds in appropriate sense — and the relatively old claim that massive quantum fields can be used as a *quantum accelerometer*, distinguishing the two setups locally simply by the transition probability of the detector [2].

Chapter 4 turns to the use of periodic boundary condition for massless quantum scalar fields. In this scenario, a *zero mode* can arise and we will discuss its properties and its effect on particle detector phenomenology. We show that while it may appear appealing to ignore the zero mode, this breaks causality in the relativistic sense and one can use this to

indeed send superluminal signals. We describe the situations in which the zero mode can arise and discuss how it ought to be handled when relativity is relevant for the physics in question.

Chapter 5 covers the use of a *moving* Dirichlet boundary condition — also known as a *moving mirror* — for a $(1+1)$-dimensional massless quantum scalar field. We will call the spacetime with a mirror a *mirror spacetime*. In this chapter we focus on how two detectors coupled to the field in mirror spacetime can or cannot harvest entanglement. This scenario provides another vantage point for understanding entanglement structure of quantum fields on black hole spacetimes, since moving mirrors were originally designed to mimic Hawking radiation in the context of black hole physics. We will see that indeed entanglement harvesting provides a complementary picture to the current analogy between mirror and black hole spacetimes that uses non-local quantities, namely the matching of Bogoliubov coefficients. We will obtain a side bonus that entanglement extraction between detectors turns out to be robust against the IR structure of the theory, thus providing a reason for trusting aspects of $(1+1)$-dimensional massless field theory, which is known to be IR-ambiguous.

Chapter 6 consists of a small detour into numerical integration used in Chapter 5, which appears often in investigations involving Unruh-DeWitt models. We provide examples and compare several methods to demonstrate and propose that in many situations, the $i\epsilon$ prescription as it appears may be inferior to a more complex-analytically motivated contour integration and how to perform this numerically. We believe this discussion is potentially of great use for readers who are working with this model or integrals of similar form.

Finally, Chapter 7 provides some summary and thoughts on the research presented in this thesis. A set of appendices has been included to demonstrate details that may distract from the main ideas presented in the main body of the thesis.

Chapter 2

Quantum field theory in curved spacetimes and particle detectors

In this chapter we will review the quantization of classical scalar field in arbitrary curved spacetime satisfying certain nice properties and also Unruh-DeWitt particle detector model. Our aim is to first show how the notion of particle creation arises within the context of quantum field theory, which will then provide us with some basic motivations to employ particle detector models to probe the field properties in relativistically covariant manner.

Although the contributions in this thesis are concerned with mostly with scalar fields on flat spacetime, we will work with the most general coordinates in curved spacetimes as it simplifies and unifies some treatment in non-inertial frames. For instance, the Klein-Gordon equation in arbitrary curved spacetime can easily account for Klein-Gordon equation in Rindler coordinates (cf. Chapter 3).

2.1 Classical scalar field

Let (M, g_{ab}) be a $(D+1)$-dimensional Lorentzian manifold. A real-valued scalar field is a smooth function $\phi : M \to \mathbb{R}$. The dynamics of a classical scalar field ϕ with mass parameter m minimally coupled to the metric $g_{\mu\nu}$ has the following action functional[1]

$$S[\phi] = -\frac{1}{2}\int \mathrm{d}^{D+1}x\sqrt{-g}\,\left(\nabla_\mu\phi\,\nabla^\mu\phi + m^2\phi^2\right). \tag{2.1}$$

[1]We take the following opportunity to express variational quantities in slightly more rigorous manner.

Let $h : M \to \mathbb{R}$ be a test function on M in the sense of distribution theory. For our purposes, it suffices that the test function belongs to the space of compactly supported, smooth, real test functions $C_0^\infty(M)$, as is usually required for algebraic formulation of scalar field quantization [29]. For a given test function h, the *functional derivative* of $S[\phi]$, denoted $\delta S/\delta\phi$, is defined via the integral over test function h:

$$\int_M \mathrm{d}^{D+1}x \frac{\delta S}{\delta\phi} h := \lim_{\epsilon\to 0} \frac{S[\phi+\epsilon h] - S[\phi]}{\epsilon} \equiv \left.\frac{\mathrm{d}}{\mathrm{d}\epsilon}\right|_{\epsilon=0} S[\phi+\epsilon h]\,.$$

The function ϵh is usually called the *variation* of ϕ, often denoted by $\delta\phi$ in physics literature. Therefore, the variation of the action δS encountered in physics literature really means

$$\delta S \equiv \langle \delta S[\phi], h\rangle := \left.\frac{\mathrm{d}}{\mathrm{d}\epsilon}\right|_{\epsilon=0} S[\phi+\epsilon h]\,, \tag{2.2}$$

where the inner product notation is used to make the dependence on the test function clear[2]. If the action is given by the following integral of Lagrangian $\mathcal{L}[\phi, \nabla_\mu\phi]$, i.e.

$$S[\phi] = \int_M \mathrm{d}^{D+1}x\, \mathcal{L}[\phi, \nabla_\mu\phi]\,, \tag{2.3}$$

then imposing the requirement that the test functions h vanish on the boundary ∂M, we obtain

$$\delta S = \int_M \mathrm{d}^{D+1}x \left(\frac{\partial\mathcal{L}}{\partial\phi} - \nabla_\mu \frac{\partial\mathcal{L}}{\partial(\nabla_\mu\phi)}\right) h\,. \tag{2.4}$$

In physics, the dynamics of a physical system is given by Hamilton's principle, which in this case dictates that this variation δS vanishes for all test functions h which vanish on ∂M. Therefore, by the fundamental lemma of variational calculus, we must have that the functional derivative of S identically vanishes, i.e. we obtain the *Euler-Lagrange equations* for the scalar field:

$$0 = \frac{\delta S}{\delta\phi} \equiv \frac{\partial\mathcal{L}}{\partial\phi} - \nabla_\mu \frac{\partial\mathcal{L}}{\partial(\nabla_\mu\phi)}\,. \tag{2.5}$$

This expression involving the full covariant derivative with respect to Levi-Civita connection ∇ is convenient even in flat space, since for non-trivial coordinate systems e.g.

[2]This is the same notation as when one defines (distributional) derivative of one-dimensional Heaviside function: $\Theta'(x) := \langle\Theta'(x), h(x)\rangle = h(0) =: \langle\delta(x), h(x)\rangle$, where for test function h, $\langle f, h\rangle = \int_{\mathbb{R}} f(x)h(x)\,\mathrm{d}x$.

involving accelerating observers, the connection coefficients $\Gamma^{\rho}_{\mu\nu}$ will generally be non-zero. For the scalar field minimally coupled to the metric in Eq. (2.1), one can show that the Euler-Lagrange equation implies the *Klein-Gordon equation in generic curved spacetime*:

$$\nabla_\mu \nabla^\mu \phi - m^2 \phi \equiv \frac{1}{\sqrt{-g}} \partial_\mu \left(\sqrt{-g} g^{\mu\nu} \partial_\nu \phi \right) - m^2 \phi = 0 \,. \tag{2.6}$$

The second expression can be obtained from the first using the fact that ϕ is a smooth function (0-form) over M hence $\nabla_\mu \phi = \partial_\mu \phi$ and also the identity

$$\Gamma^{\mu}_{\mu\nu} = \partial_\nu \log \sqrt{-g} \,. \tag{2.7}$$

The expression in Eq. (2.6) will be used for the rest of the thesis since the metric $g_{\mu\nu}$ and its determinant $\sqrt{-g}$ will be relevant for various non-trivial coordinates even in flat spacetime, such as when using Rindler coordinates.

An important classical observable which is very useful for quantum field theory is the Hamiltonian associated to the field. The Hamiltonian can be obtained using the Legendre transformation, as is done for classical mechanics of particles. The main difficulty in doing this for a given manifold M is that we will need single out a preferred time direction in M. In flat space, this is straightforward due to the full Poincaré symmetry which provides global timelike Killing vectors to label time. In the most generic spacetimes, this cannot be unambigously done.

However, it can be shown that if M is *globally hyperbolic*, then the spacetime admits a $(3+1)$-decomposition (*ADM decomposition*) [4]: that is, the spacetime has natural topology $M = \mathbb{R} \times \Sigma$ where $\mathbb{R}$ is along the timelike direction. In other words, one can foliate spacetime into one-parameter family of spacelike hypersurfaces Σ_t, where $t \in \mathbb{R}$. In particular, if the spacetime is *static*, i.e. it admits a global timelike Killing vector ξ, i.e.

$$\mathcal{L}_\xi g_{ab} = 0 \,, \quad \xi^a \xi_a < 0 \,, \tag{2.8}$$

then together with global hyperbolicity[3] one can label Σ_t with time parameter associated with the timelike Killing vector ξ. For example, in Minkowski space ∂_t is a valid timelike Killing vector and the time parameter t is the global time associated to this Killing field. Global hyperbolicity is important because it implies that the Klein-Gordon equation is *well-posed*, i.e. it has a well-defined initial value problem: that is, if one is given an initial data on one slice Σ_{t_0}, then Klein-Gordon equation will evolve the initial data for all $t \in \mathbb{R}$.

[3]It is not true that if the spacetime admits a timelike Killing vector then it must be globally hyperbolic, as some pathological examples show [4]. I thank José de Ramon for pointing this out.

In other words, one can know the values of the scalar field at all spacetime points $p \in M$.

As such, we will restrict ourselves to globally hyperbolic static spacetimes. Let t be a global time function associated to the timelike Killing vector ξ, i.e. we write $\xi = \partial_t$. Since the spacetime is static, Σ_t is time-translation invariant and so we write Σ for all of the spacelike slices. The foliation implies we can write the action as

$$S[\phi] = \int_{\mathbb{R}} \mathrm{d}t \int_{\Sigma} \mathrm{d}^D x \mathcal{L}(\phi, \nabla_\mu \phi) \equiv \int_{\mathbb{R}} \mathrm{d}t L(\phi, \dot{\phi}, \nabla_j \phi)\,, \tag{2.9}$$

$$L \coloneqq \int_{\Sigma} \mathrm{d}^D x \mathcal{L}(\phi, \dot{\phi}, \nabla_j \phi)\,, \tag{2.10}$$

where L is the Lagrangian projected to Σ and $\dot{\phi} = \partial_t \phi \equiv \mathcal{L}_\xi \phi$. Now, the conjugate momentum can be defined by[4]

$$\pi \coloneqq \frac{\delta L}{\delta \dot{\phi}} = \frac{\partial \mathcal{L}}{\partial \dot{\phi}}\,. \tag{2.11}$$

Finally, the Hamiltonian functional can be defined by

$$H[\phi, \pi] \coloneqq \int_{\Sigma} d^D x \left(\pi \dot{\phi} - \sqrt{-g} \mathcal{L}[\phi, \dot{\phi}(\phi, \pi)] \right)\,. \tag{2.12}$$

2.2 Quantization of scalar field

2.2.1 General picture of quantization

In general, a physical system is specified by three basic ingredients: its state, an *algebra* of fundamental observables that provides quantities one can measure and build more complicated observables, and an equation of motion (with suitable boundary conditions, if applicable). In classical mechanics, the state is encoded in the phase space, e.g. by specifying position and momentum (which is a point in phase space). The equation of motion in this case can be given by Hamilton's equation of motion, which is equivalent to Newton's second law. The fundamental observables are position and momentum satisfying Poisson algebra, and one can build more complicated observables as a function of position and momentum, such as the total energy (Hamiltonian). In quantum mechanics, the state is specified by a state in a Hilbert space $\mathcal{H}$. The equation of motion is provided

[4]Note that if we use different slicing with different normal vector n^μ to Σ, the conjugate momentum is strictly speaking is given by $\pi = \sqrt{\gamma} n^\mu \partial_\mu \phi$, where γ is the determinant of the *induced metric* on Σ.

by the Schödinger equation or equivalently the Heisenberg equation. The fundamental observables are provided by certain set of operators acting on $\mathcal{H}$ whose eigenvalues can be associated to measurable outcomes (through the "projection postulate", among others). The fundamental observables can be e.g. position and momentum operators satisfying canonical commutation relations (so-called "CCR algebra" for obvious reason), and more complicated observables such as the Hamiltonian can be built from these. Other technical requirements may or may not be required to make this general 3-ingredient picture work.

In our case, the physical system of interest is a real scalar field ϕ on a spacetime M that we would like to quantize, and canonical quantization is a prescription that provides us with the same three basic ingredients — the space of states, observables, and dynamics. Complication arises for many (technical) reasons, one of which being the Hilbert space is necessarily infinite-dimensional in a manner much more complicated than the quantum harmonic oscillator. Note that canonical quantization is one of the many ways to quantize a physical system: the so-called *path-integral quantization* does not, for example, work with operators and Hilbert space directly and instead directly go for correlation functions and expectation values[5]. We will not pursue path-integral quantization here.

At the heart of canonical quantization, we wish to make the classical field observable (field amplitude) $\phi : M \to \mathbb{R}$ into an operator acting on a Hilbert space $\mathcal{H}$, i.e. $\hat{\phi} : \mathcal{H} \to \mathcal{H}$. The Hilbert space contains quantum states $\{|\phi\rangle\}$ associated to the quantum field. In $\mathcal{H}$, one expects to have a state corresponding to the "lowest energy state" in an appropriate sense (unique or otherwise), called a vacuum state $|0\rangle$ (ground state) of the field, and hope to generate all other states by suitable operators acting on $|0\rangle$. This is usually done most easily using the so-called *Fock representation*, where the Hilbert space basis is countable — the number state basis $\{|n\rangle : n \in 0 \cup \mathbb{N}\}$ — and the fundamental operators are now the ladder operators $\{\hat{a}_{\boldsymbol{k}}, \hat{a}^\dagger_{\boldsymbol{k}} : \boldsymbol{k} \in \mathbb{R}^n\}$. These operators can be used to generate all the "n-particle states" of the theory, which provides us with a notion of (anti-)particle excitations. And finally, among all other operators that one can build using the basic operators, one of the most important ones is the *Hamiltonian* operator $\hat{H} : \mathcal{H} \to \mathcal{H}$, whose eigenvalues provide energy spectrum of the theory. In particular, a vacuum state (suitably regularized) is one which is annihilated by the Hamiltonian, i.e. $\hat{H}\,|0\rangle = 0$. Once the algebra (i.e. operators and commutation relation) and states are available, one can then start to compute physical quantities of interest, such as the S-matrix in scattering theory (see e.g. [30,31] for standard calculations in various quantum field theoretic contexts, from high-energy physics to condensed matter physics).

As it turns out, the field operator $\hat{\phi}$ as described above is an *operator-valued distribution*,

[5]These contain all the information about the system packaged differently, i.e. in the partition function.

i.e. it is not a well-defined operator at a spacetime point $p \in M$ and is only defined over suitable space of test functions $\mathcal{T}$ (which may or may not contain Dirac delta function [32]). That is, if $h \in \mathcal{T}$, then $\hat{\phi}(h)$ is a valid operator in a distributional sense. These operators will then define a valid *algebra of observables*, which in the case of scalar field, is known as the **CCR algebra**.

As this algebra is (schematically) not too difficult to understand and relate to standard QFT formulation, we state it here (with slight modification) [29]. We will not attempt to explain every technical point but instead loosely describe what they mean as a whole.

Definition 1. *A* **CCR algebra** *of the quantum field ϕ on M is the unital $*$-algebra $\mathcal{A}$ with the following presentation and relation: the generators of the algebra are* **(smeared abstract) field operators**, *$\hat{\phi}(f)$, labelled by the test functions $f \in C_0^\infty(M)$ which satisfy the following relations:*

(*a*) **($\mathbb{R}$-linear)** $\hat{\phi}(af + bg) = a\hat{\phi}(f) + b\hat{\phi}(g)$ *for all* $f, g \in C_0^\infty(M)$.

(*b*) **(Hermiticity)** $\hat{\phi}(f)^* - \hat{\phi}(f) = 0$ *for* $f \in T$.

(*c*) **(Klein-Gordon)**[6] $\hat{\phi}\left((\nabla_a \nabla^a - m^2)f\right) = 0$ *for* $g \in C_0^\infty(M)$.

(*d*) **(Commutation relation)** $[\hat{\phi}(f), \hat{\phi}(g)] - iE(f,g)\mathbb{1} = 0$, *where E is the* **causal propagator**.

The causal propagator E is formally a map from the space of test functions to the space of solutions of the Klein-Gordon equation, i.e. $E : C_0^\infty(M) \to \mathrm{Sol(KG)}$ with the property that with the property that

- $E(f, \cdot) = Af - Rf$, where Af, Rf are advanced and retarded solutions with source f respectively,
- $E(f,g) \coloneqq \int_M (gAf - gRf)\sqrt{-g}\,\mathrm{d}^n x$.

Another formal ingredient we need is the notion of state of a quantum field.

Definition 2. *Given a unital $*$-algebra $\mathcal{A}$, an (algebraic)* **state** *ω over $\mathcal{A}$ is a $\mathbb{C}$-linear map $\omega : \mathcal{A} \to \mathbb{C}$ which is both positive (i.e. $\omega(\hat{a}^\dagger \hat{a}) \geq 0$ for all $\hat{a} \in \mathcal{A}$) and normalized (i.e. $\omega(\mathbb{1}) = 1$, where $\mathbb{1}$ is multiplicative identity element of $\mathcal{A}$).*

[6] Note that in the context of PDE, the space of test functions may include non-smooth functions and distributions; usually g is then known as *weak solution* to the field equation.

Loosely translated to the standard QFT notions, the definition of CCR algebra $\mathcal{A}$ and algebraic state ω suggest the following picture: canonical quantization of the scalar field *phi* is a specification of an algebra of Hermitian operators $\hat{\phi}$ with a specific canonical commutation relations between these operators. The Hilbert space of states as we usually understand is obtained from $\mathcal{A}$ and ω using the so-called *GNS representation theorem* [29]. Note that relations (c) and (d) in Definition 1 tell us that indeed our field is a scalar field satisfying a specific equation of motion, namely the Klein-Gordon equation, which in turn encodes that our construction obeys relativistic dispersion relation. Furthermore, these operators are formally distributional, which is why Dirac delta functions appear in commutation relations in standard texts (compare e.g. [3, 30, 31] and [29, 32]). What remains missing from the CCR algebra is how to specify "lowest-energy state" and hence other states in $\mathcal{H}$: in standard QFT, one passes to the Fock representation for $\mathcal{H}$ just obtained from GNS construction, whose fundamental operators are ladder operators with which one can then construct explicitly the "n-particle states" of the theory.

The above discussion is meant to illustrate roughly what one would need to perform canonical quantization and what comes out of the procedure. Much of the framework in *algebraic quantum field theory* (AQFT) are concerned with making these procedures mathematically rigorous and fundamentally as satisfactory as possible in generic curved spacetimes. Unfortunately, to date most interacting field theories have not been rigorously proven to exist in $(3+1)$ dimensions[7] [36].

2.2.2 Quantization procedure

From the above discussion, we see that we more or less have canonically quantized the theory if we specify the field operators $\hat{\phi}$ and its associated commutation relations. We also need to specify the Hilbert space of states $\mathcal{H}$ (e.g. as a span of simple basis), and a way to construct n-particle states from the vacuum state of the theory — in particular, we need to construct the Hamiltonian operator $\hat{H}$ which certifies our vacuum state $|0\rangle$. Finally, we need to specify the equation of motion which specifies how the states and/or operators evolve with respect to some time parameter: whether states and/or operators evolve in time depends on which picture we adopt (Schrödinger, Heisenberg, or Dirac/interaction picture). We will, in view of AQFT framework, adopt the less rigorous approach to canonical quantization as is done in e.g. [3, 31].

This proceeds in **three** basic steps.

[7] An interesting fact is that the usual ϕ^4 theory and other self-interacting scalar theories have been proven to not exist in five dimensions or more [33–35].

Step 1: The quickest way to quantize the theory will be to elevate the field ϕ and its conjugate momentum π to operators acting on Hilbert space $\mathcal{H}$ and impose canonical commutation relations between them. That is, we now have $\hat{\phi}, \hat{\pi} : \mathcal{H} \to \mathcal{H}$ and for a given coordinate system $(t, \boldsymbol{x})$, the equal-time commutation relations are

$$\left[\hat{\phi}(t, \boldsymbol{x}), \hat{\pi}(t, \boldsymbol{y})\right] = \mathrm{i}\delta^D(\boldsymbol{x} - \boldsymbol{y}) \,, \tag{2.13}$$

$$[\hat{\pi}(t, \boldsymbol{x}), \hat{\pi}(t, \boldsymbol{y})] = \left[\hat{\phi}(t, \boldsymbol{x}), \hat{\phi}(t, \boldsymbol{y})\right] = 0 \,. \tag{2.14}$$

Step 2: We write down the Fourier decomposition of the scalar field ϕ. Promoting ϕ into an operator $\hat{\phi}$ then amounts to promoting the Fourier coefficients into ladder operators. More specifically, we write[8]

$$\phi(t, \boldsymbol{x}) = \sum_{\boldsymbol{k}} \left(a_{\boldsymbol{k}} u_{\boldsymbol{k}}(t, \boldsymbol{x}) + a^*_{\boldsymbol{k}} u^*_{\boldsymbol{k}}(t, \boldsymbol{x})\right) \,, \quad a_{\boldsymbol{k}} \in \mathbb{C} \,, \tag{2.15}$$

and $u_{\boldsymbol{k}}(t, \boldsymbol{k})$ are a complete set of orthonormal mode functions of the decomposition. If we define the real-valued solution space of the Klein-Gordon equation to be **Sol**, then this decomposition can be written as

$$\mathbf{Sol}^{\mathbb{C}} = \mathrm{span}\{u_{\boldsymbol{k}}, u^*_{\boldsymbol{k}} : \boldsymbol{k} \in \mathbb{R}^D\} \,, \tag{2.16}$$

where $\mathbf{Sol}^{\mathbb{C}}$ is the enlarged solution space which includes complex-valued solutions of the Klein-Gordon equation. These mode functions are orthogonal with respect to the Klein-Gordon inner product, defined by

$$(f, g) = -i \int_\Sigma \mathrm{d}\Sigma^\mu \sqrt{-g} \, \left(f^* \partial_\mu g - g^* \partial_\mu f\right) \,, \tag{2.17}$$

where $\mathrm{d}\Sigma^\mu = n^\mu \mathrm{d}\Sigma$, n^μ is future-directed unit normal orthogonal to spacelike hypersurface Σ. Since the spacetime is globally hyperbolic, the ADM foliation allows us to take Σ to be a Cauchy surface. By Stokes' theorem, this inner product is independent of which Σ_t we use (hence we drop the t subscript). The orthonormality relations between mode functions are as follows:

$$(u_{\boldsymbol{k}}, u_{\boldsymbol{k}'}) = \delta_{\boldsymbol{k},\boldsymbol{k}'} \,, \quad (u^*_{\boldsymbol{k}}, u^*_{\boldsymbol{k}'}) = -\delta_{\boldsymbol{k},\boldsymbol{k}'} \,, \quad (u_{\boldsymbol{k}}, u^*_{\boldsymbol{k}'}) = 0 \,. \tag{2.18}$$

Note that the Klein-Gordon inner product not a valid inner product on the entire $\mathbf{Sol}^{\mathbb{C}}$, but

[8] We have for simplicity used the summation instead of integral, analogous to quantizing the field with periodic boundary conditions and take the periodic length $L \to \infty$ at the end [3]

it is positive-definite or negative definite on subspaces spanned by $u_{\boldsymbol{k}}$ and $u^*_{\boldsymbol{k}}$ respectively. In view of this, we can write the complexified solution space as a direct sum of a *Hilbert space* and its complex conjugate, i.e.

$$\mathbf{Sol}^{\mathbb{C}} = \mathcal{H}_{\mathbf{Sol}} \oplus \mathcal{H}^*_{\mathbf{Sol}}\,, \quad \mathcal{H} := \mathrm{span}\{u_{\boldsymbol{k}}\}\,. \tag{2.19}$$

This splitting has an intuitive interpretation. The mode function $u_{\boldsymbol{k}}(t,\boldsymbol{x})$ is said to be *positive frequency* mode with frequency $\omega_{\boldsymbol{k}}$ if it is an eigenfunction of the operator $i\mathcal{L}_\xi$ with positive eigenvalue $\omega_{\boldsymbol{k}}$, i.e.

$$i\mathcal{L}_\xi u_{\boldsymbol{k}} = \omega_{\boldsymbol{k}} u_{\boldsymbol{k}}\,, \quad \omega_{\boldsymbol{k}} > 0\,, \tag{2.20}$$

where $\mathcal{L}_\xi$ is the Lie derivative with respect to timelike Killing vector ξ. Therefore, we can think of $\mathcal{H}_{\mathbf{Sol}}$ as the space of the positive frequency solutions, and we can say that a real scalar field is an (infinite) linear combinations of positive and negative frequency modes.

By quantizing the field, we obtain the field operator $\hat{\phi}$, written as

$$\hat{\phi}(t,\boldsymbol{x}) = \sum_{\boldsymbol{k}} \left(\hat{a}_{\boldsymbol{k}} u_{\boldsymbol{k}}(t,\boldsymbol{x}) + \hat{a}^\dagger_{\boldsymbol{k}} u^*_{\boldsymbol{k}}(t,\boldsymbol{x})\right)\,, \tag{2.21}$$

where $\hat{a}_{\boldsymbol{k}}, \hat{a}^\dagger_{\boldsymbol{k}}$ are ladder operators satisfying the commutation relation

$$\left[\hat{a}_{\boldsymbol{k}}, \hat{a}^\dagger_{\boldsymbol{k}'}\right] = \delta_{\boldsymbol{k},\boldsymbol{k}'}\,, \quad [\hat{a}_{\boldsymbol{k}}, \hat{a}_{\boldsymbol{k}'}] = \left[\hat{a}^\dagger_{\boldsymbol{k}}, \hat{a}^\dagger_{\boldsymbol{k}'}\right] = 0\,. \tag{2.22}$$

These commutation relations are required for the original commutation relations in terms of field operators and its conjugate momentum to hold.

Step 3: Finally, we can construct the vacuum state upon which all other states can be built from. The field decomposition above provides us with a characterisation of the Hilbert space $\mathcal{H}$ of the quantum field in terms of a very convenient basis representations known as *Fock representation*. This is the representation of the Hilbert space using a complete set of basis states constructed out of the vacuum state $|0\rangle$ by applying all possible and finitely many creation operators on $|0\rangle$. The vacuum state with respect to Killing time t is defined by the state annihilated by any $\hat{a}_{\boldsymbol{k}}$:

$$\hat{a}_{\boldsymbol{k}}\,|0\rangle = 0 \quad \forall \boldsymbol{k} \in \mathbb{R}^D\,.$$

This matches what we had previously about characterising the vacuum state using the

Hamiltonian, since the (background-subtracted, i.e. normal-ordered) Hamiltonian reads

$$\hat{H} = \sum_{\boldsymbol{k}} \omega_{\boldsymbol{k}} \hat{a}^\dagger_{\boldsymbol{k}} \hat{a}_{\boldsymbol{k}} \Longrightarrow \hat{H} \left|0\right\rangle = 0 \,. \tag{2.23}$$

In this Fock representation, the Hilbert space is a Fock space[9], formally written as

$$\mathcal{H} = \bigoplus_{n=0}^{\infty} \mathcal{H}^S_n \,, \quad \mathcal{H}^S_n := S\left(\bigotimes_{j=1}^{n} \mathcal{F}\right) \,, \tag{2.24}$$

where $\mathcal{F} = \text{span}\left\{\hat{a}^\dagger_{\boldsymbol{k}} \left|0\right\rangle : \boldsymbol{k} \in \mathbb{R}^D\right\}$ is the *one-particle Hilbert space* spanned by "1-particle states" $\hat{a}^\dagger_{\boldsymbol{k}} \left|0\right\rangle$, i.e. states acted by one creation operator of some momentum $\boldsymbol{k}$, and $S(\cdot)$ here refers to the symmetrisation operator, i.e. the n-particle states are symmetrised in the sense that $\hat{a}^\dagger_{\boldsymbol{k}} \hat{a}_{\boldsymbol{k}'} \left|0\right\rangle = \hat{a}_{\boldsymbol{k}'} \hat{a}^\dagger_{\boldsymbol{k}} \left|0\right\rangle$ whenever $\boldsymbol{k} \neq \boldsymbol{k}'$. This symmetrisation reflects the bosonic character of the real scalar field. The $n = 0$ case is the subspace spanned by the vacuum state, i.e. $\mathcal{H}^S_0 := \text{span}\left\{\left|0\right\rangle\right\}$.

An operator closely related to the Hamiltonian is the number operator $\hat{N}$ with respect to some momentum $\boldsymbol{k}$, defined to be

$$\hat{N}_{\boldsymbol{k}} := \hat{a}^\dagger_{\boldsymbol{k}} \hat{a}_{\boldsymbol{k}} \,. \tag{2.25}$$

This operator, in the language of quantum harmonic oscillator, counts the number of particle excitations with momentum $\boldsymbol{k}$. This operator will be essential to show how particle creation first arises in quantum field theory.

2.3 Particle creation

Recall that in flat spacetime, one can identify a preferred vacuum by the existence of global timelike Killing field — this is usually called the global Minkowski vacuum. The existence of this Killing field allows us to define uniquely the positive and negative frequency modes, and consequently a preferred vacuum state. We will see that even in flat space this choice is not unique. This lack of uniqueness is in fact physical — it is the origin of the phenomenon of *particle creation*.

[9] One might wonder how the Hilbert space of solutions $\mathcal{H}_{\mathbf{Sol}}$ is related to the Hilbert space $\mathcal{H}$ of our quantum field here. This connection is quite non-trivial but is described by algebraic framework of QFT: it has to do with how one relates positive frequency solutions with "particle excitations" and negative frequency solutions with "anti-particle" excitations. See [32] for details.

Since $\mathbf{Sol}^{\mathbb{C}}$ admits many different basis decomposition, we can write (after quantization)

$$\hat{\phi} = \sum_j \hat{a}_j u_j + \hat{a}_j^\dagger u_j^* = \sum_j \hat{b}_j v_j + \hat{b}_j^\dagger v_j^* \,. \tag{2.26}$$

Here we have used discrete index j to label the modes for clarity[10]. Since $\{u_j, u_j^*\}, \{v_j, v_j^*\}$ are different bases, we can relate them by

$$v_j = \sum_i \alpha_{ji} u_i + \beta_{ji} u_i^* \,. \tag{2.27}$$

The coefficients $\alpha_{ji}, \beta_{ji} \in \mathbb{C}$ are called *Bogoliubov coefficients* and this relation between two bases is called a *Bogoliubov transformation*. Given the basis modes, we can find these coefficients using the Klein-Gordon inner product:

$$\alpha_{ji} = (v_j, u_i) \,, \qquad \beta_{ji} = -(v_j, u_i^*) \,. \tag{2.28}$$

Using Eq. (2.26) and Klein-Gordon inner product, together with the Bogoliubov transformation, we can relate the ladder operators as

$$\hat{a}_j = \sum_i \alpha_{ji} \hat{b}_j + \beta_{ji}^* \hat{b}_j^\dagger \,. \tag{2.29}$$

Together with commutation relations, the Bogoliubov transformation obeys two constraints:

$$\sum_k \alpha_{ik} \alpha_{jk}^* - \beta_{ik} \beta_{jk}^* = \delta_{ij} \,, \tag{2.30}$$

$$\sum_k \alpha_{ik} \beta_{jk} - \beta_{ik} \alpha_{jk} = 0 \,. \tag{2.31}$$

We are now ready to see how particle creation arises in QFT, even in flat spacetime. Suppose we quantize the field using two different bases, $B_1 = \{u_j, u_j^*\}$ and the other using $B_2 = \{v_j, v_j^*\}$. Then we will obtain two distinct Fock spaces $\mathcal{H}_1, \mathcal{H}_2$ with their own vacuum states $|0\rangle_1 , |0\rangle_2$ respectively. By construction we described in the previous subsection, the

[10]Strictly speaking, we are summing over $\mathbb{Z}^D$ since the mode decomposition was written as sum over momenta $\sum_{\boldsymbol{k}}$, but we can make this into a sum over $\mathbb{Z}$ by virtue of countability. This is the notation used in standard texts e.g. [3], with the advantage that the change of basis can be properly thought of as (infinite-dimensional) matrices (i.e. encoded in an invertible object with two indices). If we sum over the wavevector $\boldsymbol{k}$, the argument still holds but we will have to think of the change of basis "matrix" as something with more than two indices.

vacuum states are defined by

$$\hat{a}_j \left|0\right\rangle_1 = \hat{b}_j \left|0\right\rangle_2 = 0 \quad \forall j \,. \tag{2.32}$$

However, using the Bogoliubov transformation, we can see that for example,

$$\hat{a}_j \left|0\right\rangle_2 = \left(\sum_i \alpha_{ij}\hat{b}_i + \beta^*_{ij}\hat{b}^\dagger_i\right)\left|0\right\rangle_2 = \sum_i \beta^*_{ij}\hat{b}^\dagger_i \left|0\right\rangle_2 \,. \tag{2.33}$$

This relation shows that $\left|0\right\rangle_2$ is generically not a vacuum state of the first Fock representation. In particular, if we now use the number operator of the first basis $\hat{N}^{(1)}_j := \hat{a}^\dagger_j \hat{a}_j$, we see that

$$\left\langle 0\right|_2 \hat{N}^{(1)}_j \left|0\right\rangle_2 = \sum_i |\beta_{ji}|^2 \geq 0 \,. \tag{2.34}$$

This says that the vacuum state $\left|0\right\rangle_2$ in fact contains $\sum_i |\beta_{ji}|^2$ excitations in the j-th mode. In standard QFT interpretation, this means that, for example, two observers quantizing in different frames *even in flat spacetime* will not in general agree about the particle content of the field, unless they are both in specially related frames — such as inertial frames. This is the phenomenon of particle creation in QFT.

In other words, we can characterise the relationship in terms of the mode frequencies. Clearly, if v_j can be written as linear combinations of only positive frequency modes u_j, then all $\beta_{ji} = 0$. This in turn implies that $\hat{a}_j \left|0\right\rangle_2 = 0$, thus the two quantization procedures employing different bases will agree on what is the vacuum state of the theory (and hence the particle content). This problem is worse in curved spacetimes, since in general spacetimes, no timelike Killing vectors exist to even pick out a vacuum state, so vacuum states are not even well-defined at all times.

2.4 Summary 1: how to count particles?

We started from classical scalar field and performed canonical quantization on the field. We briefly discussed certain algebraic aspects which lend credence to the less rigorous treatment of the quantization. We found at the end that there is generically particle creation even in flat spacetimes. Equivalence principle then dictates that this expectation should hold for gravitation, i.e. a gravitational field induces particle creation. This is true even in static spacetimes with timelike Killing vectors: in generic spacetimes, vacuum states are

not even well-defined at all times. This is the case for example in expanding cosmological spacetimes, where a vacuum state is only well-defined only on one spatial hypersurface. This phenomenon underlies the famous Unruh and Hawking effects, describing particle creation due to acceleration and gravitational collapse respectively.

While we do not focus on Unruh and Hawking effects specifically for this thesis, we should point out that the description of particle creation in this chapter has one unsatisfactory aspect: it is not clear how the particle content can be operationally understood without some sort of measurement protocols. The number operator $\hat{a}^\dagger_{\boldsymbol{k}}\hat{a}_{\boldsymbol{k}}$ is highly non-local in spacetime since it is localised in momentum space (at $\boldsymbol{k}$), thus no reasonable observer can in fact measure quantities such as the number expectation $\langle \hat{N}^{(1)}_{\boldsymbol{k}} \rangle_2$. This is true even in presence of timelike Killing vectors where one has natural choices of vacua, since any quantum state of the field is "global" in spacetime, i.e. not defined as tensor product of states at each point $p \in M$. This is worsened by the fact that there is no satisfactory measurement theory for the quantum field without additional, non-QFT ingredients [19].

In view of this difficulty, we will study in the next section the notion of *particle detectors*, which is a simple quantum-mechanical system coupled weakly to the quantum field $\hat{\phi}$ in background spacetime M. Unlike QFT, quantum mechanics does have a well-established measurement theory, such as projective measurements, and so the burden of measuring particle creation phenomena is shifted to how detectors respond to these excitations. It turns out that this model can be treated *relativistically* and even employ quantum information theory involving these detectors (e.g. how two detectors can be entangled). This is the starting point of the relatively new field of *relativistic quantum information* (RQI).

2.5 Unruh-DeWitt (UDW) model

In view of the considerations in the previous section, we now review the *Unruh-DeWitt* (UWD) model. The study of quantum fields via particle detectors has been a fruitful avenue of research in quantum field theory in curved spaces, quantum optics and in relativistic quantum information [20, 26, 27, 37, 38]. Particle detectors are non-relativistic localized quantum systems that couple locally to quantum fields obtaining information about the field state. This allows us to probe the field without invoking projective measurements [19, 39–41]. The paramount example of a particle detector is an atom coupled to the electromagnetic field. Among the most successful models of particle detectors we have the Unruh-DeWitt (UDW) model, consisting of a two-level quantum system coupled locally to a scalar field [21]. Despite its simplicity, this model has been shown to capture the main features of the light-matter interaction [42, 43] and has been extensively used to study

fundamental properties of quantum fields [44, 45]. It also turns out that particle detectors serve as a basic example of local measurement theory for QFT which can be formalized in algebraic settings [46].

At the heart of the Unruh-DeWitt model is bilinear weak coupling between a simple, well-controlled quantum-mechanical system ("detector") such as a two-level system or quantum harmonic oscillator, and a quantum field of interest. In this thesis we focus on a qubit detector. In the interaction picture, the interaction Hamiltonian in the detector's frame takes the form

$$\hat{H}_I(\tau) = \lambda\chi(\tau)\hat{\mu}(\tau) \otimes \hat{\phi}(\mathsf{x}(\tau)) \,, \tag{2.35}$$

where τ is the proper time of the detector, λ is the coupling constant, and $\hat{\mu}(\tau)$ is the monopole coupling of the detector, given by

$$\hat{\mu}(\tau) = \hat{\sigma}^+ e^{\mathrm{i}\Omega\tau} + \hat{\sigma}^- e^{-\mathrm{i}\Omega\tau} \,, \tag{2.36}$$

with $\hat{\sigma}^\pm$ being the ladder operators of $\mathfrak{su}(2)$ algebra and Ω is the energy gap between the detector's ground state $|g\rangle$ and excited state $|e\rangle$. The ladder operator acts in such a way that $\hat{\sigma}^+ |g\rangle = |e\rangle \,, \hat{\sigma}^+ |e\rangle = 0$ and $\hat{\sigma}^- |e\rangle = |g\rangle \,, \hat{\sigma}^- |g\rangle = 0$. Here we use x to denote the spacetime coordinates for notational compactness. The switching function $\chi(\tau)$ governs how the detector is "switched on/off", effectively controlling the strength and duration of interaction (beyond the constant coupling parameter λ). Note that the field operator is evaluated on the detector's trajectory $\mathsf{x}(\tau)$.

To describe the dynamics involving this bilinear interaction, we need an initial state of the field and the detector. In general this could be any arbitrary entangled state, but for simplicity we always choose our initial state to be a product state of the field and the detector density matrices, which reads

$$\hat{\rho}_0 = \hat{\rho}_{0,\mathrm{D}} \otimes \hat{\rho}_{0,\hat{\phi}} \,. \tag{2.37}$$

For example, if both are in ground state, we may write $\hat{\rho} = |g\rangle\langle g| \otimes |0\rangle\langle 0|$. If there are n detectors coupled to the field, we can prepare a general product state

$$\hat{\rho}_0 = \prod_{j=1}^{n} \hat{\rho}_{\mathrm{D},n} \otimes \hat{\rho}_{0,\hat{\phi}} \,, \tag{2.38}$$

which will be the case if we are studying for example entanglement dynamics between two detectors coupled locally to the quantum field (cf. Chapter 5).

The last piece we need is the time evolution operator that implements the dynamics of the detector-field interaction. This is given, as in the usual QFT, by a unitary operator in interaction picture:

$$\hat{U} = \mathcal{T} \exp\left(-\mathrm{i}\int_{-\infty}^{\infty} \mathrm{d}\tau \hat{H}_I(\tau)\right) \equiv \mathcal{T} \exp\left(-\mathrm{i}\int \mathrm{d}\tau \hat{H}_I(\tau)\right) , \tag{2.39}$$

where $\mathcal{T}$ is the time-ordering operator. In the last expression we have suppressed the integration limit since it is implicitly assumed that we are integrating over $\mathbb{R}$, and any "finite-time" requirement is implemented by the switching function that appears in the interaction Hamiltonian $\hat{H}_I$.

At this point, one can choose two routes: perturbative or non-perturbative calculations. In general, the latter is extremely difficult to achieve except in very special cases even-though formally all information is contained in the partition function of the field (hence in the correlation functions). In Unruh-DeWitt model, one example of non-perturbative calculations involve using "delta interaction", i.e. when detectors interact at exactly one instant in time — this completely removes the need for time-ordering and integral in $\hat{U}$ (see e.g. [47–50]). Another alternative is to restrict to the use of harmonic oscillators as qubits in which there are (formidable but executable) ways to perform non-perturbative calculations involving Gaussianity property (see e.g. [51–53]). In this thesis, we focus on the use of time-dependent perturbation theory which already displays many interesting physics despite rendering some physical effects invisible [52, 54].

With perturbation theory, we can employ the standard Dyson series expansion in coupling constant λ, written schematically as

$$\hat{U} = \mathbb{1} + \hat{U}^{(1)} + \hat{U}^{(2)} + O(\lambda^3) , \tag{2.40}$$

where $\hat{U}^{(n)}$ is of order λ^n in the series expansion. The operator $\hat{U}^{(1)}, \hat{U}^{(2)}$ take the form

$$\hat{U}^{(1)} = -\mathrm{i}\int \mathrm{d}\tau\, \hat{H}_I(\tau) , \tag{2.41}$$

$$\hat{U}^{(2)} = -\int \mathrm{d}\tau \int^{\tau} \mathrm{d}\tau'\, \hat{H}_I(\tau)\hat{H}_I(\tau') . \tag{2.42}$$

This expansion has the benefit that it preserves the trace of the density matrix and hence at all orders in the expansion the time-evolution we have a valid density matrix. At first glance, one may wonder why there is no prefactor of $1/2!$ in $\hat{U}^{(2)}$ in the Dyson series, since after all we used series expansion of the exponential map. We derive this in Appendix A.

With this expansion, the time-evolved density matrix can be schematically written as

$$\begin{aligned}\hat{\rho} &= \hat{U}\hat{\rho}_0\hat{U}^\dagger \\ &= \hat{\rho}_0 + \hat{\rho}^{(1)} + \hat{\rho}^{(2)} + O(\lambda^3)\,, \qquad (2.43)\\ \hat{\rho}^{(1)} &= \hat{U}^{(1)}\hat{\rho}_0 + \hat{\rho}_0\hat{U}^{(1)\dagger}\,, \qquad (2.44)\\ \hat{\rho}^{(2)} &= \hat{U}^{(2)}\hat{\rho}_0 + \hat{\rho}_0\hat{U}^{(2)\dagger} + \hat{U}^{(1)}\hat{\rho}_0\hat{U}^{(1)\dagger}\,. \qquad (2.45)\end{aligned}$$

Strictly speaking, we are almost done since the burden of extracting the physics lie mostly in evaluation $\hat{\rho}^{(1)}$ and $\hat{\rho}^{(2)}$, which can be formidable if the problem lacks symmetries or further simplifications.

The last step involves extracting information from this model. Recall that there is no valid local measurement protocols intrinsic to quantum fields in the sense of standard quantum mechanics which respect causality [19]: for example, it is not possible to respect causality if we insist one can perform projective measurement on the field in a compact subregion $U \subset M$. The Unruh-DeWitt model circumvents this problem by the fact that we indirectly probe the field by measuring the detector. In practice this means we first trace out the field state and obtain the detector's reduced density matrix:

$$\hat{\rho}_{\text{D}} = \text{tr}_\phi\, \hat{\rho}\,. \qquad (2.46)$$

If we have more than one detectors, tracing out the field gives us the reduced joint density matrix of the detectors.

The detector's reduced density matrix contains all the information we can extract to the order of perturbation theory we perform. In particular, truncation of the Dyson series effectively implements "selection rule" at each order. Trivially, at zeroth order the detector does not evolve. To first order in λ, one can show that ground state detector cannot be excited by the vacuum of the field as the excitation probability is of order λ^2. To be more specific, if we consider a *smeared detector*, i.e. a detector of finite size given by smearing function $F(\boldsymbol{x})$ centred at the detector's centre of mass, then the transition probability is given by the coefficients of the $|e\rangle\langle e|$ if we expand $\hat{\rho}_{\text{D}}$ in the $\{|g\rangle\,, |e\rangle\}$ basis, namely

$$\begin{aligned}P &= \lambda^2 \iint \mathrm{d}\tau\, \mathrm{d}\tau' \mathrm{d}^D\boldsymbol{x}\, \mathrm{d}^D\boldsymbol{x}'\, e^{-\mathrm{i}\Omega(\tau-\tau')}\chi(\tau)\chi(\tau')F(\boldsymbol{x})F(\boldsymbol{x}')W(\mathsf{x}(\tau),\mathsf{x}(\tau'))\,, \qquad (2.47)\\ W(\mathsf{x}(\tau),\mathsf{x}(\tau')) &\coloneqq \langle 0|\,\hat{\phi}(\mathsf{x}(\tau))\hat{\phi}(\mathsf{x}(\tau'))\,|0\rangle\ . \qquad (2.48)\end{aligned}$$

The function $W(\mathsf{x}(\tau),\mathsf{x}(\tau'))$ is known as two-point Wightman function of the field $\hat{\phi}$ evaluated along the trajectory of the detector (or pullback of the Wightman function to the

detector's trajectory $\mathsf{x}(\tau)$). If more than one detector is involved, one can also compute useful quantities such as signalling estimators (cf. Chapter 4) and entanglement measures (cf. Chapter 5), and one can also explore higher-order effects (see e.g. [55]). Up to second-order in perturbation theory, one essentially only requires the knowledge of the Wightman function to proceed to extract the physics of the problem.

2.6 Summary 2: fine details of UDW model

We saw how one could probe a quantum field operationally using the Unruh-DeWitt model via linear coupling. In essence, the model is extremely *flexible*: one can consider, for example, more complicated and nonlinear coupling to mimic e.g. fermionic interactions (see e.g. [56]). One could also modify the problem so as to exploit non-perturbative methods, use harmonic oscillators instead of qubits, etc. In view of this flexibility, more specific extensions of this model and how to extract useful information from this model will be relegated to the subsequent chapters depending on the physical setup: for example, in Chapter 3 we encounter the use of non-vacuum field states while in Chapter 4 and Chapter 5 we use two detectors coupled to the field.

We stop here to emphasize that in the context of time-dependent perturbation theory, the burden of computing the time evolution of the detector's density matrix and hence various useful quantities such as entanglement measure or transition probability lies in the computation of integrals over the two-point function modulated by the switching function $\chi(\tau)$, smearing function $F(\boldsymbol{x})$, and the phase factor with respect to energy gap Ω. Even for the simplest observable such as transition probability $P(\Omega)$, this is generically an $2(D+1)$-dimensional integral over a *distribution* (two-point functions are distributions). Even for $(1+1)$-dimensional spacetime, this is a four nested integral that is difficult to evaluate. The first natural simplification that comes to mind is to consider the *pointlike detector limit*, where we assume the detector to be very small relative to all length scales of the problem. This reduces the problem to two nested integrals for arbitrary spacetime dimensions, which is still quite formidable to evaluate. Next, one often exploits the simplicity of the trajectory and time-translation symmetry to reduce the integral into a Fourier transform (see e.g. [43, 55, 57, 58]). Alternatively, in the case of Unruh-Dewitt models involving cavities or boundary conditions, the integral reduces to summations that can still be computationally intensive (as exemplified by four-dimensional black hole scenarios due to higher harmonics [59–62]) though they are less ill-behaved (see e.g. [37, 63–65]).

In the worst case scenario, one is faced with lack of time-translation symmetry, which in most cases means that the computation is difficult even with direct numerical integration,

despite the closed-form expression of the full Wightman function [66]. In this last case, rewriting the integrals in certain manner and evaluating them in a slightly different manner from "plug-in-and-integrate" will be necessary while maintaining reasonable computational resources. This "worst-case scenario" occurs in one of our investigations, which we describe in Chapter 5 where we have a non-uniformly accelerating boundary condition. In view of this, it seems appropriate to introduce a trick that may be applicable for similar problems in future, in Chapter 6. Note that this "worst-case scenario" does *not* occur if we are computing *transition rate* for pointlike detectors (as is done e.g. in [67–69]), since by definition it is a single integral and not nested integrals, and there are more ways to make this both numerically and analytically tractable.

Chapter 3

Particle detectors and weak equivalence principle

In this chapter we analyse a quantum version of the weak equivalence principle, in which we compare the response of a static particle detector crossed by an accelerated cavity with the response of an accelerated detector crossing a static cavity in (1+1)-dimensional flat spacetime. In this context, we show that qualitatively the weak equivalence principle holds and discuss how the setup works in Unruh-DeWitt model. We also clarify the role of field mass parameter on this setup.

3.1 Introduction

The weak equivalence principle (WEP) has been one of the central tenets of gravitational physics. It has a variety of formulations, but it asserts that the local effects of motion in a curved spacetime cannot be distinguished from those of an accelerated observer in flat spacetime. The proviso of locality eliminates measurable tidal forces (that would originate, for example, from a radially convergent gravitational field) acting upon finite sized physical bodies. It implies that the trajectories of bodies with negligible gravitational binding energy are independent of their composition and structure, and depend only their initial positions and velocities.

With the development of the Unruh-DeWitt (UDW) model in quantum field theory, WEP can be analyzed in the presence of quantum fields in contrast to the original classical formulation. While not equivalent to a full quantum version of the WEP, this approach

provides an operational means of understanding some important aspects of the WEP in a quantum context. In particular, since UDW detectors capture fundamental features of the light-matter interaction for atomic systems [70], one can operationally study the WEP by asking if a free-falling detector in a stationary cavity in a uniform gravitational field has a different response from that of a stationary detector surrounded by a free-falling cavity. This problem has recently been revisited in the context of moving mirrors [1].

Renewed effort has been expended in recent years towards reanalyzing the role of atomic detector models coupled to a real scalar field with regards to the connection to gravitational phenomena. It has been argued that non-inertiality can be distinguished locally by exploiting nonlocal correlations of the field [2, 63, 71], effectively providing an accelerometer. An analysis of the behaviour of a UDW detector in a static cavity indicated that QFT may provide a way of distinguishing between flat-space acceleration and free-fall in the near-horizon regime [71]. More recently [72] atoms falling through a cavity near an event horizon, together with short-wavelength approximations, led to radiation that is Hawking-like as seen by observers at spatial infinity. Even more recently, an analysis of a moving mirror in cavity [1] has been used to argue once and for all that a "qualitative WEP" should hold in a quantum-field theoretic setting, and emphasized the importance of the initial state of the field in determining radiation from a moving mirror. This investigation focused on mirrors lacking internal degrees of freedom, but nonetheless had the advantage of providing information about the stress-energy tensor in the cavity, which was apparently missed in the past.

Here we will complement these recent studies, especially the one by [1], by showing that atomic UDW detectors also exhibit a qualitative WEP. In particular, we revisit the old problem of computing the response of a static detector surrounded by an accelerating cavity, and the response of an accelerating detector that is surrounded by a static cavity. The key issue here is not the composition of the detector (the body), but rather of its quantum field (vacuum) environment. We consider the response for various field states, including the (scalar) vacuum, excited Fock states, and also single-mode coherent field states. We find that the mass of the quantum scalar field does not enter into the response of the detector in an important way apart from the 'usual' amplitude degradation compared to the massless counterpart.

For non-vacuum field states, we show how resonance can be used to amplify the transition probability via co-rotating terms and demonstrate the qualitative irrelevance of the mass of the field in the physics underlying WEP. This result is to be contrasted with the findings in [2].

This chapter is organized as follows. In Section 3.2, we revisit the formulation of WEP

and clarify the contexts in which this work and others, in particular [1, 72], are performed. In Section 3.3 we provide the standard setup and generic expressions for a UDW detector coupled to a Klein-Gordon field, without restriction to the vacuum state of the field. In Section 3.3.1 we consider an accelerating detector traversing the entire static cavity, noting the necessary changes if detector starts accelerating somewhere within the cavity. In Section 3.3.2 we consider a static UDW detector that encounters an accelerating cavity, entering one end and leaving the other due to the motion of the cavity; we also note the necessary modifications if the trajectory of the detector is changed. In Section 3.4 we consider various non-vacuum field excitations and the role of resonance between atomic gap and excited cavity modes. In Section 3.5 we discuss the interpretation of our results.

3.2 Weak equivalence principle revisited

It is a remarkable property of gravity, in contrast to other non-gravitational forces, that every test particle equally and universally experiences the influence of gravitational fields. This underlies the WEP, which states that phenomenology of bodies observed from frames in uniform gravitational fields is equivalent to that of frames that accelerate uniformly relative to inertial [free-falling] frames [73]. In other words, WEP states that a mass free-falling in a stationary cavity with uniform gravitational field $\boldsymbol{g} = -g\boldsymbol{e}_z$ is completely equivalent to a stationary mass with uniformly accelerating cavity[1] with $\boldsymbol{a} = g\boldsymbol{e}_z$, as shown in Figure 3.1. This principle has been verified to great accuracy through various experiments and effectively sets inertial mass and gravitational mass to be equal.

The purely classical version of the WEP, while asserting that free-fall is independent of a body's composition, does not consider internal quantum degrees of freedom of a body. For example, the body is considered to be uncharged and the space inside the cavity to be free of electromagnetic fields. In a semi-classical setting using the UDW model, our setup will involve an atomic detector (qubit) coupled to some field prepared in some state, as shown in Figure 3.2. The state most closely resembling the classical environment of the WEP would be the quantum vacuum. Other field states can of course be considered, but they will in general produce environments analogous to those of air or some other fluid that produces drag on the body. For example [1], having an electromagnetic field makes the argument less trivial: a classical electric charge in uniform accelerated motion radiates and it is nontrivial to ask whether a *free-falling* charge radiates. The reason is because in general

[1] Alternatively, the normal force experienced by a test mass on the floor of a closed cavity cannot be attributed to cavity acceleration or a uniform gravitational field without additional non-local information (e.g. by looking out of the cavity).

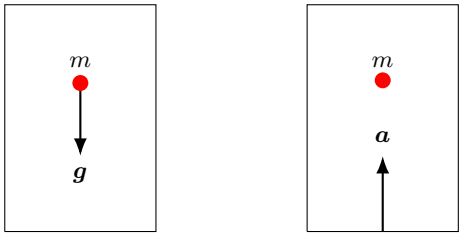

Figure 3.1: Classical WEP setup: test mass m in a closed cavity. WEP claims that these two are kinematically indistinguishable in absence of second-order effects such as tidal forces or non-uniform acceleration. The space inside the cavity is a true vacuum in the classical sense, apart from existence of gravitational field to mimic acceleration.

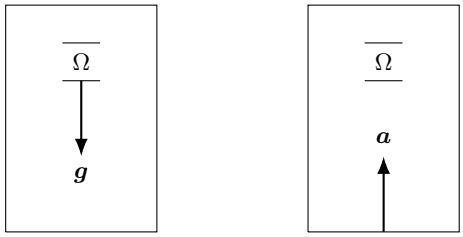

Figure 3.2: Quantum WEP setup: a two-level atomic 'detector' with gap Ω (with respect to its proper frame) in a cavity. The cavity contains a quantum field whose modes may lead to atomic excitations (even in the vacuum state), and hence detector responses. The atom serves as a detector in the sense that a particle is detected when the atom is excited and then emit radiation [3].

relativity, free-falling is an inertial motion (geodesic motion) and acceleration corresponds to non-geodesics in spacetime. According to the equivalence principle, however, we should be able to speak of uniform acceleration and constant gravitational field intercontrovertibly. Where is the problem?

Here we revisit this problem using an Unruh-DeWitt (UDW) detector to replace the mirror in [1]. Specifically, we consider two different "Experiments":

(1) **Stationary cavity, accelerating detector:** In this scenario, we let an atomic detector undergo uniform acceleration as it crosses the cavity containing the quantum field. This mimics the scenario of free-falling atom in gravitational field e.g. outside a black hole especially near the horizon, when the metric is approximately Rindler-like [72].

(2) **Stationary detector, accelerating cavity:** In this scenario, a rigid cavity is accelerating such that a stationary detector traverses across the cavity. This mimics a free-falling cavity in gravitational field under appropriate quasilocal approximations.

If WEP holds, then we should expect that Experiment 1 and Experiment 2 should be qualitatively symmetric in some regimes for the scalar field vacuum. More generally, we might expect that for other field states that the motion of the body is independent of the field mass. In order to make useful and valid comparisons in the context of WEP, we generally need to ensure two additional 'requirements' on the setup in question.

First of all, we will need to be able to set up a kind of cavity undergoing constant acceleration across its full spatial extent. This is forbidden in special relativity without abandoning the rigidity condition [74–76] (static boundary condition in Rindler coordinates). Therefore, a rigid accelerating cavity suitable for WEP is necessarily in a *quasilocal* regime in the sense of $aL \ll 1$ where L is the proper length of the cavity at rest as measured in the lab frame and a is the spatial acceleration. Outside this regime, we see that the accelerating cavity will have detectable non-uniform proper accelerations across the cavity: in this case, with respect to the co-moving frame of the cavity, the stationary detector does *not* undergo uniform acceleration since the worldline of the detector crosses hypersurfaces of constant but varying accelerations. Therefore, Experiment 1 and Experiment 2 are only equivalent in quasilocal approximations, or at most qualitatively equivalent.

Secondly, we will need to show that the distinction between detector responses in Experiments 1 and 2 should be qualitatively independent of the mass of the quantum field and the initial state of the field within the quasilocal regime. In other words, *quantitative* differences between Experiments 1 and 2 would then be attributed to nonlocal correlations: the atom is sensitive to the inequivalent setups in the two experiments and also the fact that moving-boundary/stationary-atom is not the same as a moving-atom/stationary-boundary from a physical point of view.

We make a remark that the role of the field mass should only serve to degrade non-local correlations of the field and hence diminish transition amplitudes, all else being equal. This requirement, however, is in slight tension with previous results [2] claiming (in the non-relativistic regime) that the field mass term can enhance the transition probability of a detector, making it a better accelerometer in the case of highly excited field states. This would mean that the mass of a scalar field leads to additional physical effects *beyond* suppressing correlations. For the WEP in particular, one could imagine increasing the mass more and more to detect increasingly small local accelerations. We will recover consistency with WEP by showing that this discrepancy is in part due to mixing conformal flatness with conformal invariance of the Klein-Gordon equation. We also note that the idea that

massive excitations should be 'harder' to detect than the massless ones, all things being equal, is not new — it has been investigated e.g. in [77]. A more complete discussion of these issues is given in Appendix B.1 and B.2.

In light of these requirements, in the next few sections we will consider the setup and demonstrate that the qualitative WEP holds.

3.3 Setup

Our starting point is the Klein-Gordon equation for a real scalar field: the covariant formulation of Klein-Gordon equation which governs the dynamics of a real scalar field reads (cf. Chapter 2)

$$\frac{1}{\sqrt{-g}}\partial_\mu\Big(g^{\mu\nu}\sqrt{-g}\partial_\nu\phi\Big) - m^2\phi = 0\,. \tag{3.1}$$

For global Minkowski spacetime, the solutions are given by plane waves. Recall that all $(1+1)$ dimensional spacetimes are conformally equivalent to Minkowski spacetime: by this we mean that there exists a coordinate system in which the metric is conformally flat, i.e. with metric that takes the form

$$g_{\mu\nu}(\mathsf{x}) = \Omega^2(\mathsf{x})\eta_{\mu\nu}\,. \tag{3.2}$$

This conformal flatness can be exploited in the case of $m = 0$ to map the solutions of the Klein-Gordon equation to the plane-wave solutions in Minkowski spacetime because the massless Klein-Gordon equation is conformally invariant in $(1+1)$ dimensions. This allows us to obtain an *exact closed form* for the spectrum of the field modes[2]. For $m \neq 0$, the conformal invariance of the wave equation is lost and hence conformal flatness provides no particular advantage. For uniform acceleration, the field modes can still be written in closed form but neither the normalization nor the spectrum can.

To probe the field, we consider a pointlike Unruh-DeWitt (UDW) detector whose interacting Hamiltonian is given by

$$\begin{aligned}\hat{H}_I(\tau) &= \lambda\chi(\tau)\hat{\mu}(\tau)\hat{\phi}(t(\tau),x(\tau))\,,\\ \hat{\mu}(\tau) &= e^{i\Omega\tau}\hat{\sigma}^+ + e^{-i\Omega\tau}\hat{\sigma}^-\,,\end{aligned} \tag{3.3}$$

[2]An important point here is that conformal invariance is convenient but not always necessary. We show this in Appendix B.1 for the case of uniform acceleration.

where τ is the proper time of the detector, λ is the coupling strength of the detector and the field, $\hat{\mu}(\tau)$ is the monopole moment of the detector, $\hat{\sigma}^{\pm}$ are $\mathfrak{su}(2)$ ladder operators characterizing the two-level atomic detector, and $\chi(\tau)$ is the switching function of the detector. Here $\hat{\sigma}^{+}|g\rangle = |e\rangle$ and $\hat{\sigma}^{-}|e\rangle = |g\rangle$ where $|g\rangle, |e\rangle$ refer to the ground and excited states of the atom respectively, separated by energy gap Ω. Note that the interacting Hamiltonian is given in the interaction picture.

We first consider the initial state to be a separable state $|g,\psi\rangle = |g\rangle \otimes |\psi\rangle$ where $|\psi\rangle$ is some initial pure state of the field. If the field is in some $|\text{out}\rangle$ state after the interaction and the detector is in excited state $|e\rangle$, then the transition probability of the detector is given by Born's rule after tracing out the field state (cf. Chapter 2):

$$P = \sum_{\text{out}} \left| \langle e, \text{out} | \hat{U} | g, \psi \rangle \right|^2 \tag{3.4}$$

where the time evolution operator in the Dirac picture is

$$\hat{U} = \mathcal{T} \exp\left(-i \int \mathrm{d}\tau \hat{H}_I(\tau) \right) , \tag{3.5}$$

where it is understood that the integral is over $\mathbb{R}$. Employing the Dyson expansion, we get

$$\begin{aligned} \hat{U} &= \mathbb{1} + \hat{U}^{(1)} + O(\lambda^2) , \\ \hat{U}^{(1)} &= -i \int \mathrm{d}\tau \hat{H}_I(\tau) \end{aligned} \tag{3.6}$$

we obtain the leading order contribution to the transition probability

$$\begin{aligned} P &= \lambda^2 \int \mathrm{d}\tau \int \mathrm{d}\tau' \chi(\tau)\chi(\tau') e^{-i\Omega(\tau-\tau')} W(\tau,\tau') + O(\lambda^4) , \\ W(\tau,\tau') &= \langle \psi | \hat{\phi}(\mathsf{x}(\tau)) \hat{\phi}(\mathsf{x}(\tau')) | \psi \rangle , \end{aligned} \tag{3.7}$$

where $W(\tau,\tau')$ is the pullback of the Wightman function on the detector's trajectory $\mathsf{x}(\tau)$. The remaining task is to compute the Wightman function for different scenarios and choose an appropriate switching function of the detector.

Recall from Section 3.2 that we are interested in two types of scenarios ("Experiments") contrasting accelerating detector and accelerating cavity scenarios. The spacetime diagram for these two setups are shown in Figure 3.3.

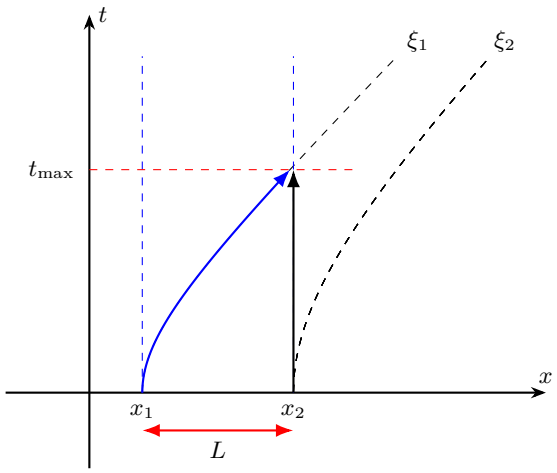

Figure 3.3: Spacetime diagram for the setup. The detector's trajectories are given by solid arrows and the cavities by the dashed lines. The accelerating detector-static cavity scenario is given in blue, while the accelerating (rigid) cavity-static detector scenario is given in black.

3.3.1 Accelerating detector, static cavity

Let us first consider the case of a static cavity relative to the lab frame (t, x). In this case, the cavity is equivalent to a Dirichlet boundary condition $\phi(x_1) = \phi(x_2) = 0$ where x_j are the locations of the boundary and the length of the cavity as measured by the lab frame is $L = x_2 - x_1$. The equation of motion for the quantized scalar field reduces to

$$(\partial_\mu \partial^\mu - m^2)\hat{\phi} = 0 \tag{3.8}$$

and the spatial part of the mode functions are standing waves:

$$\begin{aligned} \hat{\phi}(t,x) &= \sum_{n=1}^{\infty} u_n(x) \left(e^{-i\omega_n t}\hat{a}_n + e^{i\omega_n t}\hat{a}_n^\dagger \right) , \\ u_n(t,x) &= \frac{1}{\sqrt{L\omega_n}} \sin \frac{n\pi(x - x_1)}{L} , \end{aligned} \tag{3.9}$$

where $\omega_n^2 = \left(\frac{n\pi}{L}\right)^2 + m^2$ and $n \in \mathbb{N}$. The normalization of u_n can be found using the Klein-Gordon inner product [3]

$$(\phi_1, \phi_2) = -i \int_\Sigma \mathrm{d}\Sigma^\mu \sqrt{-g}\, (\phi_1 \partial_\mu \phi_2^* - (\partial_\mu \phi_1)\phi_2^*) \,, \tag{3.10}$$

where $\mathrm{d}\Sigma^\mu = \mathrm{d}\Sigma n^\mu$ and Σ is the spacelike hypersurface with unit normal n^μ (cf. Chapter 2). In this case, $\sqrt{-g} = 1$ and Σ is spacelike hypersurface at constant t.

For the detector/cavity configuration in Figure 3.3, if the detector is accelerating from the left wall to the right wall of the cavity then $x_1 = 0$; if the detector starts from the midpoint, then $x_1 = -L/2$. Starting at the midpoint (as in [2]) is useful if we wish to consider the $a = 0$ limit, since the Dirichlet boundary renders the limit ill-defined for a detector starting from the left where the field vanishes (i.e. the detector 'merges' with the wall). We will consider trajectories in which the detector travels from one wall to the other as well as from the midpoint as appropriate; we shall refer to the latter kind of trajectory as a 'midpoint trajectory'.

If the initial state the field is vacuum state $|0\rangle$ with respect to Killing time t, then the pullback of the Wightman function along the trajectory $\mathsf{x}(\tau)$ is

$$W_0(\tau, \tau') = \sum_{n=1}^{\infty} u_n(\mathsf{x}(\tau)) u_n^*(\mathsf{x}(\tau')) \,. \tag{3.11}$$

For a uniformly accelerating detector, this trajectory is given by

$$\mathsf{x}(\tau) = \frac{1}{a} (\sinh a\tau, \cosh a\tau - 1) \tag{3.12}$$

where the integration constant is chosen so that $x(\tau = 0) = 0$. Solving for the time taken to traverse the cavity, we obtain

$$\tau_{\max} = \frac{\cosh^{-1}(1 + aL)}{a} \,. \tag{3.13}$$

If the detector starts from the midpoint of the cavity, then the expression for the time to exit the cavity is given by Eq. (3.13) with $L \to L/2$. Finally, putting everything together, we obtain

$$P_0^D = \lambda^2 \sum_{n=1}^{\infty} \frac{1}{L\omega_n} \left| \int_{-\infty}^{\infty} \mathrm{d}\tau \chi(\tau) \sin \frac{n\pi}{L} \left(\frac{\cosh a\tau - 1}{a} - x_1 \right) e^{-i\Omega\tau} e^{-i\omega_n \frac{\sinh a\tau}{a}} \right|^2 \tag{3.14}$$

for the detector transition probability for the field in the vacuum state. Eq. (3.14) holds for both massless and massive scalar field, since the mass enters through ω_n. Note that the limits of integration are effectively governed by the switching function. We shall generally choose $\chi(\tau) = 1$ for the interval $[0, \tau_{\max}]$ and zero otherwise (the so-called top-hat switching). We use the superscript D to denote an accelerating detector in a cavity that is static with respect to the lab frame (t, x); otherwise we use a superscript C. The cavity forces the field to be compactly supported in the interval $[x_1, x_2]$, beyond which the detector experiences no interaction with the field.

Here we make some less important but technical remarks. For a trajectory where the detector traverses the entire cavity (from one wall to another), the divergences associated with sudden switching do not occur because the Dirichlet boundary condition causes the field to vanish there (see for instance [37]). Effectively, the detector does not see the discontinuity in the switching. Furthermore, while divergences due to sudden switching arise in quite general contexts [78], it is also now known that the spurious divergence due to sudden switching in Minkowski space is in fact dimension-dependent [68] and the setup $(1+1)$D does not suffer this problem due to logarithmic nature of the singularity in the Wightman function. Since the mode sum is convergent even without a UV regulator, imposing a UV cutoff is a computational convenience (cf. Appendix B.3). An IR cutoff naturally arises from the Dirichlet boundary condition; thus the usual IR divergence of a massless scalar field in (1+1) dimensions does not appear either.

3.3.2 Accelerating cavity, static detector

Now suppose we consider a rigid cavity of length L as measured in the lab frame at $t = 0$. The cavity is uniformly accelerating in the positive x-direction, and there is an inertial UDW detector at rest at (t, x_d) where x_d is constant. Note that by 'uniform' we mean that each point of the cavity traces a constant-acceleration trajectory at all times; different points may have different proper accelerations. This scenario corresponds to the detector passing through a cavity with moving boundary conditions. In (1+1) dimensions, there is an analytic solution to this seemingly difficult problem when $m = 0$: we perform a coordinate transformation

$$t = \frac{e^{a\zeta}}{a} \sinh a\varsigma \,, \quad x = \frac{e^{a\zeta}}{a} \cosh a\varsigma \tag{3.15}$$

where (ς, ζ) are sometimes known as the Lass or radar Rindler coordinates [79] — we will refer to these as *conformal Rindler coordinates*. This coordinate system covers the usual

Rindler wedge and has the special property that the metric is conformal to the Minkowski metric:

$$\mathrm{d}s^2 = -\mathrm{d}t^2 + \mathrm{d}x^2 = e^{2a\zeta}\left(-\mathrm{d}\varsigma^2 + \mathrm{d}\zeta^2\right). \tag{3.16}$$

Each line of constant ζ describes a uniformly accelerating trajectory with proper acceleration $|a^\mu a_\mu|^{1/2} = ae^{-a\zeta}$. Consequently the kinematical parameter a for the line $\zeta = 0$ corresponds to the proper acceleration of the test particle along this trajectory. In these coordinates, the cavity walls correspond to Dirichlet boundary conditions at $\zeta = \zeta_1, \zeta_2$. We denote $L' = \zeta_2 - \zeta_1$. Since we are comparing the scenarios in which the detector traverses the entire cavity, we will also choose $\zeta_1 = 0$ so that the proper acceleration of the left wall matches the acceleration of the detector[3]. Inverting the coordinates, the trajectory of the static detector is

$$\varsigma = \frac{1}{a}\tanh^{-1}\frac{t}{x_d}, \quad \zeta = \frac{1}{a}\log a\sqrt{x_d^2 - t^2}. \tag{3.18}$$

If we define the left wall to be at $\zeta = \zeta_1 = 0$, then the proper length of the cavity in conformal coordinates is

$$L = x_2 - x_1\Big|_{t=0} = \int_{\zeta_1=0}^{\zeta_2=L'} \mathrm{d}\zeta\, e^{a\zeta} = \frac{e^{aL'} - 1}{a}, \tag{3.19}$$

which can be inverted to give $L' = a^{-1}\log(1 + aL)$. Crucially, $x_2 - x_1 \neq \zeta_2 - \zeta_1$ and $\lim_{a\to 0} L' = L$. If the detector starts at the right wall and the cavity accelerates in the positive x-direction, then we have $x_d = a^{-1} + L$. The maximum interaction time is obtained by solving for in the detector's frame

$$a\sqrt{x_d^2 - t^2} = 1 \Longrightarrow t_{\max} = \sqrt{\frac{2L}{a} + L^2}. \tag{3.20}$$

For the massless field, the Klein-Gordon equation is conformally invariant under the above

[3]Note that if we consider the midpoint of the cavity to have acceleration a, then it is *not* true that the walls are located at $\zeta_j = \pm L'/2$: conformal transformations do not preserve distances between two points. In particular, it can be shown that

$$x_j = \frac{1}{a} \pm \frac{L}{2} \Longrightarrow \zeta_j = \log\left(1 \pm \frac{aL}{2}\right) \tag{3.17}$$

which is manifestly not symmetric with respect to the detector position $\zeta_d = 0$.

transformation and hence the spatial part of the mode functions in this coordinate system are also standing waves:

$$\begin{aligned}\hat{\phi}(\varsigma,\zeta) &= \sum_{n=1}^{\infty} v_n(\zeta)\left(e^{-i\tilde{\omega}_n\varsigma}\hat{b}_n + e^{i\tilde{\omega}_n\varsigma}\hat{b}_n^\dagger\right)\,,\\ v_n &= \frac{1}{\sqrt{n\pi}}\sin\frac{n\pi(\zeta-\zeta_1)}{L'}\,,\end{aligned} \tag{3.21}$$

where we have used the fact that the normalization simplifies due to $L'\tilde{\omega}_n = n\pi$. Here we see that the reason why $L' \neq L$ is simply because conformal transformation does not preserve length.

Since $t = \tau$ is the proper time of the detector, the full transition probability[4] for traversing the entire cavity is

$$P_0^C = \lambda^2 \sum_{n=1}^{\infty}\frac{1}{n\pi}\left|\int_{-\infty}^{\infty}\mathrm{d}\tau\chi(\tau)\sin\frac{n\pi\log\sqrt{(1+aL)^2-a^2\tau^2}}{\log 1+aL}e^{-i\Omega\tau}e^{-\frac{in\pi\tanh^{-1}\frac{a\tau}{1+aL}}{\log(1+aL)}}\right|^2 \tag{3.23}$$

with the top-hat switching in the interval $[0,\tau_{\max}]$, noting that here $t_{\max} = \tau_{\max}$.

If the field is massive ($m \neq 0$), the Klein-Gordon equation is no longer invariant under a conformal transformation, and it is more advantageous to use the manifestly simpler, standard Rindler coordinates

$$t = \xi\sinh\eta\,,\qquad x = \xi\cosh\eta\,. \tag{3.24}$$

Let us work this out explicitly from the Klein-Gordon equation: since $\sqrt{-g} = \xi$, the covariant Klein-Gordon equation gives

$$\frac{1}{\xi^2}\frac{\partial^2\phi}{\partial\eta^2} - \left(\frac{1}{\xi}\frac{\partial\phi}{\partial\xi} + \frac{\partial^2\phi}{\partial\xi^2}\right) + m^2\phi = 0\,. \tag{3.25}$$

[4]If the detector trajectory is such that at $t = 0$ it is at midpoint of the cavity ('midpoint detector'), then some parts of these expressions will need to be changed if we want the kinematical parameter a to be the proper acceleration at the centre of the cavity (such as is done in [2]). Both $t_{\max}$ and L' will change for the midpoint detector to these:

$$L' = \log\frac{2+aL}{2-aL}\,,\ t_{\max} = \sqrt{\frac{L}{a}-\frac{L^2}{4}} \tag{3.22}$$

and there will be a slight modification of Eq. (3.23). Also, clearly ζ_1 would not be zero in this case.

Separating variables $\phi = v(\xi)T(\eta)$, we can show that $T(\eta) \propto \exp \pm i\omega\eta$ and hence we obtain the modified Bessel differential equation of imaginary order for the spatial part of the mode function:

$$\xi^2 \frac{\mathrm{d}^2 v}{\mathrm{d}\xi^2} + \xi \frac{\mathrm{d}v}{\mathrm{d}\xi} + (\omega^2 - m^2\xi^2)v = 0\,. \tag{3.26}$$

Implementing the Dirichlet boundary condition $v(\xi_1) = v(\xi_2) = 0$ as before, the modes will have discrete spectrum labelled by $n \in \mathbb{Z}$ and the spatial mode can be expressed in terms of modified Bessel functions of imaginary order [80]:

$$v_n(\xi) = |A_n| \left(\mathrm{Re}\left(I_{i\omega_n}(m\xi_1)\right) K_{i\omega_n}(m\xi) - \mathrm{Re}\left(I_{i\omega_n}(m\xi)\right) K_{i\omega_n}(m\xi_1)\right)\,. \tag{3.27}$$

The Klein-Gordon inner product in Eq. (3.10) gives the normalization

$$2|A_n|^2 \omega_n \int_{\xi_1}^{\xi_2} \frac{\mathrm{d}\xi}{\xi} \left|v_n(\xi)\right|^2 = 1\,. \tag{3.28}$$

The discrete spectrum and the normalization must be solved numerically. Similar to the massless case, we can then do the pullback of the Wightman function onto the trajectory of the detector which is given by

$$\xi(\tau) = \sqrt{x_d^2 - t^2} \qquad \eta(\tau) = \tanh^{-1} \frac{t}{x_d} \tag{3.29}$$

where the constant x_d describes the static detector trajectory with respect to the lab coordinates.

We pause to comment about rigid body motion in the Rindler frame. Note that even if the leftmost wall acceleration gets arbitrarily large, the centre of mass acceleration is bounded above by the rigidity condition: a rigid cavity of length L in the lab frame must have a different proper acceleration at each point in order to remain rigid. The proper acceleration at any point x within the cavity is given by

$$a(x) = \frac{a_1}{1 + a_1(x - x_1)}\,, \tag{3.30}$$

where $x_1 = a_1^{-1}$ is the location of left wall and a_1 is the proper acceleration of the left wall. We see that at the centre $x_c = a_1^{-1} + L/2$ of the cavity we have the limit

$$\lim_{a_1 \to \infty} a_c = \lim_{a_1 \to \infty} \frac{2a_1}{2 + a_1 L} = \frac{2}{L}\,. \tag{3.31}$$

If the centre of the cavity attains an acceleration larger than this, the rear wall will cross the future Rindler horizon.

Another way to see this geometrically is by looking at the spacetime diagram (cf. Figure 3.3). For a uniformly accelerating rigid cavity, the two walls must both be on two different hypersurfaces of constant ξ in order for them to be a Dirichlet boundary i.e. $\xi = \xi_1$ and $\xi = \xi_2$. Different values of ξ correspond to trajectories with different proper accelerations, and the lab observer does not see this cavity as rigid because the the cavity shrinks across plane of simultaneity of constant t. The rigidity condition essentially means that cavity has constant length when measured in the plane of simultaneity of constant η.

3.3.3 Results for vacuum states

In Figure 3.4 we plot the absolute probability difference between the accelerating cavity and the accelerating detector scenarios as a function of the proper acceleration a. A larger energy gap generally suppresses the transition probability in massless scenario as shown in Figure 3.4, and similar qualitative suppression is observed in the massive case. For comparison of the convergence of the mode sums, we considered ranging both $N = 15$ and $N = 100$. The larger value of N is required for larger acceleration parameters a (see also Appendix B.3 for separate convergence checks).

In Figure 3.5 we compare the absolute probability difference for massless and massive fields. Here our results agree with previous work [2] in that if the initial field state is the vacuum, then for $aL \ll 1$ the difference in responses between inertial and non-inertial detectors quickly vanishes. For completeness, we plot in Figure 3.6 the transition probability of the accelerating cavity scenario for very small mass. We see that indeed it provides the correct massless limit despite the rather complicated mode functions involving modified Bessel functions. The accelerating detector case will trivially have the correct limit since the functional form of the Wightman functions is the same.

Furthermore, we do see considerable distinction between the massive and massless cases once a becomes sufficiently large (cf. Figure 3.5). The larger difference in response for the two setups at large a should not be taken to be a fundamental violation of the WEP: for large a, the non-uniformity of the cavity acceleration at different points is more pronounced, similar to how the non-uniformity of Earth's gravitational field is detectable if we consider a large enough region in space.

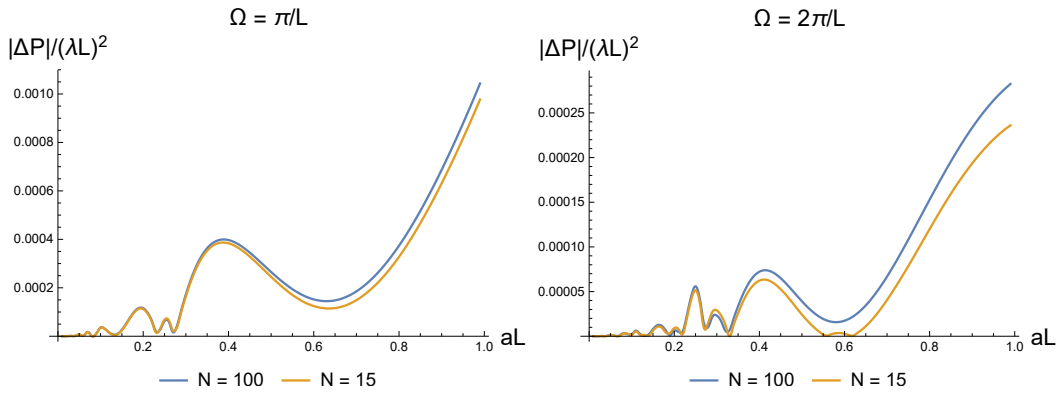

Figure 3.4: Absolute difference in probability $|\Delta P| = |P_0^C - P_0^D|$ as a function of acceleration aL for $m = 0$. For small accelerations, the mode sums quickly converge for small N and the difference in transition probability of the two scenarios is vanishingly small in low acceleration limit. **Left:** for $\Omega = \pi/L$. **Right:** for larger gap $\Omega = 2\pi/L$.

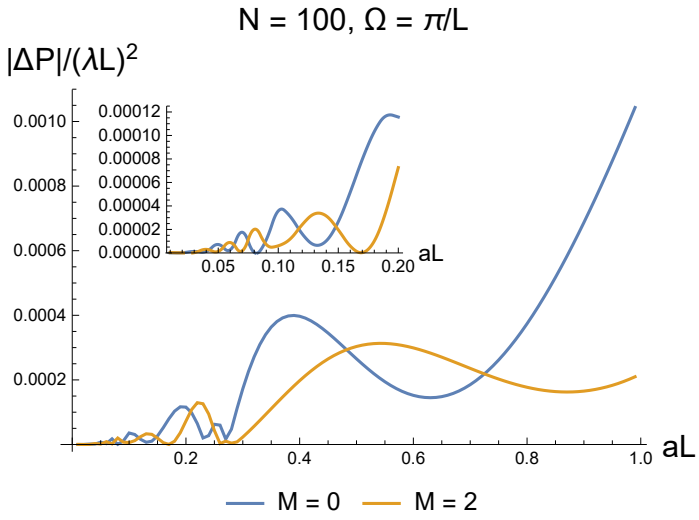

Figure 3.5: Comparing the absolute difference in probability $|P_0^C - P_0^D|/\lambda^2$ as a function of acceleration for $\Omega = \pi/L$ when the field is initially in the vacuum state. The difference vanishes quickly for $aL \ll 1$.

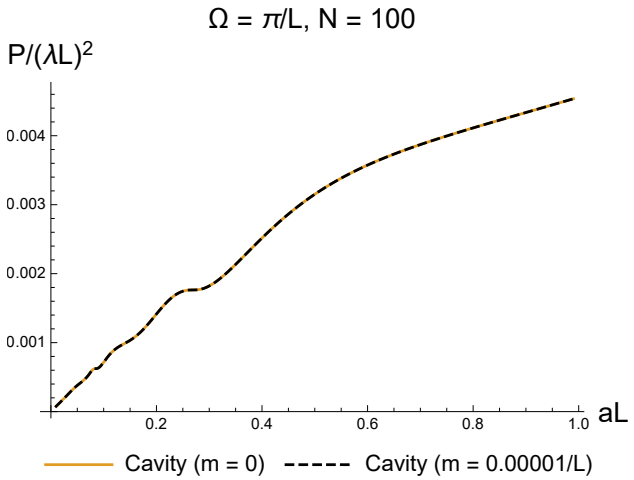

Figure 3.6: Transition probability as a function of acceleration for $\Omega = \pi/L$, showing that in the small mass limit the results agree with massless case. Note that a value of $m = 0.0001/L$ is small enough to be indistinguishable from the $m = 0$ case, with relative difference in probability of 2 parts in a billion (10^{-9}) at $aL \approx 0.01$.

3.4 Excited field states

The results in the previous section show that qualitatively WEP holds when the field is prepared in vacuum state[5]. After considering the vacuum state of the field, a natural question then arises: can sensitivity to non-inertiality be enhanced if the field state is not a vacuum state? The additional terms in the Wightman function due to the excited field states may have co-rotating term of the form $\Omega - \omega_n$ which may produce resonant-like behaviour, while for the vacuum state this cannot occur for a ground state atom. For simplicity, we will consider both single-mode excited Fock states and single-mode coherent states.

[5]This is interesting partly because the two setups involve unitarily inequivalent vacua, just as Rindler and Minkowski vacua are not unitarily equivalent [32]. It is an interesting question to see if for large acceleration the unitary inequivalence manifests itself, in addition to the "non-uniformity" of the acceleration across the cavity; or perhaps the two cavity vacua are *physically equivalent* [81].

3.4.1 Single-mode excited Fock state

The simplest excited field state we can consider is a single-mode non-vacuum Fock state, i.e. when the k-th momentum has n_k excitations. This is a straightforward generalization from the expression found in [2]. We denote this by $|n_k\rangle$ which formally reads $|n_k\rangle \sim |000...0\ n_k\ 000...\rangle$ (i.e. the zeros are suppressed), where the enumeration is valid because of the countably infinite spectrum. The corresponding Wightman function is given by

$$W(\mathsf{x},\mathsf{x}') = \langle n_k|\phi(\mathsf{x})\phi(\mathsf{x}')|n_k\rangle \tag{3.32}$$

Employing the result

$$\phi(\mathsf{x}')\,|n_k\rangle = \sum_{l\neq k} u_l^*(\mathsf{x}')\,|1_l, n_k\rangle + \sqrt{n_k+1}u_l^*(\mathsf{x}')\,|n_k+1\rangle + \sqrt{n_k}u_l(\mathsf{x}')\,|n_k-1\rangle\ , \tag{3.33}$$

where the $\{u_j\}$ are the eigenmodes of the Klein-Gordon equation (not just the spatial part), we obtain

$$\begin{aligned} W(\mathsf{x},\mathsf{x}') &= \sum_{j,l\neq k} u_j(\mathsf{x})u_l^*(\mathsf{x}') + (n_k+1)u_k(\mathsf{x})u_k^*(\mathsf{x}') + n_k u_k^*(\mathsf{x})u_k(\mathsf{x}') \\ &= \sum_j u_j(\mathsf{x})u_j^*(\mathsf{x}') + n_k u_k(\mathsf{x})u_k^*(\mathsf{x}') + n_k u_k^*(\mathsf{x})u_k(\mathsf{x}') \\ &\coloneqq W_0(\mathsf{x},\mathsf{x}') + W_{\text{exc}}(\mathsf{x},\mathsf{x}')\,. \end{aligned} \tag{3.34}$$

Here $W_0(\mathsf{x},\mathsf{x}')$ corresponds to the summation over j encoding vacuum contribution, while W_{exc} corresponds to the second and the last term proportional to n_k, the contribution from the non-zero excitations to the full expression for the Wightman function. Therefore, for a single-mode excited Fock state, the Wightman function is the sum of the vacuum Wightman function W_0 and an additional piece W_{exc} that is explicitly dependent on which mode is excited. Since the transition probability is linear in $W(\mathsf{x},\mathsf{x}')$, we see that the transition probability for this state reads

$$P_{\text{tot}}(n_k) = P_0 + n_k\left|\int \mathrm{d}\tau\chi(\tau)e^{-i\Omega\tau}u_k(\tau)\right|^2 + n_k\left|\int \mathrm{d}\tau\chi(\tau)e^{-i\Omega\tau}u_k^*(\tau)\right|^2\ . \tag{3.35}$$

We are interested in W_{exc} since we found W_0 in the previous section and we can always subtract off the vacuum contribution. Note that

$$\begin{aligned} e^{-i\Omega\tau}u_k(\tau) &\sim e^{-i(\omega_k T(\tau)+\Omega\tau)}\,, \\ e^{-i\Omega\tau}u_k^*(\tau) &\sim e^{-i(\omega_k T(\tau)-\Omega\tau)}\,, \end{aligned} \tag{3.36}$$

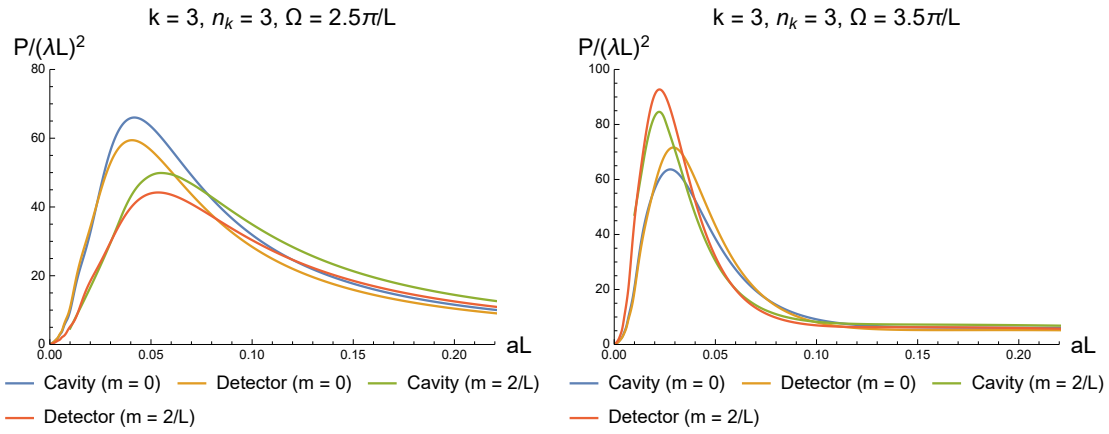

Figure 3.7: Transition probability as a function of acceleration for two different gaps, comparing massless and massive cases. The field is in the third excited state i.e. $k = 3$ and we chose $n_3 = 3$. **Top:** $\Omega = 2.5\pi/L$. **Bottom:** $\Omega = 3.5\pi/L$.

where $T(\tau)$ is the time function (which in our case is either $\eta(\tau)$ or $t(\tau)$) along the trajectory of the detector. The third term in P_{tot} is the 'co-rotating term' which will tend to dominate over the second ('counter-rotating') term.

The above results teach us that there are two ways in which one can "neglect" the vacuum contribution. One is when we have an approximate *resonance* (up to some Doppler shifts) i.e. when $\Omega \sim \omega_k$. In this case, the resonance will amplify the transition rate and the vacuum contribution can be rendered negligible compared to the rest. The other is if there is a sufficiently higher number of excitations n_k: in this case the transition probability scales as

$$P_{\text{excited}} \sim \frac{n_k}{k} \tag{3.37}$$

where the denominator $1/k$ comes from the normalization of u_k. This means for a given energy gap Ω, the higher momentum mode will need an excitation of order $n_k \sim k$ to achieve a given probability amplitude. When it is off-resonance, a larger gap tends to diminish the transition probability, which simply reflects the fact that atoms with larger energy gaps are harder to excite.

Some of these results are made more explicit in Figure 3.7. A notable result upon comparison of the two figures is that one can indeed amplify transition probability by considering gaps that are 'close' to the excited field state frequency. In Figure 3.7, by

considering 'off-resonant' gap at $\Omega = 3\pi/L \pm \epsilon$, there are regimes of accelerations in which the massive fields have better transition probabilities for both accelerating detector/cavity scenarios than do their massless counterparts, and vice versa depending whether $\Omega = \omega_n - \epsilon$ or $\Omega = \omega_n + \epsilon$ (in the plots, $\epsilon = 0.5\pi/L$). However, for each mass the distinction between an accelerating detector and an accelerating cavity quickly vanishes for small a.

Here we make a parenthetical comment that the relative magnitude of $\Omega - \omega_k$ or Ω/ω_k *does matter* for comparison purposes: for a given fixed atomic gap Ω, one can engineer a situation in which massive fields can have larger transition probability than the massless counterpart using resonance and vice versa. This is already apparent in Figure 3.7 for small a, where transition probability for massive case can be lower or higher than the massless case depending on choice of gap Ω. This is, however, a separate problem from fundamentally distinguishing local accelerations.

The relative magnitude matters less as one moves away from resonance, e.g. when $\Omega/\omega_k \gg 1$. We check this for the case of highly populated field state $n_k \gg 1$ as shown in Figure 3.8, where we choose $k = 1/L$ and $n_k = 1000$ to match the setup in [2] for convenience. In the top figure, the massive field seems to outperform the massless case for distinguishing local accelerations. However, this can be attributed to resonant effect, since for our choice of fixed Ω, the magnitude of $\Omega - \omega_k$ is smaller for the massive case than the massless case. A possibly fairer comparison would be to use the same $|\Omega - \omega_k|$ or Ω/ω_k, as shown in the middle and bottom plot of Figure 3.8. When this is done, we see that the apparent advantage of the massive field over massless one disappears and massless field seems to perform equally well if not better[6].

We conclude from these that massive fields do not seem to offer any obvious fundamental advantages at low accelerations as compared to their massless counterpart. In Appendix B.2 we suggest a possible reason for the disparity with the results found in [2].

3.4.2 Coherent field state

An interesting case to consider is when the field is in a coherent state, analogous to that of a laser field in quantum optics scenarios. For one, this state is highly non-diagonal in Fock basis, as one can verify from the density matrix. It is defined as the continuum

[6]This issue is somewhat tricky since it is arguable as to which comparison is fairer. Furthermore, one can argue whether massive and massless scalar fields should be compared with the same coupling strength λ. We brought this 'fairness' problem up since for WEP, fair comparison is analogous to "not being able to look out of the window of a rocket" to decide the asymmetry of the problem.

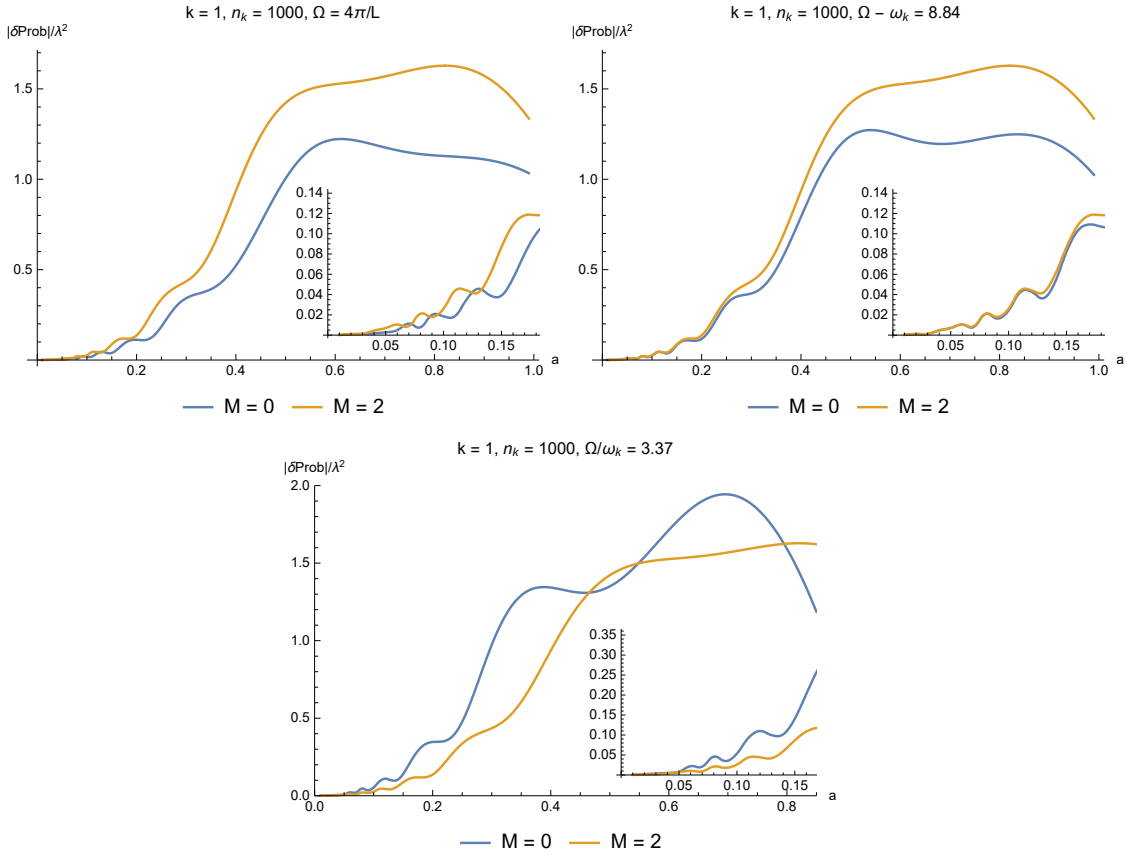

Figure 3.8: Absolute probability difference as a function of acceleration for large excitation number n_k. The field is in the third excited state i.e. $k = 3/L$ and we chose $n_3 = 3$. **Top:** $\Omega = 4\pi/L$. **Middle:** $\Omega - \omega_k = 8.84/L$ where the reference ω_k is chosen to be the angular frequency for the massive case. **Bottom:** $\Omega/\omega_k = 3.37$.

limit of a quantum-mechanical coherent state for a quantum harmonic oscillator using the displacement operator $\hat{D}_{\alpha(k)}$ (see, for instance [82]):

$$\begin{aligned} |\alpha(k)\rangle &:= \hat{D}_{\alpha(k)} |0\rangle \\ &= \exp\left[\int \mathrm{d}k \left[\alpha(k)\hat{a}_k^\dagger - \alpha^*(k)\hat{a}_k\right]\right] |0\rangle \ . \end{aligned} \tag{3.38}$$

Here $\alpha(k)$ is the *coherent amplitude distribution* defining a coherent amplitude for every mode k. As a coherent state, it satisfies the 'eigenvalue' equation

$$\hat{a}_{k'} |\alpha(k)\rangle = \alpha(k') |\alpha(k)\rangle \ , \tag{3.39}$$

noting that $|\alpha(k)\rangle$ does not mean an explicit dependence on k but rather on coherent amplitude distribution $\alpha(k)$. In a cavity, the spectrum becomes discrete and so we label the modes with integers n instead (for example, the continuous variable k becomes discrete: $k_n = n\pi/L$ in static cavity scenario). The coherent state has a simpler form

$$|\alpha(n)\rangle = \exp\left[\sum_{n=1}^{\infty}(\alpha_n \hat{a}_n^\dagger - \alpha_n^* \hat{a}_n)\right] |0\rangle \ . \tag{3.40}$$

Note that in this case we can formally write

$$|\alpha(n)\rangle \sim |\alpha_1 \alpha_2 ... \alpha_j ...\rangle \sim \bigotimes_{n=1}^{\infty} |\alpha_n\rangle \tag{3.41}$$

which denotes tensor product of coherent states each with complex coherent amplitude α_j. For single-mode coherent state, say for the j-th momentum, we have (cf. Eq. (3.39))

$$\hat{a}_j |\alpha(k)\rangle = \alpha_j \delta_{jk} |\alpha(k)\rangle \ , \quad \alpha_j \in \mathbb{C} \, . \tag{3.42}$$

For a countably infinite multimode coherent state above, we require that

$$\sum_{n=1}^{\infty} |\alpha_n|^2 < \infty \tag{3.43}$$

which means that modes with higher momenta have suppressed coherent amplitude. Here we will not employ the infinite multimode coherent state, and instead focus specifically on the more realistic single-mode coherent state as is used in quantum optics. The Wightman

function for the coherent state reads

$$\begin{aligned} W(\mathsf{x},\mathsf{x}') &= \langle 0|\hat{D}^{\dagger}_{\alpha(n)}\phi(\mathsf{x})\phi(\mathsf{x}')\hat{D}_{\alpha(n)}|0\rangle \\ &= \sum_{n=1}^{\infty} u_n(\mathsf{x})u_n^*(\mathsf{x}') + \sum_{n=1}^{\infty}\sum_{j=1}^{\infty}\alpha_n^*\alpha_j u_j(\mathsf{x})u_n^*(\mathsf{x}') + \sum_{n=1}^{\infty}\sum_{j=1}^{\infty}\alpha_n\alpha_j^* u_j^*(\mathsf{x})u_n(\mathsf{x}') \\ &\quad + \sum_{n=1}^{\infty}\sum_{j=1}^{\infty}\alpha_n\alpha_j u_j(\mathsf{x})u_n(\mathsf{x}') + \sum_{n=1}^{\infty}\sum_{j=1}^{\infty}\alpha_n^*\alpha_j^* u_j^*(\mathsf{x})u_n^*(\mathsf{x}')\,. \end{aligned} \tag{3.44}$$

Similar to the single-mode excited Fock state, the vacuum contribution to the Wightman function does not vanish. If we define the one-point function of the coherent state as

$$J(\mathsf{x}) := \langle\alpha(n)|\phi(\mathsf{x})|\alpha(n)\rangle = \sum_n \alpha_n u_n(\mathsf{x})\,, \tag{3.45}$$

we can compactly write the full Wightman function as

$$\begin{aligned} W(\mathsf{x},\mathsf{x}') &= W_0(\mathsf{x},\mathsf{x}') + J(\mathsf{x})J(\mathsf{x}') + J(\mathsf{x})J^*(\mathsf{x}') \\ &\quad + J^*(\mathsf{x})J(\mathsf{x}') + J^*(\mathsf{x})J^*(\mathsf{x}') \\ &:= W_0(\mathsf{x},\mathsf{x}') + W_c(\mathsf{x},\mathsf{x}')\,, \\ W_c(\mathsf{x},\mathsf{x}') &= 4\mathrm{Re}[J(\mathsf{x})]\mathrm{Re}[J(\mathsf{x}')]\,. \end{aligned} \tag{3.46}$$

The fact that $W_c(\mathsf{x},\mathsf{x}')$ factorizes into product of one-point functions allow us to simplify the expression for the transition probability. The transition probability due to the purely coherent part (i.e. modulo the vacuum contribution $W_0(\mathsf{x},\mathsf{x}')$) then reads

$$\begin{aligned} P_c(\Omega) &= \lambda^2\int \mathrm{d}\tau\,\mathrm{d}\tau'\chi(\tau)\chi(\tau')e^{-i\Omega(\tau-\tau')}W_c(\tau,\tau') \\ &= 4\lambda^2\left|\int \mathrm{d}\tau\chi(\tau)e^{-i\Omega\tau}\mathrm{Re}[J(\mathsf{x}(\tau))]\right|^2\,. \end{aligned} \tag{3.47}$$

With a judicious choice of $\{\alpha_n\}$, it may be possible to perform the infinite sum in $J(\tau)$ exactly. Before we proceed, it is worth noting that resonant behaviour similar to that of the previous section is expected, since the real part of $J(\tau)$ contains $\cos\omega_n t(\tau)$ term which produces co-rotating term when combined with the exponential of the gap $e^{-i\Omega\tau}$.

For single-mode coherent state, there is no real restriction on the coherent amplitude;

we obtain

$$J(\mathsf{x}) = \delta_{mn} \sum_n \alpha_n u_n(\mathsf{x}) \,, \tag{3.48}$$

where m-th mode is to be the coherent state and the rest are all vacuum modes. For simplicity we can consider, for example, $m/L = 2$ and restrict $\alpha \in \mathbb{R}$ (though α can be arbitrary complex number).

We illustrate the case when the second mode $k = 2/L$ is in a coherent state with coherent amplitude $\alpha_2 = 1$ while others are in the vacuum state, shown in Figure 3.9. We also intentionally adjust the energy gap of the detector so that $\Omega = 1.9\omega_n$, which is different for massless and massive fields. This comparison can be thought of as making the comparison somewhat fairer since the amount by which the atom is off-resonant from the mode frequency is of the same weight. We see that even with massive fields, the overall behaviour remains unchanged and as expected, the transition amplitude degrades with larger mass. While we do not probe extremely non-relativistic regimes due to computational resources, it is clear that the role of mass is vanishingly small for smaller acceleration. We have ignored the vacuum contribution because we have chosen the value of Ω such that the vacuum contribution is negligible compared to the contribution due to the excited field state and we had shown previously that vacuum states are not sensitive to local accelerations.

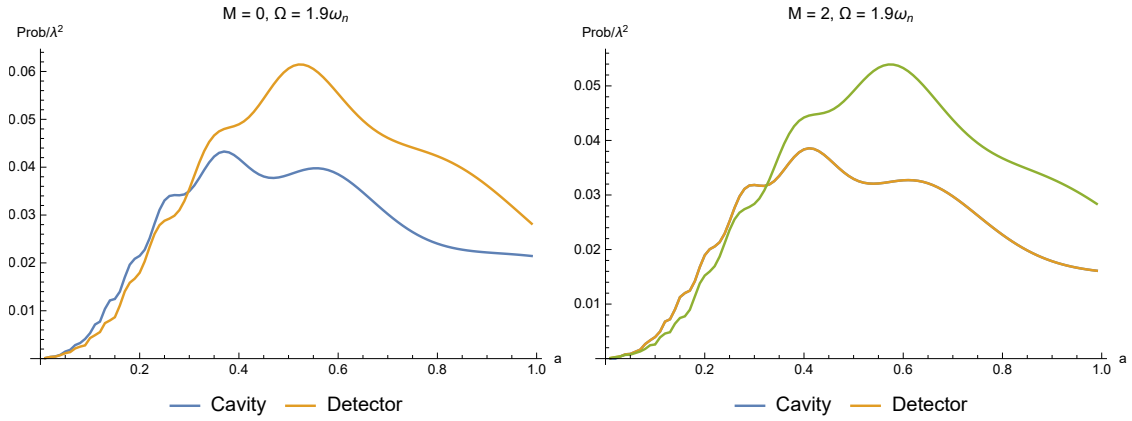

Figure 3.9: Transition probability (modulo the vacuum contribution) for an accelerating detector and an accelerating cavity for two different masses when the second mode ($k = 2/L$) is in coherent state and other modes are in vacuum state.

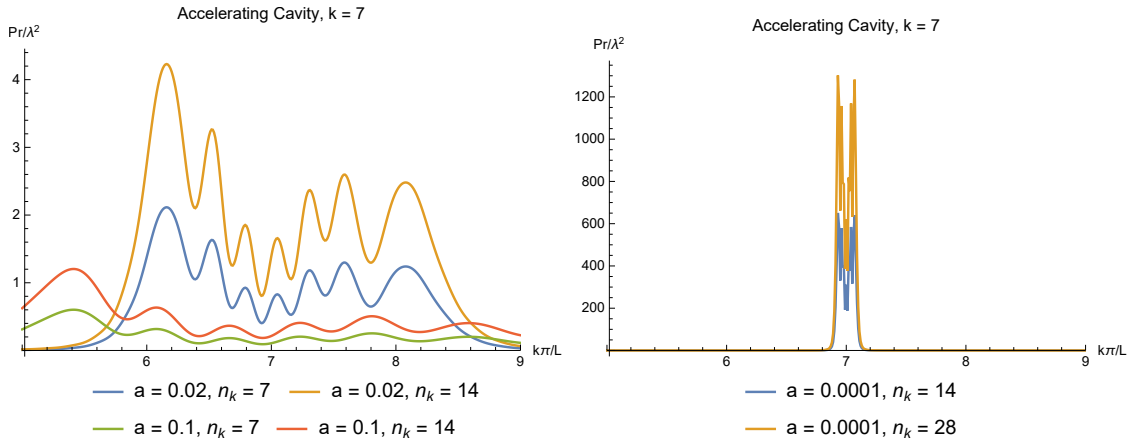

Figure 3.10: Transition probability for fixed acceleration as a function of energy gap $\Omega = k\pi/L$ where n_k is the number of excitations of the massless field in mode k, with $L = 1$.

3.4.3 Resonance

The resonance phenomenon, while not very exact due to accelerated motion of the detector or cavity, can be made manifest if we study the "resonance peak" of the detector. The resonance peak for the case of the field in a Fock state $|n_k\rangle$ is shown in Figure 3.10. Recall that in this notation, it is the k-th momentum having n_k excitations: if field is in the seventh excited state with 20 excitations, then we write $|20_7\rangle$.

From Figure 3.10 we observe that for large acceleration there is a larger Doppler shift, which smears out resonance and damps out transition probability. The number of resonance peaks matches the mode number k that defines the excited state of the field. As the acceleration decreases, the resonance peaks becomes narrower and higher, indicating that we approach resonance in static inertial scenario. Figure 3.10 also shows that resonance dominates when

$$\Omega\tau \approx \lim_{a\to 0} \omega_k t(\tau)\,, \tag{3.49}$$

where $t(\tau)$ is the pullback of the coordinate time in terms of proper time τ of the detector. Crucially, the rough estimate of the right hand side gives

$$\omega_k t(\tau) \approx \frac{k\pi}{aL}\left(a\tau + O(a^3\tau^3)\right) \sim \frac{k\pi\tau}{L} + O(a^3\tau^3)\,, \tag{3.50}$$

which is to first order the same as the case for static detector and static cavity.

We remark that near resonance $\Omega - \omega_k \approx 0$, Figure 3.10 seems to indicate that the probability amplitude may be divergent if aL is small enough, potentially breaking the perturbative calculation. We expect this to be an artefact of the approximations in the whole setup, including perturbative calculations of transition probability. As an example of such an artefact, note that in Eq. (3.35) the transition probability scales linearly with n_k (this also appears in [2]). Clearly, this cannot be valid for arbitrary n_k since for large enough excitations, the probability can be made greater than 1. These may be cancelled by higher order terms which would also contain co-rotating terms. Also, recall that since our detector starts from one end of the cavity, in the limit where $a = 0$ we should expect *no excitation* at all due to Dirichlet boundary condition given the choice of coupling. This suggests that for computations involving non-vacuum contributions and co-rotating terms, one should be careful in extrapolating results.

Nonetheless, our results so far do not change even if we stay away from the $\Omega \approx \omega_k$ limit (cf. Figure 3.9), since all that the resonance condition and large n_k limit do is allow us to ignore vacuum contributions from $W_0(\tau, \tau')$ by amplifying the non-vacuum contributions. Even if the excited parts W_{exc}, W_c of the Wightman function are smaller than W_0, we could simply subtract off the W_0 part since we find a negligible difference between the responses in Experiment 1 and Experiment 2.

As a side remark, we also checked whether some details arise if we compute instead the *transition rate* instead of transition probability, since it may be the case that transition probability (which can be thought of as integral of the transition rate) may average out some important information. We discuss these briefly in Appendix B.4. The answer is that transition rate sees nothing particularly different between massless and massive fields.

3.5 Discussion

With hindsight we should not be surprised by these results, since they are basically an Unruh-type setup confined to cavity. As clarified in [1], what is important in these WEP considerations is really the fact that there is *relative acceleration* between the atom and the cavity. In the slow acceleration limit, every point in the cavity can be approximated to have the same constant proper acceleration (hence the same clock ticking rates) and so an accelerating cavity-static detector and an accelerating detector-static cavity should lead to the same physical results. The mass parameter of the scalar field enters the quantum field via the mode frequency and amplitude, which generally degrades response since the integral over Wightman function is more oscillatory and the normalization for each mode is smaller than those for a massless field. In this respect, if a 'fair' comparison is made

between the massless and massive cases (e.g. adjusting Ω/ω_k or $|\Omega - \omega_k|$ instead of fixing Ω, cf. Section 3.4), the massless field should lead to larger detector responses because mass suppresses nonlocal correlations. Note that this suppression is *independent* of WEP.

Why would the responses be different at large a? As argued in the context of mirrors [1], the accelerating cavity-static detector and the accelerating detector-static cavity setups are also not mathematically equivalent: if our experiments are sensitive enough to non-uniformity of acceleration across the cavity, then the notion of "relative acceleration" becomes blurred. For an accelerating detector, in the cavity frame one observes that the detector has a constant-acceleration trajectory; for an accelerating cavity, in the cavity frame observes that the detector is not uniformly accelerating because its worldline crosses all the hypersurfaces of constant ξ between one cavity wall $\xi = \xi_2$ to another $\xi = \xi_1$. In the slow acceleration limit, these constant-ξ surfaces describe approximately the same acceleration and hence the detector is observed to be approximately uniformly accelerating. We can think of the correlation functions of the field as capturing this non-local difference and the inequivalent setups lead to unequal responses. It is in this spirit that WEP makes sense — the responses between the free-falling cavity-stationary detector and free-falling detector-stationary cavity will be different once the non-uniformity of the gravitational field is detectable.

Finally, a small qualification about the comparison between the two different scenarios (accelerating detector and accelerating cavity) is in order. There are a couple of ways in which the two scenarios can be argued not to be on equal footing, First, we note that in relativity there is no absolute rigidity [74–76]; it is impossible to maintain fixed coordinate distance between two cavity walls in *all frames*. Accelerating the cavity whilst keeping it rigid in the cavity rest frame (Fermi-Walker rigidity) is the simplest and most natural setup. The fact that for accelerating cavities the detector is seen to be non-uniformly accelerating from the cavity's frame, is sufficient to show that the detector response should be different from the constantly accelerating detector scenario.

There is one possible alternative interpretation for the lack of equivalence between the two scenarios: The accelerating cavity is a setup of accelerating mirrors, which are perfectly reflecting boundary conditions, whereas an accelerating detector is a quantum object that can absorb, transmit and reflect parts of an illuminating plane wave. Consequently, they constitute rather distinct field configurations (e.g., dynamical Casimir effect and Unruh radiation respectively) and the two setups are not identical beyond the 'non-uniformity' of the acceleration. This interpretation is likely to be relevant when we consider the "energy" cost of carrying out the acceleration, since different amount of effort is likely to be required

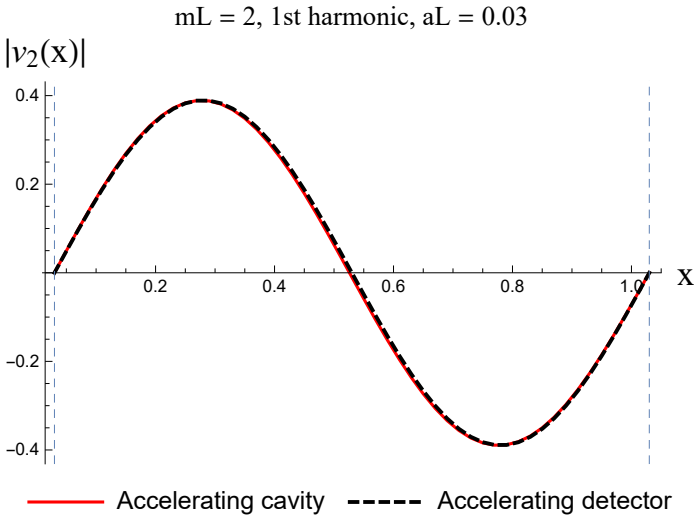

Figure 3.11: The amplitude of the first harmonic for $mL = 2$. It is clear that the accelerating detector and accelerating cavity scenario have practically indistinguishable mode function even for $aL \sim 0.03$, not yet a highly non-relativistic regime. Since distinguishability rests solely on the field modes being different, this shows that massive fields cannot do better than massless one.

to accelerate perfectly reflecting cavity and a transmissive detector[7]. In this setup, since the trajectories are fixed from the outset, only relative motion matters and hence any distinction must come from non-uniformity of acceleration. If so, then it is likely that in the deep non-relativistic regime, *both* massless and massive fields *cannot* distinguish local accelerations, a conclusion that [1] supports.

We can make this argument even more explicit. Suppose we choose to take the quasilocal regime and non-relativistic regime. Then, we effectively disregard variations of acceleration across the cavity, similar to how we disregard spacetime curvature ('spacetime is locally flat'). For WEP to hold, it must mean that both massless and massive cases are equally bad at distinguishing *relative local acceleration*. For massless case, it is easy: we perform Taylor series expansion in acceleration $a\tau \in [0, a\tau_{\max}]$ and show that the transition probability in Eq. (3.23) and Eq. (3.14) are equal. In this sense, the claim of [2] is correct: massless fields are not able to distinguish relative local accelerations, however conformal invariance is really just the 'easy' way to show it (the hard way would be the way done in Appendix B.1).

[7]This conclusion is somewhat different from the one given in the paper [64] which this chapter was based, after some additional thoughts during the writing of this thesis.

For massive case, we cannot do this analytically but there is actually a simple numerical check, as exemplified in Figure 3.11. Here we compare the first harmonic of the field mode for $mL = 2$, and it is easy to see that *with proper normalization* (which we believe is not done in [2], cf. Appendix B.2), accelerating cavity and accelerating detector scenarios have practically identical mode function, and this is not even highly non-relativistic ($aL \sim 0.03$). Since for arbitrary state of the field the local distinguishability via detector responses depends on the mode function, the fact that the mode functions are indistinguishable in non-relativistic limit must imply that massive fields cannot be used for distinguishing relative local acceleration either, contrary to the claim [2].

3.6 Conclusion

We have investigated a quantum version of the WEP in which we consider the response of a particle detector in two scenarios: a) a detector accelerating in a static cavity and b) a static detector in an accelerating cavity. We found that the qualitative WEP is indeed satisfied insofar as quasilocal approximations are valid. We do this by investigating the transition probability of a two-level atomic detector on various field states, namely vacuum state (Minkowski-like and Rindler-like vacuum), arbitrary Fock state, and single-mode coherent state. We also check the effect of bringing the atomic gap closer to the resonant frequency when we have co-rotating terms and clarify the validity of some approximations such as large n_k limit for Fock state of the field. We believe that these results support that WEP holds in semiclassical settings; in this sense, our results complement those of [1, 72].

Chapter 4

Zero mode and superluminal signalling

In this chapter we turn to Unruh-DeWitt detectors coupled to a scalar field in the presence of periodic and Neumann boundary conditions. With these boundary conditions, the so-called *zero mode* — an oscillator with vanishing frequency — appears. We investigate the impact of this mode to particle detector phenomenology. We show that in the relativistic regime, the zero mode has direct consequence on causality, namely it may lead to superluminal signalling if the zero mode is not treated properly.

4.1 Motivation

In applied settings such as in solid state physics and quantum optics, the spatial topology of the setup is something that can be given by the particular experimental setup. For example, one can have an optical fibre coiled around itself to have periodic boundary conditions in one dimension. Hence, it is natural to ask what the role of boundary conditions have in modeling the light-matter interaction, and whether assuming simpler models could lead to faster-than-light signalling between spacelike separated operators of particle detectors. For instance, it has been recently studied how factors such as the detector smearing, rotating-wave approximations or the introduction of UV regularization have implications on causality in particle detector models [57].

It is known that in $(1+1)$ dimensional flat spacetime, a scalar field subjected to periodic boundary conditions has a zero mode which contributes to a particle detector's

response, the field's stress-energy tensor, and the ability for particle detectors to get entangled through the field [54, 83]. Zero modes also appear in other contexts such as two-dimensional conformal field theories (CFTs) and in the minimal coupling of massless scalar field in certain spacetimes with nontrivial compact topology [84–88], where regularization schemes for the Wightman function have impacts on the zero modes. However, the zero mode is peculiar as compared to the regular oscillator modes since it does not admit a Fock space representation. For this reason, it is perhaps desirable to be able to ignore or remove the zero mode from any calculation by hand. In some contexts, such as the UDW model coupled via derivative coupling, its effect can indeed be made negligible at the level of detector responses in appropriate limits [83], but in some other contexts it has significant impact on detector dynamics and entanglement [54, 83, 89, 90]. There are also cases when the zero mode has been excluded by assumption from a setup with periodic boundary conditions (e.g., in [91–95]), thus it is of interest to further study the impact of the zero mode may have on the relativistic nature of the interaction within particle detector model.

Here we will investigate how neglecting the zero mode of a massless scalar field can lead to faster-than-light signalling between particle detectors via violations of microcausality[1]. We will show how two particle detectors coupled locally to the field can non-negligibly communicate faster than light when the zero mode is neglected. As a consequence, we show that whenever a zero mode arises, one cannot remove it by hand and only consider the oscillator part if relativistic phenomenology is important in the setup under study. We will also show how this zero mode-induced causality violation is alleviated in higher dimensions. In this paper, we first study the causality with respect to zero mode in $(1+1)$ and $(2+1)$ dimensions and then make an argument for arbitrary dimensions.

The chapter is organized as follows. In Section 4.2 we briefly review the UDW model and the notion of signalling estimator, and its relation to microcausality. In Section 4.3 we study microcausality in $(1+1)$ dimensions. In Section 4.4 we study several cases in $(2+1)$ dimensions for different choices of spatial section topology. In Section 4.5 we briefly discuss the general case in arbitrary dimensions.

4.2 How do we evaluate causality?

When microcausality is violated, the commutator between two observables at two spacelike separated events may no longer be zero. This in turn can be used to perform faster-than-

[1]Note that in the context of algebraic quantum field theory (AQFT), sometimes this is known (modulo some technical subtleties) as a version of *locality* [81, 88].

light signalling with particle detectors. To make this idea precise in an operational manner we follow [57] and we consider two observers Alice and Bob who are spacelike separated, each carrying a particle detector that can interact with the field locally. We model these detectors using a pair of Unruh-DeWitt detectors consisting of two-level quantum systems (qubits). The monopole moment of each detector in the interaction picture is given by

$$\hat{\mu}_\nu(\tau) = \hat{\sigma}_\nu^+ e^{i\Omega_\nu \tau} + \hat{\sigma}_\nu^- e^{-i\Omega_\nu \tau} \tag{4.1}$$

where $\nu = \{\text{A}, \text{B}\}$ denotes Alice or Bob respectively. Here we have $\hat{\sigma}_\nu^+ = |e_\nu\rangle\langle g_\nu|$, $\hat{\sigma}_\nu^- = |g_\nu\rangle\langle e_\nu|$ are the usual $\mathfrak{su}(2)$ ladder operators, $|g_\nu\rangle, |e_\nu\rangle$ are the ground and excited states of the qubit, Ω_ν is the gap of the qubit and τ is the proper time of the the qubits. Since we are in flat space, the proper time for both detectors will be the same.

The linear UDW model prescribes the following interaction between the field and a stationary detector [42] (cf. Chapter 2)

$$\hat{H}_\nu = \lambda_\nu \chi_\nu(t) \hat{\mu}_\nu(t) \int \mathrm{d}^n \boldsymbol{x}\, F_\nu(\boldsymbol{x} - \boldsymbol{x}_\nu) \hat{\phi}(t, \boldsymbol{x}) \,, \tag{4.2}$$

where $F(\boldsymbol{x} - \boldsymbol{x}_\nu)$ is the spatial smearing of the detector ν, centred at $\boldsymbol{x}_\nu$, $\chi_\nu(t)$ is the switching function of the detector, and λ_ν is the coupling strength. We can assume that the Hamiltonians generate translations with respect to the same time parameter for both detectors assuming they are at rest relative to each other and also relative to the lab frame where the field quantization is performed.

The full interaction Hamiltonian for the field and the two detectors is given by

$$\hat{H}_I(t) = \hat{H}_\text{A}(t) + \hat{H}_\text{B}(t) \,. \tag{4.3}$$

We assume that the system is initialized in the completely uncorrelated state

$$\hat{\rho}_0 = \hat{\rho}_\text{A} \otimes \hat{\rho}_\text{B} \otimes \hat{\rho}_{\hat{\phi}} \tag{4.4}$$

where $\hat{\rho}_\phi$ is an arbitrary field state, which in the presence of a zero mode we can split as $\hat{\rho}_{\hat{\phi}} = \hat{\rho}_\text{osc} \otimes \hat{\rho}_\text{zm}$ where $\hat{\rho}_\text{osc}$ is the state of all the modes that admit a Fock quantization and $\hat{\rho}_\text{zm}$ is the state of the zero mode. The state $\hat{\rho}_\text{A} \otimes \hat{\rho}_\text{B}$ is the most general product state of both detectors, which in a matrix representation in the basis

$$|e\rangle = \begin{pmatrix} 1 \\ 0 \end{pmatrix} \,, \quad |g\rangle = \begin{pmatrix} 0 \\ 1 \end{pmatrix} \tag{4.5}$$

reads

$$\hat{\rho}_{\mathrm{A}} \otimes \hat{\rho}_{\mathrm{B}} = \begin{pmatrix} \alpha_{\mathrm{A}} & \beta_{\mathrm{A}} \\ \beta_{\mathrm{A}}^* & 1-\alpha_{\mathrm{A}} \end{pmatrix} \otimes \begin{pmatrix} \alpha_{\mathrm{B}} & \beta_{\mathrm{B}} \\ \beta_{\mathrm{B}}^* & 1-\alpha_{\mathrm{B}} \end{pmatrix} . \tag{4.6}$$

where $\alpha_\nu \in \mathbb{R}$.

Notice that while there is an ambiguity to choose the physically meaningful state for a zero mode, all the results in this paper are independent of the state of the field, therefore we do not need to concern ourselves with discussing what would be a reasonable state for the field in general and in particular for the zero mode as long as the expectation values of the field commutators are well defined.

The state evolves as

$$\hat{\rho} = \hat{U}\hat{\rho}_0\hat{U}^\dagger \,, \tag{4.7}$$

where the time evolution operator is

$$\hat{U} = \mathcal{T} \exp\left(-\mathrm{i}\int_{-\infty}^{\infty} \mathrm{d}t\, \hat{H}_I(t)\right) \tag{4.8}$$

and $\mathcal{T}$ denotes time-ordering. The time evolution can be found perturbatively order-by-order in the coupling strengths λ_ν. The final state of the two-detector subsystem is then given by the reduced joint density matrix

$$\hat{\rho}_{\mathrm{AB}} = \mathrm{tr}_{\hat{\phi}}\, \hat{\rho} = \hat{\rho}_{\mathrm{AB},0} + \hat{\rho}^{(1)}_{\mathrm{AB}} + \hat{\rho}^{(2)}_{\mathrm{AB}} + O(\lambda^3) \,, \tag{4.9}$$

where the superscript (j) denotes the contribution to the time-evolved density matrix of order λ^j.

In order to see how signalling using particle detectors is connected to microcausality, we first note that any contributions linear in λ_{A} or λ_{B} are local, thus $\hat{\rho}^{(1)}$ cannot contribute to signalling. The signalling part of the detectors' density matrix $\hat{\rho}_{\mathrm{AB}}$ must be of second order in the product of coupling strengths $\lambda_{\mathrm{A}}\lambda_{\mathrm{B}}$ [57]. Therefore, we can split the second order term into three parts, namely

$$\hat{\rho}^{(2)}_{\mathrm{AB}} = \hat{\rho}^{(2)}_{\mathrm{AB,signal}} + \hat{\rho}^{(2)}_{\mathrm{A,noise}} + \hat{\rho}^{(2)}_{\mathrm{B,noise}} \,. \tag{4.10}$$

The last two terms are of the order λ_{A}^2 and λ_{B}^2 respectively, hence they are local noise terms that do not contribute to signalling between the two detectors. The first term is the signalling term, which is of the order $\lambda_{\mathrm{A}}\lambda_{\mathrm{B}}$. This can also be seen by finding the reduced

state of detector B alone and only the signalling term will survive:

$$\hat{\rho}_{\mathrm{B,signal}} = \mathrm{tr}_{\mathrm{A}}\left(\hat{\rho}^{(2)}_{\mathrm{AB,signal}}\right) . \tag{4.11}$$

In order to cleanly separate effect of zero mode on microcausality from the smearing and switching effects, we consider both compactly supported smearing and switching function. That is,

$$\begin{aligned} \mathrm{supp}[\chi_\nu(t)] &= \left[T^{\mathrm{on}}_\nu, T^{\mathrm{off}}_\nu\right] , \\ \mathrm{supp}[F(\boldsymbol{x}-\boldsymbol{x}_\nu)] &= \left[\boldsymbol{x}_\nu - \frac{\sigma}{2}, \boldsymbol{x}_\nu + \frac{\sigma}{2}\right] , \end{aligned} \tag{4.12}$$

where σ is the width of the spatial smearing (i.e. an effective detector diameter). We require that these supports do not overlap, i.e.

$$\begin{aligned} T^{\mathrm{off}}_{\mathrm{A}} &< T^{\mathrm{on}}_{\mathrm{B}} , \\ \boldsymbol{x}_{\mathrm{A}} + \frac{\sigma}{2} &< \boldsymbol{x}_{\mathrm{B}} - \frac{\sigma}{2} . \end{aligned} \tag{4.13}$$

Under these conditions, it can be shown that

$$\begin{aligned} \hat{\rho}^{(2)}_{\mathrm{B,signal}} = 2\int_{\mathbb{R}} \mathrm{d}t \int_{\mathbb{R}} \mathrm{d}t' \chi_{\mathrm{A}}(t)\chi_{\mathrm{B}}(t')\mathrm{Re}\left(\beta_{\mathrm{A}} e^{\mathrm{i}\Omega_{\mathrm{A}}t}\right)\mathcal{C}(\mathsf{x}_{\mathrm{A}},\mathsf{x}'_{\mathrm{B}}) \\ \begin{pmatrix} -2\mathrm{Im}(\beta_{\mathrm{B}} e^{\mathrm{i}\Omega_{\mathrm{B}}t'}) & -\mathrm{i}e^{-\mathrm{i}\Omega_{\mathrm{B}}t'}(1-2\alpha_{\mathrm{B}}) \\ \mathrm{i}e^{-\mathrm{i}\Omega_{\mathrm{B}}t'}(1-2\alpha_{\mathrm{B}}) & 2\mathrm{Im}(\beta_{\mathrm{B}} e^{\mathrm{i}\Omega_{\mathrm{B}}t'}) \end{pmatrix} . \end{aligned} \tag{4.14}$$

The function $\mathcal{C}(\mathsf{x}_{\mathrm{A}},\mathsf{x}_{\mathrm{B}}) \equiv \mathcal{C}(t,\boldsymbol{x}_{\mathrm{A}},t',\boldsymbol{x}_{\mathrm{B}})$ in the integrand is the spatially smeared pull-back of the field commutator, as shown in detail in [57]:

$$\mathcal{C}(t,\boldsymbol{x}_{\mathrm{A}},t',\boldsymbol{x}_{\mathrm{B}}) := \int_{\mathbb{R}^n} \mathrm{d}^n\boldsymbol{x} \int_{\mathbb{R}^n} \mathrm{d}^n\boldsymbol{x}' F_{\mathrm{A}}(\boldsymbol{x}-\boldsymbol{x}_{\mathrm{A}}) F_{\mathrm{B}}(\boldsymbol{x}'-\boldsymbol{x}_{\mathrm{B}}) \left\langle[\phi(t,\boldsymbol{x}),\phi(t',\boldsymbol{x}')]\right\rangle , \tag{4.15}$$

where $\boldsymbol{x}_j$ are the centres of mass of the smearings of the detectors used to probe causality. To estimate the ability of A and B to perform faster-than-light signalling we analyze the causality estimator $\mathcal{E}$ proposed in [57], which is proportional to the signal strength of the contributions to the density matrix of detector B coming from the presence of detector A:

$$\mathcal{E}(\boldsymbol{x}_{\mathrm{A}},\boldsymbol{x}_{\mathrm{B}}) := \left| \int_{\mathbb{R}} \mathrm{d}t \int_{\mathbb{R}} \mathrm{d}t' \, \chi_{\mathrm{A}}(t)\chi_{\mathrm{B}}(t')\mathcal{C}(t,\boldsymbol{x}_{\mathrm{A}},t',\boldsymbol{x}_{\mathrm{B}}) \right| . \tag{4.16}$$

Furthermore, it has been shown that channel capacity, measured by a lower bound to the

number of bits per unit time that can be sent from Alice to Bob, is directly related to $\mathcal{E}$ [96, 97].

Notice that one can also particularize to a delta switching (that can be understood as the limit of very short time Gaussian switching when the total strength of the interaction over time is fixed, see, e.g., [98]). In the case of this instantaneous switching, the reduced density matrix of detector B will simply be proportional to $\mathcal{C}$, thus this function is a legitimate measure of signalling between detectors. For this reason we will make use of both $\mathcal{E}$ and $\mathcal{C}$ as causality estimators in the subsequent sections.

4.3 Causality and zero mode in (1+1) dimensions

We consider massless scalar field on the Einstein cylinder with the metric [3]

$$\mathrm{d}s^2 = -\mathrm{d}t^2 + \mathrm{d}x^2 \,, \tag{4.17}$$

where the spacetime has topology $\mathbb{R} \times S^1$. The topological identification is made for $x \sim x + L$, where L is the circumference of the cylinder. This is the same as having a periodic cavity in $(1+1)$ dimensions, i.e. implementing periodic boundary condition for the scalar field in Minkowski spacetime. The field operator can be decomposed into two parts, namely

$$\hat{\phi}(t,x) = \hat{\phi}_{\mathrm{zm}}(t) + \hat{\phi}_{\mathrm{osc}}(t,x) \,. \tag{4.18}$$

The first term $\hat{\phi}_0$ is the *zero mode* term which is spatially constant. The spatially constant nature can be understood from the standard Fourier series: the zero mode corresponds to the constant c_0 term in complex Fourier series expansion [99]. The second term $\hat{\phi}_{\mathrm{osc}}(t,\boldsymbol{x})$ is the harmonic oscillator term whose mode decomposition reads

$$\hat{\phi}_{\mathrm{osc}}(t,x) = \sum_{n\neq 0} \frac{1}{\sqrt{4\pi\,|n|}} \left[e^{-\mathrm{i}|k_n|t + \mathrm{i}k_n x} \hat{a}_n + \mathrm{h.c.} \right] , \qquad k_n = \frac{2\pi n}{L} \,, n \in \mathbb{Z} \setminus \{0\} \,. \tag{4.19}$$

The oscillator modes have a Fock vacuum $|0\rangle$ defined by $\hat{a}_n |0\rangle = 0$ for all $n \in \mathbb{Z} \setminus \{0\}$ and the usual canonical commutation relation for the ladder operators $[\hat{a}_j, \hat{a}_k^\dagger] = \delta_{jk}$.

Note that the zero mode behaves as a "free-particle": specifically, the Lagrangian only contains the kinetic part [83, 84]

$$\mathcal{L}_{\mathrm{zm}} = \frac{L\dot{Q}^2}{2} \,, \tag{4.20}$$

where $Q := \tilde{\phi}_0$ is the Fourier component of the zero mode. We can think of this as an "oscillator" with zero frequency, since after a Legendre transformation the zero-mode free Hamiltonian (after quantization) is given by:

$$\hat{H}_{\rm zm} = \frac{\hat{P}^2}{2L}\,, \quad P = \frac{\partial \mathcal{L}_{\rm zm}}{\partial \dot{Q}}\,. \tag{4.21}$$

In the interaction picture, we have that

$$\hat{Q}(t) = \hat{Q}_S + \frac{\hat{P}_S t}{L} \tag{4.22}$$

where the subscript S means Schrödinger picture operator. The Heisenberg equation of motion then implies that

$$\hat{\phi}_{\rm ZM}(t) = \hat{Q}(t) = \hat{\phi}_{\rm ZM}(0) + \frac{\hat{P}_S t}{L}\,. \tag{4.23}$$

The field commutator can be written as the sum of the commutator for the oscillator modes and the zero mode,

$$[\hat{\phi}(\mathsf{x}), \hat{\phi}(\mathsf{x}')] = [\hat{\phi}_{\rm zm}(t), \hat{\phi}_{\rm zm}(t')] + [\hat{\phi}_{\rm osc}(\mathsf{x}), \hat{\phi}_{\rm osc}(\mathsf{x}')]\,. \tag{4.24}$$

The oscillator contribution to the commutator is given by (see Appendix C.1)

$$\begin{aligned}[\hat{\phi}_{\rm osc}(\mathsf{x}), \hat{\phi}_{\rm osc}(\mathsf{x}')] = &-\frac{1}{4\pi}\log\left(1 - e^{-\frac{2i\pi(\Delta u - i\epsilon)}{L}}\right) - \frac{1}{4\pi}\log\left(1 - e^{-\frac{2i\pi(\Delta v - i\epsilon)}{L}}\right) \\ &+ \frac{1}{4\pi}\log\left(1 - e^{\frac{2i\pi(\Delta u - i\epsilon)}{L}}\right) + \frac{1}{4\pi}\log\left(1 - e^{\frac{2i\pi(\Delta v - i\epsilon)}{L}}\right)\,,\end{aligned} \tag{4.25}$$

where $u = t - x$ and $v = t + x$ are the double null coordinates in Minkowski space and $\Delta u = u - u'$ and $\Delta v = v - v'$. The commutator due to the zero mode reads [83]

$$[\hat{\phi}_{\rm zm}(\mathsf{x}), \hat{\phi}_{\rm zm}(\mathsf{x}')] = -\frac{i\Delta t}{L}\,, \quad \Delta t = t - t'\,. \tag{4.26}$$

Let us now check the causality estimators in $(1+1)$ dimensions. The simplest case is when we take pointlike detectors and instantaneous switching, which reduces the estimators $\mathcal{E}$ to be proportional to $\mathcal{C}$. Note that even if we do not know the ground state for the zero mode, commutator is a c-number so the causality estimator is state-independent.

In general, for a pointlike detector in arbitrary dimensions and delta switching, one can

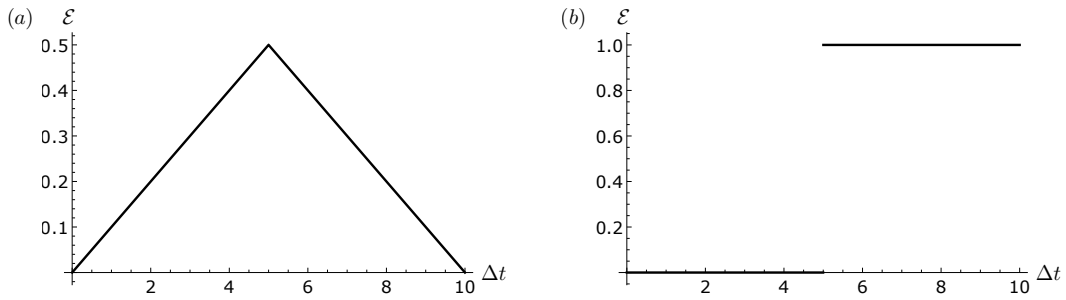

Figure 4.1: Causality estimator for delta switching and pointlike detector, with $\Delta x = 5$ in natural units. **(a):** excluding the zero mode. The commutator does not vanish even for spacelike separated regions. **(b):** including the zero mode. Microcausality is recovered as commutator vanishes identically for $|\Delta t| < |\Delta x|$.

run into UV-divergent detector reduced density matrix. However, the causality estimator is UV-safe and does not have such problems even in the limiting cases where UV-divergences may appear [100, 101]. Note as well that we can always avoid this problem by not taking both limits (infinitely fast switching and pointlike smearing) simultaneously.

In Figure 4.1(a) we show the causality estimator (4.16) for a delta switching and pointlike detectors for $L = 10$, $\Delta x = 5$ (that is, the separation between the detectors so that $\Delta t < 5$ corresponds to spacelike separation). The figure demonstrates causality violation when one removes the zero mode contribution. The causality violation coming from ignoring the zero mode is very strong as it can be seen in the figure. The decay of the signalling contributions (thus the decay of the superluminal channel capacity between Alice and Bob) decays only linearly with the distance to the light cone.

When we plot the whole commutator including the zero mode in Figure 4.1(b) we recover the full causal behaviour: the commutator vanishes in the spatial separation domain $\Delta t < 5$. We should also note that in $(1 + 1)$ dimensions we have a violation of *strong Huygens' principle* [97, 100–103], i.e. the support of the commutator is on the whole timelike region bounded by the light cone, and in fact it is constant inside the lightcone.

Note that the zero mode contribution is inversely proportional to L. As one may have expected, the oscillator mode contribution to the commutator dominates at large L and also uniformly becomes microcausal for large L, as shown in Figure 4.2(a). In other words, if the cavity is large, the causality violation is small when one ignores zero mode contribution of the quantum field. Consequently, the usual "toroidal" quantization used e.g. in [3] where one puts a field in a torus and take $L \to \infty$ to reproduce free space

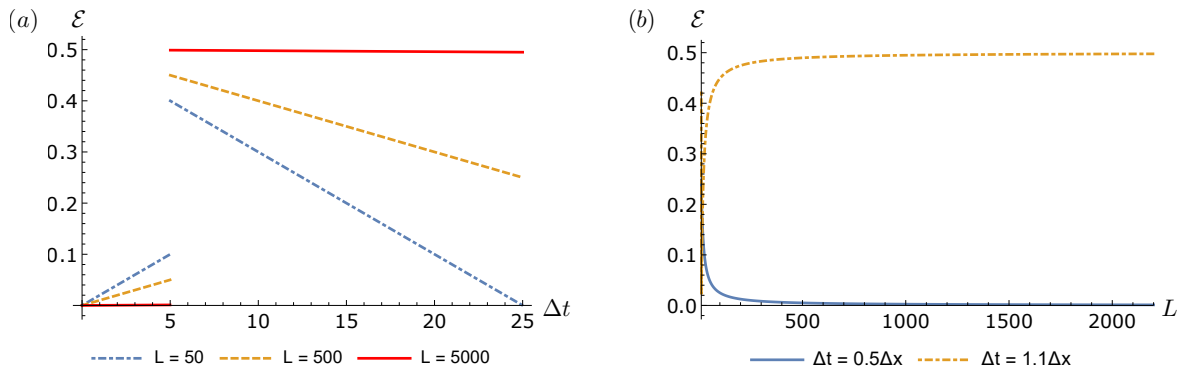

Figure 4.2: **(a):** Causality estimator of the purely oscillator part as a function of time gap between detector switching times Δt for several choices of L. For large L microcausality is approximately recovered. **(b):** Causality estimator of the purely oscillator part as a function of L. We see that the causality estimator falls quickly with increasing L when detectors are spacelike separated and quickly approaches constant value when timelike separated.

quantization does not suffer causality violation because of the limit taken. However, one has to be careful since the superluminal signaling decays only linearly with the length L, hence the faster-than-light signalling will not be strongly suppressed. This is illustrated in Figure 4.2(b).

In a more general setting, we could consider the presence of compactly supported spatial smearing and switching functions. In Figure 4.3 we show the causality estimator $\mathcal{E}$ when we include the zero mode for various choices of detector size σ and duration of switching δ for each detector. In this plot we used the hard-sphere smearing and finite Heaviside switching of the form

$$\begin{aligned} \chi_\nu(t) &= \begin{cases} 1/\delta & t \in \left[T_\nu^{\text{on}}, T_\nu^{\text{off}}\right] \\ 0 & \text{otherwise} \end{cases}, \\ F_\nu(x - x_\nu) &= \begin{cases} 1/\sigma & x \in \left[\boldsymbol{x}_\nu - \frac{\sigma}{2}, \boldsymbol{x}_\nu + \frac{\sigma}{2}\right] \\ 0 & \text{otherwise} \end{cases} \end{aligned} \tag{4.27}$$

where $\delta := T_\nu^{\text{on}} - T_\nu^{\text{off}}$ is the duration of the switching which we set to be equal for both detectors and σ is the finite size of both detectors. We also fix the time gap between the

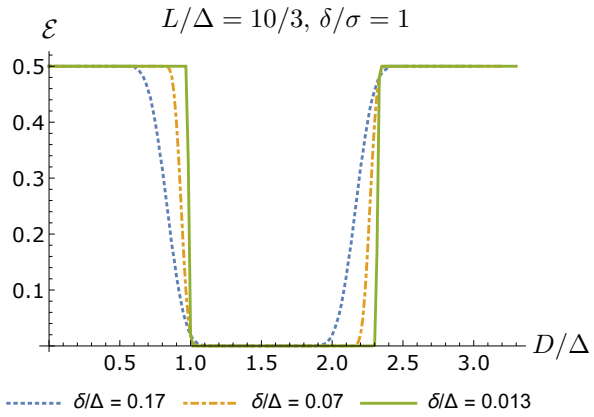

Figure 4.3: Causality estimator $\mathcal{E}$ as a function of outer distance of the finite-sized detectors D for various switching duration δ and size of detector σ. The time gap between the switch-off of detector A and switch-on of detector B is denoted Δ.

two detector's switch-on/off times $\Delta := T_{\rm B}^{\rm on} - T_{\rm A}^{\rm off}$ and D is the surface-to-surface distance between both detectors. We choose $\delta/\sigma = 1$ in all cases but we decrease the value of δ/Δ, which amounts to shorter switching duration *and* smaller detector size. Indeed, we see that the causality estimator approaches the delta switching and pointlike limit. These results also indicate that causality estimator $\mathcal{E}$ is largely independent of the type of switching or smearing functions and mainly dependent on their durations/lengths. Therefore, to discuss causality violations in detector signalling for higher dimensional cases it suffices to focus on the pointlike and fast-switching limits for $\mathcal{E}$.

We also note here that when we impose Neumann boundary condition instead of periodic boundary condition, it will also yield a zero mode. In this case, the spacetime still has the same metric as Minkowski space, but now we consider homogeneous Neumann boundary condition

$$\left.\frac{\partial\hat{\phi}}{\partial x}\right|_{x=0} = \left.\frac{\partial\hat{\phi}}{\partial x}\right|_{x=L} = 0\,. \tag{4.28}$$

The eigenfunctions now take the form

$$u_n(t,x) = N_n \cos\frac{n\pi x}{L} e^{-\mathrm{i}|k_n|t}\,, \qquad n \in \mathbb{N}\cup 0\,. \tag{4.29}$$

The spatially constant solution $u_0(t,x) \equiv u_0(t)$ corresponds to the zero mode. Therefore, the Klein-Gordon inner product only works for $n \in \mathbb{N}$ which gives $N_n = 1/\sqrt{n\pi}$ and the

zero mode $u_n(t,x)$ has to be treated separately. The oscillator part of the commutator now reads (see Appendix C.1)

$$[\hat{\phi}_{\text{osc}}(\mathsf{x})\hat{\phi}_{\text{osc}}(\mathsf{x}')] = \frac{1}{4\pi}\Bigg[\log\left(1-e^{\frac{\mathrm{i}\pi(\Delta u-\mathrm{i}\epsilon)}{L}}\right)+\log\left(1-e^{\frac{\mathrm{i}\pi(\Delta v-\mathrm{i}\epsilon)}{L}}\right) \tag{4.30}$$

$$+\log\left(1-e^{\frac{\mathrm{i}\pi(u-v'-\mathrm{i}\epsilon)}{L}}\right)+\log\left(1-e^{\frac{\mathrm{i}\pi(v-u'-\mathrm{i}\epsilon)}{L}}\right)$$

$$-\log\left(1-e^{-\frac{i\pi(\Delta u-\mathrm{i}\epsilon)}{L}}\right)-\log\left(1-e^{-\frac{i\pi(\Delta v-\mathrm{i}\epsilon)}{L}}\right)$$

$$-\log\left(1-e^{-\frac{i\pi(u-v'-\mathrm{i}\epsilon)}{L}}\right)-\log\left(1-e^{-\frac{i\pi(v-u'-\mathrm{i}\epsilon)}{L}}\right)\Bigg]\,. \tag{4.31}$$

This commutator differs from the case for periodic boundary conditions shown in Eq. (4.25) by a factor of 2 in the momentum k_n and the fact that the commutator is no longer translationally invariant. The zero mode commutator remains the same as before. The estimator $\mathcal{E}$ for Neumann boundary condition will be qualitatively similar to the periodic boundary case shown previously in Figure 4.1, thus we do not repeat the plot for Neumann boundary conditions.

Last but not least, there is an interesting observation we can make regarding the expressions for the commutators: if we invoke the identity

$$\log\frac{(1-e^{\mathrm{i}\phi})(1-e^{\mathrm{i}\psi})}{(1-e^{-\mathrm{i}\phi})(1-e^{-\mathrm{i}\psi})} \equiv \log e^{\mathrm{i}(\phi+\psi)} = i(\phi+\psi)+2\pi\mathrm{i}n\,,\qquad n\in\mathbb{Z}\,, \tag{4.32}$$

the expression seems to simplify considerably. However, one has to be careful with the branch cuts of the logarithm when applying this simplification. When the detectors are spacelike separated we do not cross the branch cut of the of the logarithm when taking its principal branch ($n=0$). In that case, taking the principal branch of the logarithm, the oscillator contribution $[\hat{\phi}_{\text{osc}}(\mathsf{x}),\hat{\phi}_{\text{osc}}(\mathsf{x}')]$ for *both* the periodic and Neumann boundary conditions in Eq. (4.25) and Eq. (4.31) appear to simplify further into

$$[\hat{\phi}_{\text{osc}}(\mathsf{x}),\hat{\phi}_{\text{osc}}(\mathsf{x}')] = \frac{1}{4\pi}\log\left[e^{\frac{4\pi\mathrm{i}(\Delta t-\mathrm{i}\epsilon)}{L}}\right] = \frac{\mathrm{i}\Delta t}{L}+\frac{\epsilon}{L}\,. \tag{4.33}$$

Consequently, by adding Eq. (4.25) or Eq. (4.31) to $[\hat{\phi}_{\text{zm}}(\mathsf{x}),\hat{\phi}_{\text{zm}}(\mathsf{x}')]$, followed by the limit $\epsilon\to 0$, we get the following simple result for for spacelike separated x,x':

$$[\hat{\phi}(\mathsf{x}),\hat{\phi}(\mathsf{x}')] = 0\,, \tag{4.34}$$

as it should be if microcausality is not violated.

However, there are some subtleties associated with the above simplifications. For one, the identity seems to hide the role of spatial separation Δx because only Δt appears in the expression for $[\hat{\phi}_{\text{osc}}(\mathsf{x}), \hat{\phi}_{\text{osc}}(\mathsf{x}')]$ in Eq. (4.33). It turns out that depending on the values of t, t', x, x', we may cross branch cuts and the terms in the commutator may refer to different branches of the logarithm. For arbitrary separation, from Eq. (4.32) the simplification reads

$$[\hat{\phi}(\mathsf{x}), \hat{\phi}(\mathsf{x}')] = \frac{n}{2}\,, \qquad n \in \mathbb{Z}\,. \tag{4.35}$$

Here n refers to different branches of the full simplified logarithm in Eq. (4.33) which depends on t, t', x, x' in nontrivial manner. The timelike separated case as shown in Figure 4.1(b) is in fact the $n = 2$ branch. For arbitrary values of x, x', t, t' the value of n will depend on how many logarithms in the sums in Eq. (4.25) and (4.31) cross branch cuts for the value of the parameters. The consequent piecewise simplification of the zero-mode commutator would in general be cumbersome so we only included it in detail for the spacelike case which is the one we focus on to study causality.

As a side remark, it has been argued that microcausality as we describe here is in fact a property of causal structure of *classical* theory rather than Lorentz invariance, since Lorentz invariance is manifestly broken in generic curved spacetimes [104]. This suggests that our results should hold even for non-flat background.

4.4 Causality and zero mode in (2+1) dimensions

In (1+1) dimensions, we showed that both periodic and (homogeneous) Neumann boundary conditions have zero modes which lead to causality violations when they are removed unjudiciously. Both boundary conditions are essentially unique since there is only one way to implement them. For example, in $(1 + 1)$ dimensions there is a unique spatial topology corresponding to periodic boundary conditions, namely S^1. Similarly, there is only one possible homogeneous Neumann boundary condition, namely spatial derivatives at both ends are set to zero. In higher dimensions, there are more possibilities due to more freedom in imposing the boundary conditions. For instance, homogeneous Neumann boundary conditions can be implemented for various boundary shapes, and one can impose periodic boundary condition in one dimension and, e.g., Dirichlet boundary condition on the remaining spatial dimensions.

4.4.1 Annular boundary condition

The simplest case we consider will involve a two-dimensional 'annular' cavity, where the spatial topology is $I \times S^1$ where $I \subset \mathbb{R}$ is a compact interval. This is equivalent to taking the massless scalar field in Minkowski spacetime but impose Dirichlet boundary conditions in one direction and periodic boundary conditions in another. If we let x to be the coordinate with the periodic boundary condition and y the coordinate with the Dirichlet boundary condition, we have

$$\begin{aligned} \hat{\phi}(t,x,y) &= \hat{\phi}(t,x+L_1,y)\,, \\ \hat{\phi}(t,x,0) &= \hat{\phi}(t,x,L_2) = 0\,. \end{aligned} \tag{4.36}$$

For convenience we consider the case with $L_1 = L_2 = L$. The positive eigenmodes with respect to Minkowski timelike Killing vector for this case is given by

$$\begin{aligned} u_{nl}(t,x,y) &= N_{nl} e^{-\mathrm{i}|\boldsymbol{k}_{nl}|t} \exp\frac{2\mathrm{i}\pi n x}{L} \sin\frac{l\pi y}{L}\,, \\ |\boldsymbol{k}_{nl}| &= \sqrt{\left(\frac{2\pi n}{L}\right)^2 + \left(\frac{\pi l}{L}\right)^2}\,, n \in \mathbb{Z}, l \in \mathbb{N}\,, \end{aligned} \tag{4.37}$$

where N_{nl} is a normalization constant. For clarity, we explicitly derive the normalization using the Klein-Gordon inner product:

$$\delta_{nn'}\delta_{ll'} = -\mathrm{i}\int_0^L \mathrm{d}x \int_0^L \mathrm{d}y \left(u_{nl}\frac{\partial u^*_{n'l'}}{\partial t} - u^*_{n'l'}\frac{\partial u_{nl}}{\partial t}\right) \tag{4.38}$$

For $n = n', l = l'$, this leads to

$$2\,|\boldsymbol{k}_{nl}|\,|N_{nl}|^2 \int_0^L \mathrm{d}x \int_0^L \mathrm{d}y \sin^2\frac{n\pi y}{L} = |\boldsymbol{k}_{nl}|\,|N_{nl}|^2 L^2 = 1 \tag{4.39}$$

and hence we can set $N_{nl} = 1/\sqrt{2L\,|\boldsymbol{k}_{nl}|}$.

The above expression alone is sufficient to conclude that there is no zero mode problem even though we have $n = 0$ eigensolutions. The reason is because since $l \in \mathbb{N}$, we have $|\boldsymbol{k}_{nl}| \neq 0$ for all $n \in \mathbb{Z}$ including $n = 0$. Consequently, under canonical quantization every mode with a definite n, l is an oscillator mode with nonzero frequency $|\boldsymbol{k}_{nl}|$. Without computing the commutator, we will know that microcausality is fully governed by the oscillator modes. We show this concretely in Figure 4.4, where we highlight the differences

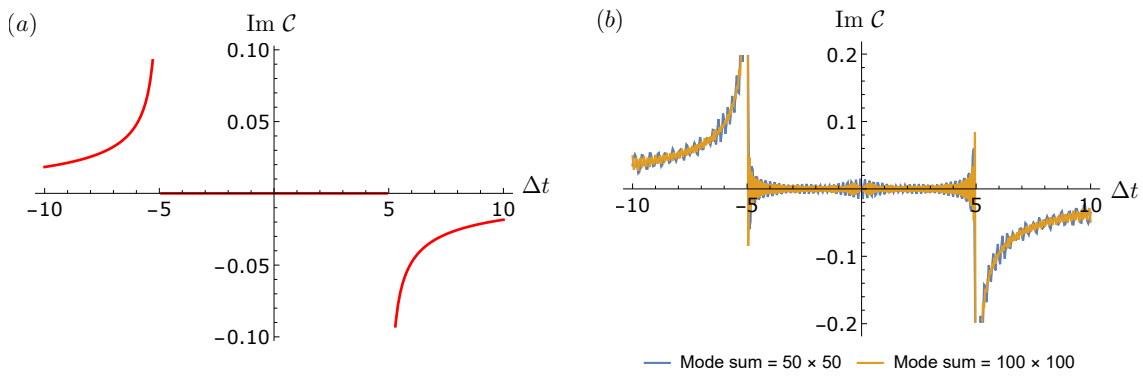

Figure 4.4: **(a)** Free space commutator. **(b)** Commutator for finite cylindrical spacetime with spatial topology $\Sigma = I \times S^1$ for 50×50 and 100×100 modes. Within the timelike interval, as we sum more higher mode, the estimator uniformly approaches zero (here the average is already zero). At the null boundary there is Gibbs phenomenon [99] due to the UV cutoff.

between the signalling of the detectors in free space studied in [57] (Fig. 4a) and detectors in finite cylindrical cavity of topology $I \times S^1$ (Fig. 4b).

To have a zero mode in $(2+1)$ dimensions, we must consider the case where we have the "harmonic" solution with vanishing frequency $|\boldsymbol{k}_{00}| = 0$. This suggests two other nontrivial cases: (1) toroidal boundary and (2) a $(2+1)$ dimensional Einstein cylinder.

4.4.2 Toroidal boundary condition

For the case with toroidal boundary, the spatial topology is $S^1 \times S^1$, i.e. both x, y have periodic boundary conditions,

$$\begin{aligned} \hat{\phi}(t,x,y) &= \hat{\phi}(t,x+L_1,y)\,, \\ \hat{\phi}(t,x,y) &= \hat{\phi}(t,x,y+L_2)\,. \end{aligned} \tag{4.40}$$

Again for simplicity let us set $L_1 = L_2 = L$. This gives us the positive frequency eigenmodes of the form

$$\begin{aligned} u_{mn}(t,x,y) &= N_{mn} e^{-\mathrm{i}|\boldsymbol{k}_{mn}|t} \exp\frac{2\mathrm{i}\pi m x}{L} \exp\frac{2\mathrm{i}\pi n y}{L}\,, \\ |\boldsymbol{k}_{mn}| &= \sqrt{\left(\frac{2\pi m}{L}\right)^2 + \left(\frac{2\pi n}{L}\right)^2}\,, \\ N_{mn} &= \frac{1}{\sqrt{2L\,|\boldsymbol{k}_{mn}|}}\,, \end{aligned} \tag{4.41}$$

where in this case the zero mode will appear. The oscillator part of the commutator is given by (see Appendix C.1)

$$\begin{aligned} &\langle[\hat{\phi}_{\mathrm{osc}}(\mathsf{x}), \hat{\phi}_{\mathrm{osc}}(\mathsf{x}')]\rangle \\ &= \sum_{m=-\infty}^{\infty} \sum_{n\neq 0} \frac{1}{\sqrt{2L\,|\boldsymbol{k}_{mn}|}} \left(u_{mn} u'^{*}_{mn} - u'_{mn} u^{*}_{mn}\right) + \\ &\quad \sum_{m\neq 0} \frac{1}{\sqrt{2L\,|\boldsymbol{k}_{m0}|}} \left(u_{m0} u'^{*}_{m0} - u'_{m0} u^{*}_{m0}\right)\,. \end{aligned} \tag{4.42}$$

Since the sum cannot be done analytically, we resort to partial sums for the computation of estimator $\mathcal{C}$ and take the imaginary part, Im $\mathcal{C}$. This will give us the same information about superluminal signalling due to the absence of zero mode, since from Eq. (4.16) and for a delta-switching and pointlike detector the estimator $\mathcal{E}$ is the modulus of $\mathcal{C}$, which is purely imaginary. Plotting Im $\mathcal{C}$ is visually clearer.

The results are shown in Figure 4.5(a). It is clear that there is a causality violation and superluminal signalling between detectors when one discounts zero mode. Causality is recovered when the zero mode contribution is included, even at the level of partial sums. Furthermore, note that the zero mode commutator is different from the one in $(1+1)$ dimensions, namely

$$[\hat{\phi}_{\mathrm{zm}}(\mathsf{x}), \hat{\phi}_{\mathrm{zm}}(\mathsf{x}')] = -\frac{\mathrm{i}\Delta t}{L^2}\,. \tag{4.43}$$

4.4.3 (2+1) dimensional Einstein cylinder

The other nontrivial case involves the Einstein cylinder, where the only difference is that the sum over modes along one direction is a continuum (hence an integral over modes

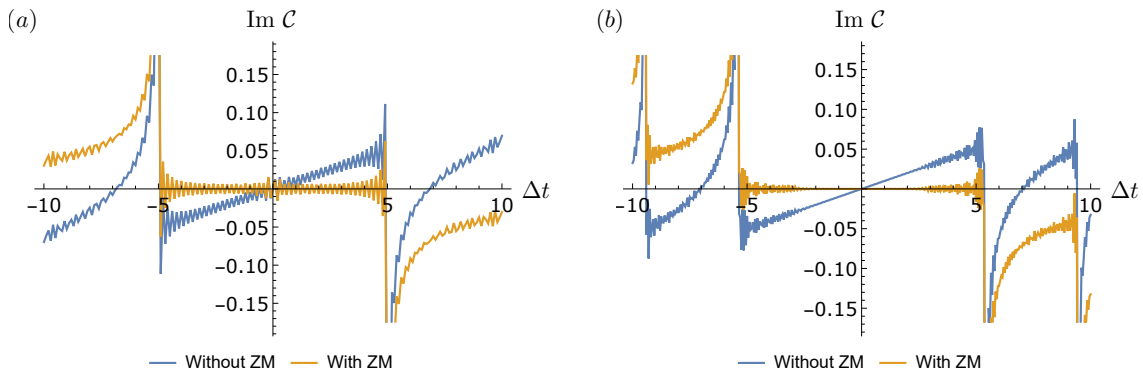

Figure 4.5: Commutator for toroidal spacetime with spatial topology $\Sigma = S^1 \times S^1$. **(a)** 50×50 modes, $\Delta x = 5, \Delta y = 0$. **(b)** for 100×100 modes, $\Delta x = 5, \Delta y = 2$.

instead of a summation). The mode decomposition is given by

$$\begin{aligned} u_{nl}(t,x,y) &= N_{nl} e^{-\mathrm{i}|\boldsymbol{k}_{nl}|t} e^{\mathrm{i}ly} \exp \frac{2\mathrm{i}\pi n x}{L}\,, \\ |\boldsymbol{k}_{nl}| &= \sqrt{\left(\frac{2\pi n}{L}\right)^2 + l^2}\,, \qquad n \in \mathbb{Z}, l \in \mathbb{R}\,, \\ N_{nl} &= \frac{1}{\sqrt{2L\,|\boldsymbol{k}_{nl}|}}\,. \end{aligned} \tag{4.44}$$

While formally it appears that the result should be the same as the case for toroidal scenario, we should be careful because from the perspective of the y-modes, the ω_{00}-mode is a point and hence is a measure zero proper subset of the real line $\mathbb{R}$ which has strictly greater measure. The partially mode-summed estimator is shown in Figure 4.6, where we can see the faster-than-light signalling that appears when the zero mode is ignored. Indeed one can check that taking the principal value integral for the full commutator

$$\begin{aligned} &[\hat{\phi}(\mathsf{x}), \hat{\phi}(\mathsf{x}')] \\ &= \sum_{n\in\mathbb{Z}} \int_{-\infty}^{-\epsilon} \mathrm{d}l \, (u_{nl}(\mathsf{x}) u^*_{nl}(\mathsf{x}') - u_{nl}(\mathsf{x}') u^*_{nl}(\mathsf{x})) + \\ &\sum_{n\in\mathbb{Z}} \int_{\epsilon}^{\infty} \mathrm{d}l \, (u_{nl}(\mathsf{x}) u^*_{nl}(\mathsf{x}') - u_{nl}(\mathsf{x}') u^*_{nl}(\mathsf{x})) \end{aligned} \tag{4.45}$$

does not violate microcausality as $\epsilon \to 0$.

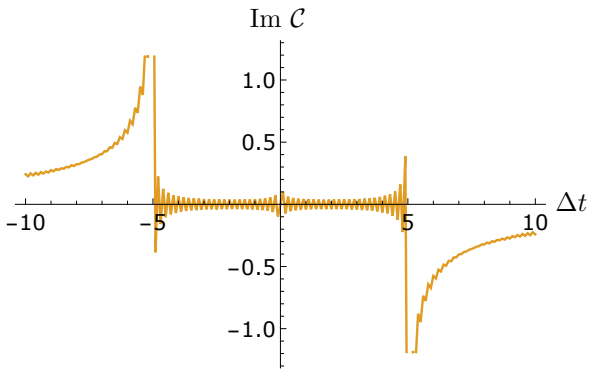

Figure 4.6: Commutator for $(2+1)$ dimensional Einstein cylindrical spacetime with spatial topology $\Sigma = \mathbb{R} \times S^1$ for $(k_{\min}, k_{\max}) = (-50, 50)$. It does not display causality violation despite the integral domain excluding the zero mode.

Again we note that Neumann boundary conditions similarly produce a zero mode, as in $(1+1)$ dimensions. However, in $(2+1)$ dimensions it is now possible to have periodic boundary conditions in one direction and Neumann boundary conditions on another. A zero mode will arise whenever there is "zero frequency" component of the eigenfunctions which is spatially constant (see Appendix C.1 and Appendix C.3 for more details).

4.5 Results in higher dimensions

Based on our results in $(2+1)$ dimensions, we can easily generalize the results to higher dimensions. In particular, the toroidal case with topology $S^1 \times S^1 \times ... \times S^1$ will present a zero mode in arbitrary dimensions since the construction is analogous. The oscillator part of the commutator for arbitrary dimensions with toroidal boundary conditions (and more general boundary conditions) is given by Eq. (C.3) in Appendix C.1. Another notable feature is that in higher dimensions, one can have strong Huygens' principle, e.g. in $(3+1)$ dimensions [102,103]. This is shown in Figure 4.7, where the support of the full commutator (including the zero mode) is only on the light cone. Notice that the zero mode commutator in arbitrary dimensions is given by (see Appendix C.3 for derivation)

$$[\hat{\phi}_{\rm zm}(\mathsf{x}), \hat{\phi}_{\rm zm}(\mathsf{x}')] = -\frac{\mathrm{i}\Delta t}{L^n}\,, \qquad \Delta t = t - t'\,. \tag{4.46}$$

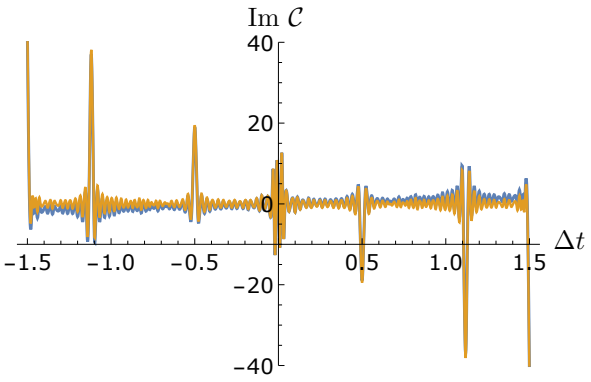

Figure 4.7: Commutator for $(3+1)$ dimensional toroidal spacetime with spatial topology $\Sigma = S^1 \times S^1 \times S^1$ for $30 \times 30 \times 30$ oscillator modes. Here $L = 1$ and $\Delta x = 0.5, \Delta y = \Delta z = 0$. The curve without zero mode is somewhat tilted clockwise relative to the origin, reflecting causality violation. The spikes correspond to the divergences due to the support of the commutator on the null cone.

That is, the impact of the zero mode is polynomially weaker in higher dimensions. In Figure 4.7 we already see that the estimator Im $\mathcal{C}$ is not very much different visually, but removing zero mode nonetheless leads to causality violation and, in this case, also violation of strong Huygens' principle in $(3+1)$ dimensions.

Another feature of higher dimensional cases is that there are more transverse dimensions in which one can impose boundary conditions. For example, to have zero mode, strictly speaking one does not need toroidal boundary condition. One could instead use a combination of periodic boundary condition in some transverse dimensions and Neumann boundary condition on the remaining dimensions (see Appendix C.1 for details).

4.6 Conclusion

In this chapter we have shown that when zero modes are present due to periodic or Neumann boundary conditions (associated either to cavities or spacetimes with compact spatial topology), excluding them in modelling light-matter interactions using particle detector models can lead to faster-than-light signalling between two detectors.

We explicitly quantify the amount of violation in terms of the strength of the superluminal signal that one emitter operating a particle detector can send to another if the

detector is not coupling to the zero mode, and find that for a fixed spatial separation $\Delta\boldsymbol{x}$, the causality violation decays polynomially with the temporal separation Δt, and the length across the boundary condition L. The power law of this decay is given by the number of spatial dimensions n so that the decay is linear in $(1+1)$ dimensions, quadratic in $(2+1)$, etc. Therefore, any relativistic scenario where we analyze the light-matter interaction, communication, entanglement harvesting, or any other phenomenological study where relativity is of importance should consider that particle detectors couple to the zero mode explicitly. As a corollary, in such scenarios one might need to care about the state of the zero mode, whose impact on detector dynamics is non-trivial [83], and one cannot get around the ambiguity of establishing the state of a zero mode just by ignoring its presence.

Chapter 5

Entanglement harvesting with moving mirrors

In this chapter we study how two Unruh-DeWitt detectors extract entanglement from the quantum vacuum of a massless scalar field in $(1+1)$ dimensional spacetime in presence of a moving Dirichlet boundary condition. We will call this spacetime with moving mirrors as "mirror spacetime". We consider a variety of non-trivial trajectories for these accelerating mirrors and find (1) an entanglement inhibition phenomenon similar to that recently seen for black holes, as well as (2) trajectory-independent entanglement enhancement in some regimes. We show that qualitative result obtained is the same for both linear and derivative couplings of the detector with the field. This provides an additional validity of studying entanglement dynamics of massless scalar field with Dirichlet boundary condition in (1+1) dimensions despite the fact that the theory has infrared divergences in free space [105–107].

5.1 Introduction

The study of quantum entanglement has far-reaching consequences in many fields, such as in the study of black hole entropy [108, 109] and the anti-de Sitter/conformal field theory (AdS/CFT) correspondence [15]. In more formal algebraic quantum field theory, it was shown that the vacuum state of a quantum field can maximally violate Bell's inequalities [11]. A more operational approach to study quantum field entanglement was initiated in [22], where it was shown that atoms initialized as uncorrelated states can become entangled after some time due to the global nature of field correlators. This particle detector model,

now known as the Unruh-DeWitt (UDW) model [20, 21], has been extensively used to study the phenomenon of entanglement harvesting [110, 111], discerning the topology of spacetime [55] and distinguishing a thermal bath from an expanding universe at the same temperature [112], among others.

In this chapter we study the phenomenon of entanglement harvesting in the context of *mirror spacetimes*, i.e. the Minkowski spacetime spatially divided by a (possibly dynamical) Dirichlet boundary condition, in $(1+1)$ dimensions. This would constitute the first investigation of entanglement harvesting in a highly non-stationary background quantum field essentially due to the Dynamical Casimir effect (DCE). The DCE has been recently observed experimentally [113, 114] thus motivating the use of mirror spacetimes to study aspects of particle creation in quantum field theory.

The conformal invariance of the massless wave equation in $(1+1)$ dimensions, together with the ease of obtaining exact analytic expressions for the Wightman functions of moving mirrors in certain classes of trajectories, make the study of mirror spacetimes a very attractive toy model to gain insights into the physics of quantum fields in curved spacetimes. The study of responses and transition rates of UdW detectors in receding mirror spacetimes was first investigated decades ago [3, 115, 116]. For some classes of trajectories, one can even match certain mirror trajectories to Hawking radiation associated with black hole spacetimes, whether at the level of the response rate [59] or at the level of the Bogoliubov transformation and stress-energy tensor [117]. More recently it has been shown that for some generic trajectories certain limits can also be taken to obtain thermal responses [118] or even model black hole collapse from a null shell [119–121]. We note in this context that a study of entanglement harvesting in black hole spacetimes was recently initiated for the first time for $(2+1)$-dimensional black holes [58], and so it is of further interest to investigate entanglement harvesting in spacetimes with non-trivial boundary conditions that could simulate the collapse of matter into a black hole.

We will see that, despite the differences between the physics of mirrors and black holes, a pair of atoms can experience (1) entanglement inhibition and even "entanglement death"[1] near a mirror, an effect recently associated with the event horizon of a black hole [58], as well as (2) trajectory-independent entanglement enhancement in some regimes.

This chapter is organized as follows. In Section 5.2 we describe the setup involving the UDW model and provide several *ray-tracing functions* for the mirror trajectories that will be studied in this paper. In Section 5.3 we study entanglement harvesting between two detectors in the presence of a static mirror and also a non-inertial mirror first studied

[1] In other contexts, the term *separability island* has been used due to the island-like region in the contour plot (see e.g. [62, 122]).

in [117]. In Section 5.4 we show that the same qualitative results are obtained using a derivative-type coupling.

5.2 Setup

In this section we recall the standard UDW model in the context of a massless scalar field in (1+1) dimensions interacting with two first quantized atom ("detectors") which we label A and B. In the interaction picture, the light-matter interaction between each detector and the field is provided by the interacting Hamiltonian of the form

$$\hat{H}_I^j(\tau) = \lambda_j \chi_j(\tau) \hat{\mu}_j(\tau) \otimes \hat{\phi}(\mathsf{x}_j(\tau)) \,, \quad j = A, B \,. \tag{5.1}$$

Here index j labels each detector, λ_j is the coupling strength, $\chi_j(\tau)$ is a switching function, $\hat{\phi}$ is the field operator and $\mathsf{x}_j(\tau) = (t_j(\tau), x_j(\tau))$ is the trajectory of detector j parametrized by its proper time τ. In addition, $\hat{\mu}_j(\tau) = \hat{\sigma}_j^+ e^{i\Omega_j \tau} + \hat{\sigma}_j^- e^{-i\Omega_j \tau}$ is the monopole moment of the detector, where $\hat{\sigma}^\pm$ are the ladder operators of the $\mathfrak{su}(2)$ algebra and Ω_j is the energy gap of each detector.

In order to study entanglement harvesting, we have two atomic detectors so the full interacting Hamiltonian takes the form

$$\hat{H}_I(t) = \hat{H}_I^A(t) + \hat{H}_I^B(t) \,. \tag{5.2}$$

We shall also consider for simplicity the case where the two atoms are identical so $\Omega_A = \Omega_B = \Omega$, $\chi_A = \chi_B = \chi$ and $\lambda_A = \lambda_B = \lambda$. We will also focus on the case when both detectors are static in the quantization frame (t, x), so that both detectors are at rest relative to one another and their proper times are given by $\tau = t$. This will ensure that the physical results can be attributed purely to the relative motion between the mirror and the detectors.

We consider the initial state of the full system to be a separable state $\rho_0 = |\psi\rangle\langle\psi|$ where $|\psi\rangle = |0\rangle |g\rangle_A |g\rangle_B$, and where $|0\rangle$ is the field vacuum and $|g\rangle$ is the atomic ground state. The final state of the detector ρ_{AB} is obtained by tracing out the field state after time evolution:

$$\begin{aligned} |\psi_f\rangle &= \hat{U} |\psi\rangle = \mathcal{T} \exp\left(-i \int \mathrm{d}t H_I(t)\right) |\psi\rangle \,, \\ \rho_{AB} &= \mathrm{tr}_\phi |\psi_f\rangle\langle\psi_f| \,. \end{aligned} \tag{5.3}$$

In the $\{|g\rangle_A|g\rangle_B, |e\rangle_A|g\rangle_B, |g\rangle_A|e\rangle_B, |e\rangle_A|e\rangle_B\}$ basis, the reduced joint density matrix of detectors A and B are given by

$$\rho_{AB} = \begin{pmatrix} 1-P_A-P_B & 0 & 0 & X^* \\ 0 & P_B & C & 0 \\ 0 & C^* & P_A & 0 \\ X & 0 & 0 & 0 \end{pmatrix} + O(\lambda^4)\,. \tag{5.4}$$

The expressions for X, P_j (we are not using C in this paper) are:

$$X = -\lambda^2 \iint \mathrm{d}t\,\mathrm{d}t' \chi_A(t)\chi_B(t') e^{i\Omega(t+t')} \left[\Theta(t-t')W(\mathsf{x}_A(t),\mathsf{x}_B(t')) + \Theta(t'-t)W(\mathsf{x}_B(t'),\mathsf{x}_A(t))\right], \tag{5.5}$$

$$P_j = \lambda^2 \iint \mathrm{d}t\,\mathrm{d}t' \chi_j(t)\chi_j(t') e^{-i\Omega(t-t')} W(\mathsf{x}_j(t),\mathsf{x}_j(t')) \tag{5.6}$$

where $W(\mathsf{x},\mathsf{x}') = \langle 0|\hat{\phi}(\mathsf{x})\hat{\phi}(\mathsf{x}')|0\rangle$ is the pullback of the Wightman function to the detector trajectories and $\Theta(\cdot)$ is the Heaviside step function. We derive these expressions in Appendix D.1 for completeness. Since the detectors are identical, we also choose the same Gaussian switching function $\chi(t)$ for both detectors,

$$\chi_j(t) = \exp\left[-\frac{(t-t_j)^2}{2\sigma^2}\right] \tag{5.7}$$

where the parameter σ characterises the effective duration of the interaction with the field and t_j is the temporal peak of the switching function. We specialize to the case when $t_A = t_B$.

The entanglement measure we use here is concurrence $\mathcal{C}(\rho_{AB})$, computed in this case to be [55]

$$\mathcal{C}(\rho_{AB}) = 2\max\left\{0, |X| - \sqrt{P_A P_B}\right\} + O(\lambda^4) \tag{5.8}$$

which is simple and transparent for our purposes[2].

[2]Negativity $\mathcal{N}$ is another usable well-known entanglement measure but in this context does not yield qualitatively different results. Concurrence admits a simpler interpretation due to a clean separation of local and nonlocal terms and the fact that it monotonically increases with the entanglement of formation. In fact for identical detectors, $\mathcal{C} \approx 2\mathcal{N}$ if $P_A \approx P_B$ (cf. [23, 55]), which occurs e.g. when the detectors are identical and not too far apart from one another as is the case in this chapter.

In (1+1) dimensions, the metric for Minkowski spacetime can be written in terms of double null coordinates $u, v = t \mp x$ so that

$$\mathrm{d}s^2 = -\mathrm{d}t^2 + \mathrm{d}x^2 = -\mathrm{d}u\,\mathrm{d}v\,. \tag{5.9}$$

The Wightman function for massless scalar field in $(1+1)$ dimensions in terms of these coordinates is

$$W_f(\mathsf{x},\mathsf{x}') = -\frac{1}{4\pi}\log\left[\Lambda^2(\epsilon + i\Delta u)(\epsilon + i\Delta v)\right] \tag{5.10}$$

where the logarithm is taken with respect to the principal branch, the subscript f denotes 'free space', Λ is an IR cutoff and ϵ is a small positive constant serving as the UV cutoff. In free space, the IR regulator cannot be removed, which is a peculiarity of $(1+1)$ dimensions alone [123]. This leads to the well-known IR ambiguity in the response of a detector coupled linearly to $(1+1)$ massless scalar field.

Unlike the free-space case, the presence of a (moving) mirror i.e. Dirichlet boundary condition removes this IR ambiguity. Hence our investigation does not suffer the fundamental IR cutoff problem encountered in the free-space scenario. It modifies the Wightman function via *ray-tracing functions* $p(u)$ or $f(v)$ depending on whether we use u or v to 'trace' rays: in the presence of a mirror, some of the 'reflected' right-moving modes can be written in terms of the incoming left-moving modes. Anticipating our results, we choose $p(u)$ to avoid issues involving coordinate singularities (see e.g. [117] or [118]) and the Wightman function is now given by [3]

$$W(\mathsf{x},\mathsf{x}') = -\frac{1}{4\pi}\log\left[\frac{(\epsilon + i(p(u)-p(u'))(\epsilon + i(v-v'))}{(\epsilon + i(p(u)-v')(\epsilon + i(v-p(u')))}\right] \tag{5.11}$$

For a static mirror located at the origin $x = 0$ we have $p(u) = u$, and the result reduces to the well known fact that the Wightman function is the difference between the free-space Wightman function and its parity-reversed counterpart [59].

In this paper we will consider three ray-tracing functions, corresponding to three different trajectories [118]:

$$\begin{aligned} p_0(u) &= u\,, \\ p_1(u) &= -\frac{1}{\kappa}e^{-\kappa u}\,, \\ p_2(u) &= v_H - \frac{1}{\kappa}\mathrm{W}\left(e^{-\kappa(u-v_H)}\right) \end{aligned} \tag{5.12}$$

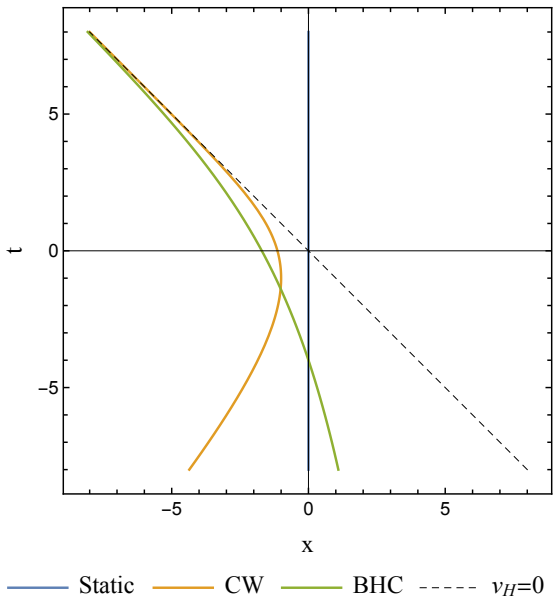

Figure 5.1: The various mirror trajectories considered in this paper are shown here, with $\kappa = 1/2$ for CW and $\kappa = 1/4$ and $v_H = 0$ for BHC.

where $\mathrm{W}(x)$ is the Lambert W function [124]. The Lambert W function (sometimes known as *product logarithm*) is not to be confused with Wightman function $W(\mathsf{x}, \mathsf{x}')$.

The ray-tracing function p_0 describes a static mirror located at the origin. The function p_1 corresponds to a mirror that emits thermal radiation just like that of an eternal black hole, and is known as the *Carlitz-Willey* (CW) trajectory [117]. We shall call the last ray-tracing function p_2 the *black hole collapse* (BHC) trajectory, since it has been shown that there is one-to-one correspondence between the Bogoliubov coefficients for this moving mirror setup and the scenario of $(1+1)$ null shockwave collapse [119, 125, 126]. In both cases the parameter κ can be interpreted as some kind of acceleration parameter since both p_1, p_2 correspond to non-inertial motion of the mirror. The corresponding trajectories are shown in Figure 5.1.

5.3 Results and discussions

We present the main findings in this section. The variable parameters will be denoted as follows: (t_j, x_j) for the time and position coordinates of the peak of the Gaussian switching of

detector j, Ω for the energy gap of the detectors, d_A for the distance of detector A from the mirror at $t = t_A$ and finally $\Delta x = x_B - x_A$ for the detector separation. The results will be presented in terms of the corresponding dimensionless variables, $\{t_A/\sigma,\, d_A/\sigma,\, \Omega_j\sigma,\, \Delta x/\sigma\}$. We first describe general results for all mirror trajectories, followed by an analysis of the effects due to specific mirror motions.

Note that the entanglement results below are strictly speaking given by $\mathcal{C}(\rho_{AB})/(\lambda^2\sigma^2)$ on dimensional grounds but for convenience we will just write $\mathcal{C}(\rho_{AB})$ as a shorthand.

5.3.1 Entanglement enhancement by a mirror

A mirror serves as a Dirichlet boundary condition for the quantum field along the mirror trajectory, i.e.

$$\hat{\phi}(z(t)) = 0 \tag{5.13}$$

where $z(t)$ is the mirror trajectory parametrized by, say, Minkowski time t. Consequently the Wightman function must also vanish wherever one of the detector trajectories coincides with the mirror trajectory. Since the Wightman function gives a measure of correlations present in the field, we would expect to see a drop in the entanglement harvested when the mirror is approached.

For a static mirror, we show in Figure 5.2 the concurrence $C[\rho_{AB}]$ against d_A/σ plot for different values of the energy gap $\Omega\sigma$. Somewhat surprisingly, for fixed detector separation $\Delta x/\sigma$, we find that the presence of a mirror can actually *enhance* entanglement.

Let us analyse the results in greater detail. Firstly, observe that for all parameter choices, the entanglement increases initially as the detectors are positioned furthered from the mirror due to Dirichlet boundary condition in Eq. (5.13). Far from the mirror, concurrence vanishes for large Δx and small $\Omega\sigma$ (the blue and orange curves in the right figure). When the detector separation Δx is decreased it becomes easier to harvest entanglement as we expect. Indeed, for very small Δx (Figure 5.2, left), the region of entanglement extraction is very large (possibly everywhere $d_A > 0$). Conversely, for sufficiently large Δx the concurrence vanishes and so entanglement cannot be extracted anywhere.

The more interesting observation from Figure 5.2 is that concurrence in the presence of a mirror can overtake the free-space result (dashed lines on the figure) at large enough d_A/σ and small enough detector separation $\Delta x/\sigma$. As a representative example, consider $\Delta x/\sigma = 3, \Omega\sigma = 1$. Noting that the free space case (dashed line) has zero concurrence, we see that entanglement harvesting would not have been possible at all if not for the presence of the mirror. Heuristically, this can be understood as a reflection effect in which

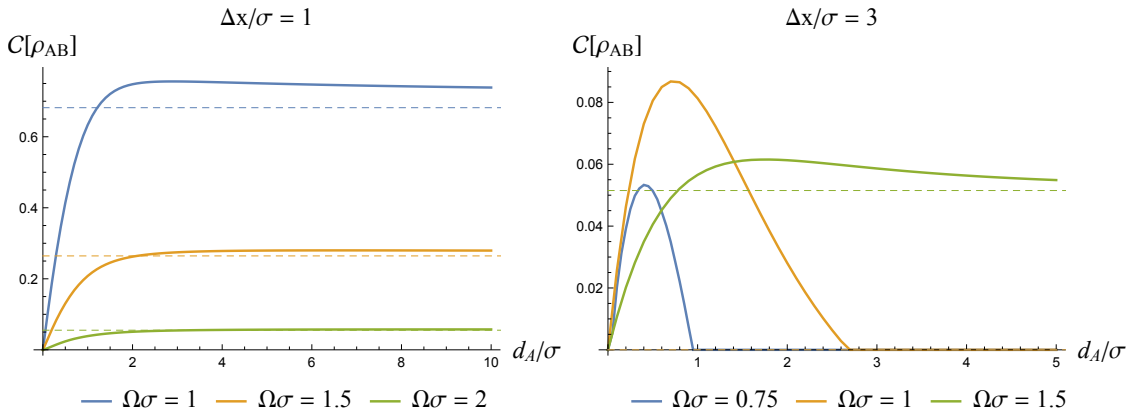

Figure 5.2: Concurrence as a function of distance from static mirror at the origin d_A with $\sigma = 1$ and for various energy gaps. The left and right plots are obtained for different detector separations $\Delta x/\sigma$ as indicated in the plots. The corresponding free space results are shown as dashed lines in each plot. We observe entanglement enhancement relative to that of free-space in some regions. For $\Delta x/\sigma = 3$ (right plot) and $\Omega\sigma = 0.75, 1$, the free space cases (computed by choosing $\Lambda = 10^{-12}$) have zero concurrence (dashed lines on d_A/σ axis).

information from one detector can reach the other detector after reflecting off the mirror. The trade off between this reflection effect and the vanishing of the Wightman function close to the mirror leads to a peak in the concurrence at some optimal d_A away from the mirror. This qualitative behaviour is also present for the other mirror trajectories considered. The main feature displayed here is that of *entanglement enhancement*: mirrors can amplify entanglement extraction relative to the free-space scenario.

Accelerating mirrors contain richer entanglement dynamics from the static one because the Wightman function is generally non-stationary. Furthermore, in this case there will be some $t \in \left[-\frac{\sigma}{2}, \frac{\sigma}{2}\right]$ in which $\hat{\phi}(z(t)) \neq 0$, so naively we do not expect entanglement to completely vanish even if the detector coincides with the mirror for a short period of switch-on time. We investigate these in more details below.

5.3.2 Entanglement death near moving mirrors

The results for the CW mirror are shown in Figures 5.3 and 5.4. Such mirrors are known to have a constant flux of Hawking radiation. We focus on one particular choice of $\kappa\sigma = 0.5, \Omega\sigma = 1$ which captures all the qualitative features we hope to highlight.

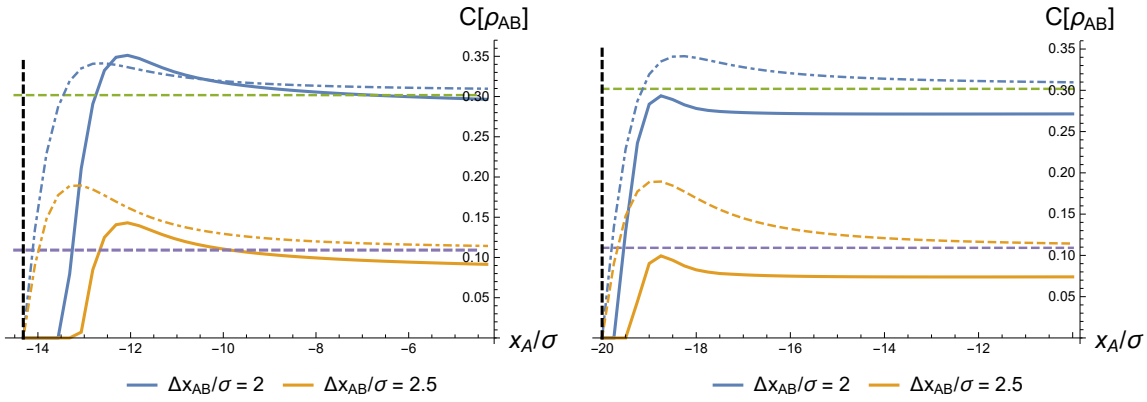

Figure 5.3: Concurrence as a function of position of detector A for fixed detector separations Δx, with $\kappa = 0.5, \Omega = 1, \sigma = 1$ for CW mirror (in red at time $t = t_A = t_B$ when the switching function is peaked). Note that $x_A/\sigma, \Omega\sigma, \kappa\sigma$ are dimensionless and numerically equal to x_A, κ, Ω since $\sigma = 1$. **Left:** $t_A/\sigma = -20$. **Right:** $t_A/\sigma = 20$. The horizontal dashed lines are the corresponding free-space limit and the dot-dashed curves are the static mirror scenarios.

The CW mirror scenario contains more interesting physics compared to its static counterpart. In contrast to the static mirror case, where entanglement vanishes strictly at the mirror due to the boundary condition (cf. Figure 5.2), we see from Figure 5.3 that there can be a small finite region of *entanglement death* near the mirror. This is reminiscent of the situation when detectors are placed too close to a black hole event horizon [58], but the physical origin is different since there is no black hole in our case. For the black hole the origin of entanglement death is due to a redshift factor diminishing the non-local correlations relative to the local noise terms. In the present case, superficially there is a (nonlinear) competition between the local noise term $\sqrt{P_A P_B}$ and the nonlocal term $|X|$ due to the logarithmic behaviour of the Wightman function since they grow at different pace with distance from mirror at some fixed time t, as shown in the left plot of Figure 5.4. Furthermore, by comparing with the static mirror case (dot-dashed curves in Figure 5.2), we can clearly see that at late times generically entanglement degrades relative to the static mirror scenario.

This result is interesting because the CW mirror trajectory $z(t)$ has a future horizon [117]. This is the line $v_H = 0$ in Figure 5.1. The trajectory is asymptotically null in the

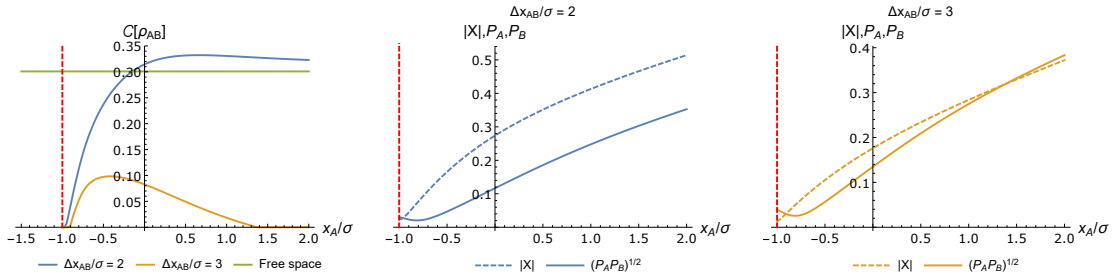

Figure 5.4: **Left:** A plot of concurrence for the CW mirror (in red at time $t = -1$), as a function of the position of detector A for various fixed detector separations Δx, with $\kappa = 0.5, \Omega = 1, \sigma = 1$. **Middle:** The nonlocal term $|X|$ and local noise $\sqrt{P_A P_B}$ terms for the $\Delta x = 2\sigma$ trajectory in the left figure. **Right:** The nonlocal term $|X|$ and local noise $\sqrt{P_A P_B}$ terms for the $\Delta x = 3\sigma$ trajectory in the left figure. The small region where the two curves intersect give the small entanglement enhancement region. Note the small zones of entanglement death near the mirror on the left plot for both cases; these appear in the other two plots where we see that $|X| < \sqrt{P_A P_B}$ very close to the mirror.

infinite past and future, i.e.

$$\frac{\mathrm{d}z(t)}{\mathrm{d}t} = \frac{2W\left(e^{-2\kappa t}\right)}{W\left(e^{-2\kappa t}\right)+1} - 1 \Longrightarrow \lim_{t\to\pm\infty}\frac{\mathrm{d}z}{\mathrm{d}t} = \pm 1\,. \tag{5.14}$$

Similar to black hole event horizon, the mirror's accelerating horizon prevents some modes at past null infinity $\mathscr{I}^-$ from reaching (being ray-traced to) null infinity $\mathscr{I}^+$. This suggests that the analogy/mapping between accelerating mirror and black hole spacetimes can be understood as mapping horizons in both spacetimes.

CW mirrors can also enhance entanglement. The size of the region of entanglement enhancement depends on the relative separation of the two detectors, as the left plot of Figure 5.4 shows. Meanwhile, Figure 5.3 demonstrates that the entanglement structure of this mirror spacetime is not time-symmetric even though the thermal spectrum is time independent; unlike the radiation spectrum, concurrence is sensitive to the non-stationary nature of the spacetime. At "early" times (left plot), in addition to a finite region of entanglement death we observe a finite region of entanglement enhancement relative to the free space result. However, at "late" times (right plot) the size of the entanglement death zone increases and the harvesting zone always yields an amount of concurrence strictly less than free-space limit. This is likely due to the fact that at $t = 10$ the mirror is already at ultrarelativistic speed. From this we see that generically at late times an accelerating

mirror inhibits entanglement compared to early times.

To summarize, we see that the main effect a non-trivial mirror trajectory has on entanglement harvesting is the generic presence of an *entanglement death zone* near the mirror. The strip where this occurs may increase or decrease in size depending on the proximity of the detectors, as shown in Figure 5.3. The fact that $\mathcal{C}(\rho_{AB})$ is sensitive to non-stationarity of the mirror also suggests that entanglement is not correlated directly with a thermal flux of radiation, since a CW mirror models a constant flux of Hawking radiation but $\mathcal{C}(\rho_{AB})$ is clearly dependent on when the detector is switched on.

5.3.3 Effect of different trajectories

While the Carlitz-Willey trajectory models black hole radiation, it does not model black hole collapse because particle creation due to an accelerating mirror following a CW trajectory is *always* thermal [126]. This is understandable since the CW trajectory has an exact one-to-one correspondence with an eternal black hole [121]. Modelling black hole collapse on the other hand requires a mirror trajectory in which particle creation is only thermal at late times. In (1+1) dimensions, the analysis is surprisingly manageable and is provided by the mirror trajectory [125, 126]

$$z(t) = v_H - t - \frac{W(2e^{2\kappa(v_H - t)})}{2\kappa} \tag{5.15}$$

where to model collapse to a black hole of mass M the identification $\kappa = 1/4M$ is made and the horizon is given by the future light cone of the point with double-null coordinate (v_H, v_0) where $v_H = v_0 - 4M$ [126]. This trajectory has zero velocity and acceleration in the asymptotic past at infinity and models the shock-wave collapse of a null shell at $v = v_0$, i.e. the spacetime that is flat for $v < v_0$ and Schwarzschild for $v > v_0$. We shall call this trajectory the "black hole collapse" (BHC) trajectory.

Since both CW and BHC trajectories are asymptotically null in the future, we might expect that their differences must arise at early and intermediate times. We note that unlike the CW trajectory, the BHC mirror is at $x = \infty$ when $t = -\infty$ whereas the CW mirror is at $x = -\infty$ (see Figure 5.1). As such, for the BHC trajectory, in principle the mirror will cross the detectors at some time; in this case, we imagine that the detectors have Gaussian switching that effectively makes the detector active only when the mirror is on the left side of both detectors and imposes the boundary condition so that the field vanishes on the left side of the mirror.

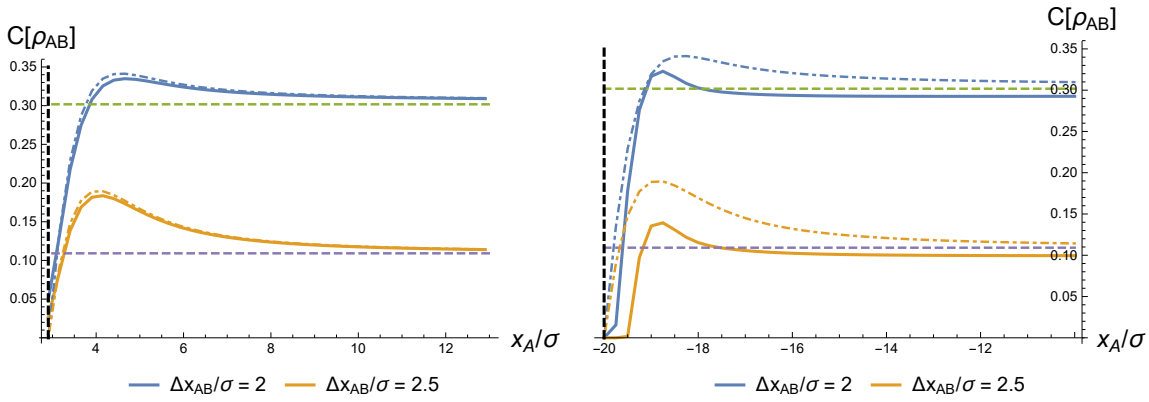

Figure 5.5: Concurrence for a BHC mirror (in red at time t when the detector is temporally peaked) for various fixed detector separations as a function of position of detector A with $\kappa = 0.25, \Omega = 1, \sigma = 1$. From left to right: **Left** $v_H = 0$, the "earlier"time $t = -20$. **Right** $v_H = 0$, the "late" time $t = 20$. The dot-dashed curves are for the static mirror case, which we include for comparison.

We are interested in the generic behaviour of entanglement between the detectors as compared to the static and CW mirror cases. First, we obtained the expected dependence on the detector separation $\Delta x/\sigma$ (not illustrated) generic to all three mirror trajectories: for small $\Delta x/\sigma$, we find that we can extract entanglement from the vacuum very far away from the mirror; for large $\Delta x/\sigma$, no entanglement can be extracted at all for any d_A/σ.

The situation becomes more interesting when we choose to turn on the detectors at different times, to see what "early" or "late" times do to the concurrence. Unlike the CW trajectory, the BHC mirror trajectory has no turning point, i.e. it always moves in the negative x direction, and so it is not obvious what will happen here. The results are illustrated in Figure 5.5, and turn out to be qualitatively similar to the CW trajectory. Again by comparing with the static mirror case (dot-dashed curves in Figure 5.5), we can clearly see that at late times generically entanglement for BHC mirror also degrades relative to the static mirror scenario.

Last but not least, we note that the overall entanglement inhibition at late times when the mirror trajectory is almost null, as well as the entanglement death near the mirror are generic features of accelerating mirror spacetimes. Since for BHC trajectory we have

$$\frac{\mathrm{d}z(t)}{\mathrm{d}t} = \frac{W\left(2e^{2\kappa(v_H - t)}\right)}{W\left(2e^{2\kappa(v_H - t)}\right) + 1} - 1 \tag{5.16}$$

which gives $\lim_{t\to-\infty}\dot{z}(t) = 0$ and $\lim_{t\to\infty}\dot{z} = 1$, the mirror only has one accelerating (future) horizon, which is similar to a collapsing Vaidja-type spacetime (which also only has one apparent horizon asymptotically approaching future event horizon $\mathcal{H}^+$).

Overall, our study on entanglement extraction by two *localized* detectors in these mirror spacetimes provide further indication that we should take seriously that one can establish correspondence between the mirror spacetimes and black hole spacetimes as argued in [118, 119, 125, 126] where the correspondence is made based on nonlocal, non-observable quantities, namely that their Bogoliubov coefficients agree.

For all the different accelerating mirror trajectories considered here, we have mostly focused on detectors which are at least separated by $\Delta x_{AB}/\sigma = 2$. As such, the entanglement dynamics is not dominated by 'reflection' effects, i.e. the physics due to signals reflecting off the mirror allowing detector A to influence detector B causally. By looking at the light cone of detector A, one can see, for e.g. the static mirror case with $\Delta x_{AB} \geq 2\sigma$, that reflection effects would start to dominate only when the switching time is at least 3σ (the detectors considered here are all switched on for about 1σ in duration). This will be generically true for accelerating mirrors here since the mirror moves away from the detectors. Therefore, the two detectors are indeed spacelike separated even in the presence of these mirrors.

5.4 Derivative coupling with moving mirrors

Upon closer scrutiny, two subtleties in the above sections may cause one to question the validity of the results. The first is the ambiguity in the free-space concurrence results due to the infrared cut-off and the second is the spurious effect of an unbounded growth in the excitation probability of a detector in the mirror spacetime (see Figure 5.4). We include an appendix D.2 detailing the origin of the blow up in $P(\Omega)$ and how $|X|$ compensates this to result in sensible results for the concurrence in mirror spacetimes. We also show there how the free-space concurrence is independent of the infrared cutoff.

However, these two subtleties can be bypassed altogether by considering a derivative type coupling (see for example [67]) between the detector and the field. In this subsection, we employ this alternative coupling, and show that in the absence of the above two effects, the qualitative results obtained in the previous sections still hold.

Instead of the linear coupling between the detector and the field operator $\hat{\phi}$ in Eq. 5.1,

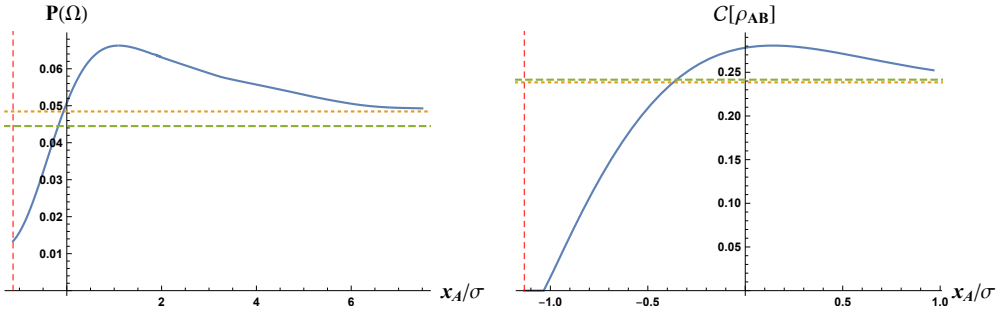

Figure 5.6: Derivative coupling results. **Left**: The use of derivative coupling removes the IR ambiguity in the free-space $P(\Omega)$ (dashed, green). The probability of excitation in the CW mirror spacetime now remains bounded at large x_A/σ. It asymptotes to a value (dotted, yellow) slightly higher than the free-space result. **Right**: The concurrence against x_A/σ plot shows the same qualitative behaviour as linear coupling. Namely, we observe a region of entanglement enhancement and a region of entanglement death close to the mirror. The concurrence will asymptote to a value (dotted, yellow) slightly below the free-space result (dashed, green). In this plot, $\kappa\sigma = 0.5$, $\Omega\sigma = 1$, $t_A/\sigma = 0$ and $\Delta x/\sigma = 1$.

we can replace $\hat{\phi}(\mathsf{x}(t))$ with its proper time derivative to obtain the derivative coupling,

$$\tilde{H}_I^j = \lambda\chi_j(\tau)\hat{\mu}_j(\tau) \otimes u^\mu \nabla_\mu \hat{\phi}(\mathsf{x}_j(\tau))\,.$$

For detectors static in the (t, x) coordinates, we have $t = \tau$ and the proper time derivative reduces to partial derivative ∂_t. As shown in [67], in addition to removing the dependence of the excitation probability on the infrared cut-off, this coupling also results in an expression for the probability that looks more similar to the $(3+1)$D case. In the current case, we can see this by the following: the expressions for $P(\Omega)$ and X given in sec. 5.2 can be easily modified to accommodate the change in coupling by making the replacement $W(\mathsf{x}_{j_1}(t), \mathsf{x}_{j_2}(t')) \to A(\mathsf{x}_{j_1}(t), \mathsf{x}_{j_2}(t')) \equiv \partial_t \partial_{t'} W(\mathsf{x}_{j_1}(t), \mathsf{x}_{j_2}(t'))$ whenever it appears. In

particular, we have

$$A_f(\mathsf{x},\mathsf{x}') = -\frac{1}{4\pi}\left(\frac{1}{\Delta u - i\epsilon} + \frac{1}{\Delta v - i\epsilon}\right), \tag{5.17}$$

$$\begin{aligned} A_m(\mathsf{x},\mathsf{x}') = -\frac{1}{4\pi}\Bigg(&\frac{p'(u)p'(u')}{\Big[p(u)-p(u')-i\epsilon\Big]^2} + \frac{1}{\Big[v-v'-i\epsilon\Big]^2} \\ &- \frac{p'(u')}{\Big[v-p(u')-i\epsilon\Big]^2} - \frac{p'(u)}{\Big[p(u)-v'-i\epsilon\Big]^2}\Bigg) \end{aligned} \tag{5.18}$$

respectively for free space and mirror spacetimes. These replace the Wightman functions in (5.10) and (5.11). Since A_f does not require an IR regulator to be well-behaved, the IR ambiguity in $P(\Omega)$ and $|X|$ is removed. Furthermore, the similarity between A_f and the $(3+1)$D Wightman function (c.f. Appendix D.2) also indicates that the results for $P(\Omega)$ and $|X|$ in $(3+1)$D using linear coupling will be similar to that obtained using derivative coupling in $(1+1)$D. In fact, for the free space scenario the Wightman function $A_f(\mathsf{x},\mathsf{x}')$ in $(1+1)$ dimensions only differs from the linear coupling Wightman function $W_f(\mathsf{x},\mathsf{x}')$ in $(3+1)$D by a constant factor of 2, so the physics is practically identical.

In Figure 5.6, we show the results obtained using derivative couplings between the detectors and the field. From the $P(\Omega)$ plot, we see that the probability in the CW mirror spacetime remains bounded at large d_A rather than blowing up as in Figure 5.4. We note also that the free-space value in this case was computed without the need for choosing an IR cut-off. In addition, we see that derivative coupling results in the same qualitative findings as the previous subsections: there is a region of entanglement enhancement over the free-space result and entanglement death near the mirror.

The derivative coupling scenario reinforces the fact that entanglement dynamics between detectors in mirror spacetimes can be understood as intrinsically the physics of horizons: even though the time-evolved reduced density matrix depends strongly on the type of coupling used, we see that entanglement itself is qualitatively robust and captures the essential physics induced by presence of horizons. Our study complements the correspondence previously established in [118, 119, 121, 125, 126] using nonlocal/non-observable quantities such as Bogoliubov coefficients and expectation value of stress-energy tensor, by establishing qualitative correspondence via local measurements using detectors.

5.5 Free-space limit

The previous sections seem to suggest that in general we should not expect our results to approach the free-space limit (without mirror) even in the large x_A limit (keeping Δx_{AB} fixed). This may appear counter-intuitive, and it turns out that this is related to the IR ambiguity of the free-space case. Recall that a massless scalar field in $(1+1)$-dimensional Minkowski spacetime is IR-ambiguous because the Wightman function is ambiguous up to an arbitrary constant which depends on the logarithm of the IR cutoff Λ (see e.g. [3, 59]). Note that we showed in Appendix D.2 that IR ambiguity does not pose problems for computations involving concurrence, so we should try to understand how the limit is approached.

The two-point Wightman function for Carlitz-Willey (CW) mirror is given by

$$W_{\rm CW}(\mathsf{x},\mathsf{x}') = -\frac{1}{4\pi}\log\left(\frac{(t-t'+x-x'-i\epsilon)\left(\frac{e^{-\kappa(t'-x')}}{\kappa}-\frac{e^{\kappa(-(t-x))}}{\kappa}-i\epsilon\right)}{\left(\frac{e^{-\kappa(t'-x')}}{\kappa}+t+x-i\epsilon\right)\left(-t'-\frac{e^{-\kappa(t-x)}}{\kappa}-x'-i\epsilon\right)}\right). \tag{5.19}$$

Now let us take the $\kappa \to 0$ limit, which should correspond to zero acceleration. This in fact goes to the *free-space limit*

$$\lim_{\kappa\to 0} W_{\rm CW}(\mathsf{x},\mathsf{x}') = \lim_{\kappa\to 0} -\frac{1}{4\pi}\log\left[\kappa^2(i\epsilon-\Delta u)(i\epsilon-\Delta v)\right] - \frac{i}{4} + O(\kappa)\,. \tag{5.20}$$

The additive constant $i/4$ agrees with what was found in [59]. Therefore, by comparing with the free-space scenario, we can identify the small small acceleration κ *for any* x,x' with the free space IR cut-off[3] Λ! In other words, the concurrence asymptotes to the free space limit only for small κ: a larger κ asymptotes to free space scenario with larger IR cutoff. Another compact way of saying this is that the accelerating mirror approaches free-space results only if $\kappa = \Lambda$. Therefore, it follows that even for large distances away from the mirror, we will not exactly recover free-space results for entanglement or transition probability if κ is not comparable to Λ. Another way of saying this is that no matter how far the mirror is, detectors *can* distinguish the presence of the mirror if the mirror has large enough acceleration parameter κ.

[3] See Appendix D.2 for further discussion of IR-cutoff in (1+1)D massless scalar field.

The result is the same for Black Hole Collapse (BHC) mirror:

$$W_{\rm BHC}(\mathsf{x},\mathsf{x}') = -\frac{\log\left(\frac{\kappa(t-t'+x-x'-i\epsilon)\left(-W\left(e^{\kappa(v_H-t'+x')}\right)+W\left(e^{\kappa(v_H-t+x)}\right)+i\kappa\epsilon\right)}{\left(W\left(e^{\kappa(v_H-t'+x')}\right)+\kappa(-v_H+t+x-i\epsilon)\right)\left(W\left(e^{\kappa(v_H-t+x)}\right)+\kappa(-v_H+t'+x'+i\epsilon)\right)}\right)}{4\pi} \tag{5.21}$$

Again taking the $\kappa \to 0$ limit, we get

$$\lim_{\kappa\to 0} W_{\rm BHC}(\mathsf{x},\mathsf{x}') = \lim_{\kappa\to 0} -\frac{1}{4\pi}\log\left(\frac{\kappa^2\,(\Delta v - i\epsilon)\,(\Delta u - i\epsilon)}{W(1)(W(1)+1)}\right) - \frac{i}{4} + O(\kappa)\,, \tag{5.22}$$

where $W(1) \approx 0.56714$. Notice that this is exactly the same as the free-space limit of CW mirror up to redefinition of κ, i.e.

$$\kappa \to \frac{\kappa}{\sqrt{W(1)(W(1)+1)}} \approx 1.06072\kappa\,. \tag{5.23}$$

Therefore, in the limit $\kappa \to 0$ they agree. This rescaling also means that a fixed small κ of CW and BHC mirrors corresponds to slightly different IR cutoff in free space. One can check that indeed, for arbitrary positive κ, the limit $x_A \to \infty$ (at fixed Δx), the limit does not approach free-space case *unless* $\kappa \approx \Lambda$.

One can repeat the same calculation for derivative coupling. Denoting the derivative coupling Wightman functions in Minkowski space, CW mirror and BHC mirrors respectively by $(\mathcal{A}_f, \mathcal{A}_{\rm CW}, \mathcal{A}_{\rm BHC})$, we can show that

$$\lim_{\epsilon\to 0}\lim_{\kappa\to 0} \mathcal{A}_f - \mathcal{A}_{\rm CW} = \lim_{\epsilon\to 0}\lim_{\kappa\to 0} \mathcal{A}_f - \mathcal{A}_{\rm BHC} = 0\,, \tag{5.24}$$

independently of x,x'.

Finally, it is important to notice that $\kappa \to 0$ does not approach the *static mirror* limit. In this sense, we should view static mirror as a quite different setup; alternatively, we should view $\kappa \to 0$ limit as the limit when the mirror does not accelerate (i.e. static) but at the same time the mirror is pushed to $x = -\infty$, thus tending towards full Minkowski space instead of Minkowski half-space (where the mirror is at the origin).

5.6 Conclusion

We have performed in $(1+1)$ dimensions the first investigation of entanglement harvesting between two detectors in the presence of mirrors using both linear and derivative couplings between the detectors and the quantum field. We looked at both static and non-inertial trajectories, focusing on the CW and BHC trajectories for the latter because of their respective correspondence to eternal black holes and black hole formation. We find that a similar correspondence exists for their entanglement structures, in particular the phenomenon of an entanglement death zone, similar to that recently found for a black hole event horizon [58]. Physically, our results provide a theoretical prediction of what to expect of the entanglement detection in the presence of the DCE.

Finally, and perhaps most interestingly, we also find that mirrors can enhance entanglement: entanglement harvested between two detectors can be greater in the presence of a mirror as compared to free space. Qualitatively this enhancement is largely trajectory-independent, and is thus attributable to the inherent presence of a Dirichlet boundary condition. Quantitatively there are distinctions between different mirror trajectories, as a comparison between Figures 5.2 and 5.3 indicates. We focused on three types of mirror trajectories that have the simplicity of having smooth ray-tracing functions $p_j(u)$ that are regular for all $u \in \mathbb{R}$. Important trajectories such as a mirror with constant uniform acceleration have ray-tracing functions that are not defined for all u, indicating that only some modes at future null infinity $\mathcal{I}^+$ can be 'ray-traced' to modes at past null infinity $\mathcal{I}^-$. We have also not investigated the case of piecewise mirror trajectories, such as a mirror that only accelerates at $t = 0$ and static at $t \leq 0$, which are often used in analyses involving Bogoliubov transformations. We defer this for future work.

Finally, we make a brief comment about physicality of the (1+1)-dimensional setup. One of the main concerns about the Unruh-DeWitt model coupled linearly to massless scalar fields in $(1+1)$ dimensions is the IR ambiguity of the field. In this work we showed that this does not pose a problem in presence of Dirichlet boundary condition, and in particular entanglement dynamics can be IR-safe. It may also be argued that $(1+1)$-dimensional setup can be used as an effective description (e.g. think about very thin optical fiber). This would make sense as a form of dimensional reduction, where $(3+1)$ massless scalar field is reduced to an effective theory of $(1+1)$ massive scalar fields, where the transverse momenta $\boldsymbol{k}_\perp^j$ of the dominant modes enter the description as effective mass $m_{\text{eff}} \sim \sqrt{\sum_j |\boldsymbol{k}_\perp^j|^2}$. The extent to which this reduction gives valid results has been recently studied in [37] in the context of scalar fields in a cavity, thus it would be interesting avenue to see how much dimensional reduction affects entanglement dynamics between Unruh-DeWitt detectors.

Chapter 6

Detour: numerical contour integral in the Unruh-DeWitt model

In this chapter we take a short detour from the main work in this thesis and explore the problem of contour integration using numerical methods, primarily using *Mathematica*[1]. This was motivated by some numerical computations undertaken in the last chapter, and we present here some discussions about what we found to be both useful and requires some explanation. This may prove relevant for future investigations in the Unruh-DeWitt model involving highly non-stationary Wightman functions which contain poles. This is the case for derivative coupling in $(1+1)$ dimensions (cf. Chapter 5) and linear coupling in $(3+1)$ dimensions.

6.1 Prelude: failing simple integral

It is well-known that numerical integration is hard to perform — much harder than differentiation. Given a closed-form expression, one can differentiate *any* differentiable function to obtain new closed form expressions but one cannot integrate any integrable function to get a closed-form anti-derivative function. This is especially the case when distributions are involved: the (distributional) derivative of the Heaviside step function is the Dirac delta *distribution*, but one cannot really integrate a Dirac delta distribution and expect to obtain Heaviside step function. Therefore, we cannot say that a Heaviside step function

[1] In this thesis version 11 of Mathematica was used.

is an antiderivative of a Dirac delta distribution. This is one of the many ways in which integration is "harder" than differentiation[2].

For our discussion, another factor that leads to difficulty in integration is related to local-versus-global information. Given $p \in \mathbb{R}^N$, differentiation at point p only requires information about the open neighbourhood $B_p(\epsilon)$. Integration however requires us to know information about the entire domain of integration. For integrals in which there is exponential suppression at large ranges, one can attempt to truncate the range to a smaller one and obtain approximate but more tractable expressions. The subject of numerical integration and how to optimise it in various settings, softwares, etc. is too broad so it suffices for our purposes that in general numerical integration is "hard" without any further simplifying conditions or nice behaviour of the integrand[3].

Let us start with a very simple integral before we focus on our real problem. This is given by the famous Gaussian integral

$$\int e^{-(x-1)^2} \mathrm{d}x = \frac{\sqrt{\pi}}{2} \mathrm{Erf}(x-1)\,, \tag{6.1}$$

where $\mathrm{Erf}(x)$ is the error function. Since $\lim_{x\to\pm\infty} \mathrm{Erf}(x) = \pm 1$, we see that

$$\int_{-\infty}^{\infty} e^{-(x-1)^2} \mathrm{d}x = \sqrt{\pi} \approx 1.77245\,. \tag{6.2}$$

Symbolic integration software such as Mathematica can do this analytically. Numerical integration along the full $\mathbb{R}$ also gives the correct numerical result. However,

$$\int_{-5}^{5} e^{-(x-1)^2} \mathrm{d}x \approx 1.77245\,, \tag{6.3}$$

$$\int_{-1000}^{1000} e^{-(x-1)^2} \mathrm{d}x \approx 1.63305\,, \tag{6.4}$$

where the first truncation to $[-5, 5]$ has error of about 10^{-12} from $\sqrt{\pi}$ (this range is considered to be a *strongly supported region* of the Gaussian function, since beyond it the integral is highly suppressed). The second integral is clearly off. This is a well-known

[2]There is a sense in which differentiation can be harder than integration: this is when we think of a *finite difference* as dividing small quantities with small quantity, a numerically unstable process; integration as Riemann sum, however, tends to average things out.

[3]For example, one of the banes of integration is "highly oscillatory" integrands, in which the Riemann sum will have to be adaptive enough to catch the oscillations, as well as integrals with singularities.

problem in Mathematica[4], and for this simple problem there is a simple solution because the problem is quite "obvious": the numerical integration did not sample enough points. For example, by increasing the option MinRecursion to 3 (default is 0), the error from $\sqrt{\pi}$ is 10^{-16}, which is even better than the strong support truncation at $[-5, 5]$ (but without additional settings). Numerically Python can do the same and obtain the correct result without fiddling[5].

While this integral does not provide insight into the problems we want to solve, it does give us one way to check consistency: namely, if the integrand is strongly supported, i.e. exponentially suppressed at large values of x, then truncation at strong support should give sensible result[6].

6.2 The problematic double integral

Consider the following double integral

$$I[\Omega, \sigma, \epsilon] := \iint_{\mathbb{R}^2} \mathrm{d}t\, \mathrm{d}T\, e^{-\frac{t^2}{2\sigma^2}} e^{-\frac{T^2}{2\sigma^2}} e^{-i\Omega(t-T)} \left(-\frac{1}{4\pi^2 (t - T - i\epsilon)^2} \right) . \tag{6.5}$$

This is in fact the integral associated to transition probability (divided by coupling strength factor λ^2) of a two-level detector initialized in its ground state and with Gaussian switching function (cf. Chapter 2) when the detector is inertial in $(3+1)$ Minskowski spacetime; the term in the bracket is the pullback of the the Wightman function in $(3+1)$ Minkowski spacetime for inertial trajectory when the field is prepared in vacuum state [3]. The $i\epsilon$ prescription ($\epsilon > 0$) is required since Wightman function is strictly speaking a distribution. Let us first consider the special case when $\sigma \to \infty$, the so-called "long interaction" limit, equivalent to an Unruh-DeWitt detector being on at all times.

[4] https://reference.wolfram.com/language/tutorial/NumericalIntegration.html

[5] I thank Erico Tjoa who works with Python for his PhD daily for checking this.

[6] We have been able to make use of this fact to verify that in some situations, *not truncating* the integral is computationally faster while in other cases the opposite is true, both with acceptable error trade-offs.

6.2.1 Long interaction limit and contour integral

In the "long interaction" limit $\sigma \to \infty$, this integral formally divergent [3]; this can be seen from the transformation $u := t - T$, $v := t + T$ which gives

$$I(\Omega, \infty, \epsilon) \propto \int_{\mathbb{R}} \mathrm{d}v \int_{\mathbb{R}} \mathrm{d}u \, e^{-i\Omega u} \left(-\frac{1}{4\pi^2 (u - i\epsilon)^2} \right) . \tag{6.6}$$

In the traditional treatment, we define the *transition rate* as

$$\frac{\mathrm{d}I(\Omega, \infty, \epsilon)}{\mathrm{d}v} = \int_{\mathbb{R}} \mathrm{d}u \, e^{-i\Omega u} \left(-\frac{1}{4\pi^2 (u - i\epsilon)^2} \right) \tag{6.7}$$

and this integral is identically zero for $\Omega > 0$ (i.e. for detectors in ground state). To see this, the $i\epsilon$ prescription requires us to deform the contour to the lower complex plane near the pole $u = 0$ and since we close the contour in the lower complex plane, Cauchy's integral theorem certifies this to be zero since the contour encloses no poles. This analytic result says that "an inertial detector which is always on detects no particles in vacuum" [3].

Now suppose we attempt to perform the integral in Eq. (6.7) *numerically* as is. It can be shown that *without truncating* the integration domain to finite $[-a, a]$, Mathematica gives the following answer ($\Omega = 1$):

$$\begin{aligned} \epsilon &= 10^{-1} \sim 10^{-14} , \\ \epsilon &= 10^{-3} \sim 10^{-15} , \\ \epsilon &= 10^{-5} \sim 10^{-14} . \end{aligned}$$

We see that the answer does converge to zero for sufficiently small ϵ but not too small. If we truncate the domain, we will see convergence to zero as the interval $[-a, a]$ widens but *not too wide*: the answer deviates greatly when $a \sim 10^3$, similar to the Gaussian integral in the previous section — i.e. for larger a we need some auxiliary settings to refine the domain subdivision by Mathematica. It turns out that this convergence issue is worse in double integral scenarios, as the subdomain division is a rectangle and in general numerical integration schemes become much harder to control than single integrals[7].

The case in Eq. (6.7) might be worrying since the example above tells us that the range of ϵ which gives sensible result is not actually very large when in theory we should be able

[7] In *Mathematica*, for instance, there are more schemes, transformations and methods that work for one-dimensional integrals but not higher dimensional integrals.

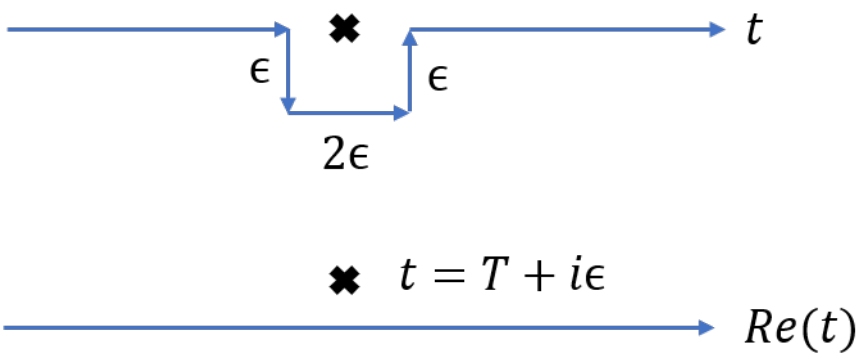

Figure 6.1: Contour for Eq. (6.7) (top), compared to the $i\epsilon$ prescription (bottom).

to take arbitrarily small ϵ. Furthermore, oftentimes we do not *a priori* knows the expected value of the integral. This might mean that for more complicated integrands, we may not be able to inspect the values to know that we are correctly computing the integral (i.e. the numerical integral converges to the *wrong* result): after all, in this example we *cheated* since we know without solving the integral (and on physical grounds) that the integral should vanish.

A potential solution comes from complex analysis: the deformation theorem [127] states that if γ_1, γ_2 are two contours with the same endpoints such that the integrand is holomorphic in the interior enclosed by these curves, then the two contour integrals agree. Loosely speaking, if we can deform the the contour without crossing any poles or singularities, then the integral should be the same. For Eq. (6.7), we can perform contour integration directly *and* numerically instead of using the $i\epsilon$ prescription. One example of the contour is given in Figure 6.1.

To test this, we consider the following one-parameter family of contours parameterized by ϵ as in Figure 6.1:

$$\tilde{I}(\Omega, \epsilon) := \int_{C(\epsilon)} \mathrm{d}u \, e^{-i\Omega u} \left(-\frac{1}{4\pi^2 u^2} \right) . \tag{6.8}$$

Basically, ϵ now parameterizes the three segments to the lower complex plane around the pole at $t = T$ (i.e. $u = 0$). Of course analytically we know the answer: it is zero. Numerically, we need to explicitly request that we integrate u in this sequence ($\epsilon > 0$):

- Along the real direction $u = -\infty$ to $u = -\epsilon$
- Along the imaginary direction $u = -\epsilon$ to $u = -\epsilon - i\epsilon$

- Along the real direction $u = -\epsilon - i\epsilon$ to $u = \epsilon - i\epsilon$
- Along the imaginary direction $u = \epsilon - i\epsilon$ to $u = \epsilon$
- Finally, along the real direction from $u = \epsilon$ to $u = \infty$.

Note that this contour parametrization is not unique, since we could choose many other ways to deform the contour on the lower half of the complex plane by the deformation theorem. Our choice here is simply the simplest to implement in Mathematica[8].

With this, we obtained similar results approaching zero ($\Omega = 1$):

$$\begin{aligned}\epsilon &= 10^{-1} \sim 10^{-9}\,,\\ \epsilon &= 10^{-3} \sim 10^{-11}\,,\\ \epsilon &= 10^{-5} \sim 10^{-12}\,.\end{aligned}$$

This appeared to be worse than the $i\epsilon$ prescription. Also, in our comparison we only chose the most minimalistic settings (we could optimize things to make both cases better). It turns out that for this integral $\tilde{I}(\Omega, \epsilon)$, numerical contour integration does not perform much better in many cases, but either way the results are both consistent with zero. This may be due to one-dimensional integrals along the real line being more robust numerically than across the complex plane and the fact that the value of the integral is very close to zero. We will see that this implementation performs much better when we encounter the integral such as $I(\Omega, \sigma, \epsilon)$ in Eq. (6.5) when σ is finite (hence the integral does not vanish).

6.2.2 Double integral revisited

Let us now try to solve the integral in Eq. (6.5). It turns out that this integral can be solved *analytically* using a judicious coordinate transformation: this reads (see e.g. [78])

$$I_{\text{exact}} := \lim_{\epsilon\to 0} I(\Omega, \sigma, \epsilon) = \frac{1}{4\pi}\left(e^{-\Omega^2\sigma^2} - \Omega\sigma\Gamma\left(\frac{1}{2}, \Omega^2\sigma^2\right)\right)\,, \tag{6.9}$$

where $\Gamma(a, b)$ is the incomplete Gamma function. For $\Omega\sigma = 1$, this gives

$$I_{\text{exact}} \approx 0.00708827\,. \tag{6.10}$$

Let us see how direct integration with $i\epsilon$ prescription fares. The results are shown in Table 6.1. It turns out that the result is very badly behaved: without any optimizations, the result does not converge properly and we get the following results with only $\epsilon \sim$

[8] In fact, given in this form, the integral is still solvable *exactly* for nonzero ϵ.

ϵ	Integral value
10^{-1}	0.00670271
10^{-2}	0.00704838
10^{-3}	$2.14412 - 1.32803i$
10^{-4}	$17.1784 + 0.732602i$
10^{-5}	$-41.3518 - 1.42294i$

Table 6.1: Integral values of $I[1, 1, \epsilon]$ using Method 0 (direct $i\epsilon$ integration) as ϵ varies.

$10^{-1}, 10^{-2}$ barely making the cut: Several choices of optimization attempts, including changing integration methods, the number of recursions for sampling points, do not appear to help reaching close to the exact answer. In principle there should be a way to reach the result, but our trials suggest that this will be far from straightforward and requires rather detailed knowledge of numerical analysis and back-end Mathematica's integration schemes. We should also make a remark that to the author's knowledge, most results involving this double integral in the literature have been mostly dealt with *analytically* due to nice symmetries of the problem, either directly such as is done in [78], or by performing some sort of Fourier transform along the way (see e.g. [43, 55, 56]). What can we do?

Below we will present *four* other methods to compute the integral above which fare better and demonstrate how contour integral can be seen as superior. We will refer to direct integration with $i\epsilon$ prescription as **Method 0**. Let us regard the exact answer I_{exact} given above as **Method 1** (thus $I_1[\Omega, \sigma] := I_{\text{exact}}$) and the rest of the methods as I_j where j is the method number.

Method 2: numerical contour integration

The principle is the same as the contour integral in the previous section, except that now we perform double integral. That is, for every fixed T, we perform contour integration as in Figure 6.1, deforming at the poles $t = T$, and then integrate over all T. If we choose to integrate T first for every fixed t, note that due to the relative sign in $e^{-i\Omega(t-T)}$, the contour deformation must be towards the *upper* complex plane instead of lower complex plane. Thus, we write the integral as

$$I_2[\Omega, \sigma, \epsilon] := \int_{\mathbb{R}} \mathrm{d}T \int_{C(\epsilon)} \mathrm{d}t \, e^{-\frac{t^2}{2\sigma^2}} e^{-\frac{T^2}{2\sigma^2}} e^{-i\Omega(t-T)} \left(-\frac{1}{4\pi^2 (t-T)^2} \right) , \tag{6.11}$$

ϵ	Integral value
10^{-1}	0.00708827
10^{-2}	0.00708827
10^{-3}	0.00708827
10^{-4}	0.00708827
10^{-5}	$0.00708827 + 1.28 \times 10^{-9} i$

Table 6.2: Integral values of $I[1, 1, \epsilon]$ using Method 2 (numerical contour integration).

where $C(\epsilon)$ is the contour towards the lower complex plane (cf. Figure 6.1), and ϵ here marks how far away the deformation is from the poles at $t = T$. The results are shown in Table 6.2. Clearly, we observe the manifestation of deformation theorem: the probability is *constant* and converge to the exact answer very satisfactorily. This is completely different outcome from the previous section.

We make a rather obvious but subtle remark that this integral is not solvable by residue theorem, as one may wish to attempt given the fact that this can be solved by contour integration. The reason is because the Gaussian switching function in the integrand renders Jordan's lemma [127] inapplicable. Also, while in theory the deformation theorem allows arbitrary $\epsilon > 0$, in practice for a fixed precision and accuracy settings, ϵ cannot be too large (otherwise the Gaussian overflows) or too small (otherwise the contour is too close numerically to the pole).

Method 3: Satz's integral

In [69], the transition probability was recast into the following form:

$$\begin{aligned} I_3[\Omega, \sigma, \epsilon] &\coloneqq 2 \lim_{\epsilon \to 0} \mathrm{Re} \int_{-\infty}^{\infty} \mathrm{d}u \, \chi(u) \int_0^{\infty} \mathrm{d}s \, \chi(u-s) e^{-i\Omega s} W_\epsilon(u, u-s) \\ &= 2 \lim_{\epsilon \to 0} \mathrm{Re} \int_{-\infty}^{\infty} \mathrm{d}u \, e^{-\frac{u^2}{2\sigma^2}} \int_0^{\infty} \mathrm{d}s \, e^{-\frac{(u-s)^2}{2\sigma^2}} e^{-i\Omega s} \left(-\frac{1}{4\pi^2 (s - i\epsilon)^2} \right) . \end{aligned} \tag{6.12}$$

It is clear from the second line that using Gaussian switching and inertial detector in free space gives a result very close to [78], since the integral in u is just Gaussian integral and the integral over s will lead to the expression in [78]. This method is nonetheless more useful since it is applicable for general switching and Wightman functions. Let us evaluate this expression numerically as it is.

It turns out that without any optimization, this integral behaves very badly, coming

ϵ	Integral value	ϵ	Integral value
10^{-1}	0.00670271	10^{-6}	0.00708827
10^{-2}	0.00704838	10^{-7}	0.00708827
10^{-3}	0.00708427	10^{-8}	0.00708827
10^{-4}	0.00708787	10^{-9}	0.00708827
10^{-5}	0.00708823	10^{-10}	0.00708816

Table 6.3: Integral values of $I[1,1,\epsilon]$ using Method 3 (Satz's integral).

close to the exact answer only for $\epsilon = 10^{-2} - 10^{-3}$. However, unlike Method 0, this is actually improvable quite easily. With MinRecursion increased to 3 and adopting Double-Exponential method, the results we get are shown in Table 6.3. This is actually much more stable than even the numerical contour integral (without optimization), since the range of convergence can be extended to 10^{-9} and with more effort and time for even smaller ϵ while for numerical contour we just performed, it was good as it is for $\epsilon \sim 10^{-5}$. Unfortunately, we will see later that this benefit only appears because the Wightman function $W_\epsilon(u, u-s)$ happens to be independent of u in this case; this effectively reduced the problem to products of single integrals. For more complicated trajectories and spacetimes, this will not be the case (e.g. the case with moving mirrors in Chapter 5) and the double integral no longer factors.

Method 4: Juárez-Aubry's integral

In [67], the transition probability is rewritten as the following integral:

$$\begin{aligned} I_4[\Omega,\sigma] \coloneqq & -\frac{\Omega}{4\pi}\int_{\mathbb{R}} \mathrm{d}u[\chi(u)]^2 + \frac{1}{2\pi^2}\int_0^\infty \frac{1}{s^2}\int_{\mathbb{R}} \mathrm{d}u\chi(u)\left(\chi(u)-\chi(u-s)\right) \\ & + 2\int_{\mathbb{R}} \mathrm{d}u \int_0^\infty \mathrm{d}s\chi(u)\chi(u-s)\mathrm{Re}\left(e^{-i\Omega s}\left(W(u,u-s)+\frac{1}{4\pi^2 s^2}\right)\right) \end{aligned} \tag{6.13}$$

Note that this form was supposed to be advantageous because it *eliminates the regulator*, i.e. there is no $i\epsilon$ anywhere [67]. For an inertial detector in free space, the second line is identically zero[9]. So what remains are the first two terms. The first two terms are

[9]This is because the Wightman function is cancelled exactly by the $1/(4\pi^2 s^2)$. Note that we need to modify here the full integral in [67] by a factor of 2π because the derivative coupling Wightman function in $(1+1)$ dimensions differs from the usual Wightman function in $(3+1)$ dimensions by a prefactor of 2π.

completely finite and hence evaluating the integral yields ($\Omega = \sigma = 1$)

$$I_4 \approx 0.00708827\,, \tag{6.14}$$

as expected. Since there is no ϵ, this method either works or does not work. A subtle point is that the second term involving $1/s^2$ is in fact a *principal value integral*: one would need to actually ask Mathematica to recognize this by using PrincipalValue $\to$ True, otherwise the integral diverges.

Interestingly, [67] actually provided an equivalent integral given by

$$\begin{aligned} I_4[\Omega,\sigma] \coloneqq & -\frac{\Omega\Theta(-\Omega)}{2\pi}\int_{\mathbb{R}} \mathrm{d}u[\chi(u)]^2 + \frac{1}{2\pi^2}\int_0^\infty \frac{\cos\Omega s}{s^2}\int_{\mathbb{R}} \mathrm{d}u\chi(u)\left(\chi(u)-\chi(u-s)\right) \\ & + 2\int_{\mathbb{R}}\mathrm{d}u\int_0^\infty \mathrm{d}s\chi(u)\chi(u-s)\mathrm{Re}\left(e^{-i\Omega s}\left(W(u,u-s)+\frac{1}{4\pi^2 s^2}\right)\right) \end{aligned} \tag{6.15}$$

which modifies the first two terms. Unlike the previous form, the second term involving $\cos\Omega s/s^2$ is now a well-defined integral on its own and not strictly a principal value integral. Of course the answer is the same.

6.3 Why should we do numerical contour integration?

Recall that our integral can be slightly generalized to take the form

$$I_{\mathrm{gen}}[\Omega,\sigma,\epsilon] := \iint_{\mathbb{R}^2} \mathrm{d}t\,\mathrm{d}T\, e^{-\frac{t^2}{2\sigma^2}} e^{-\frac{T^2}{2\sigma^2}} e^{-i\Omega(t-T)} W_\epsilon(t,T)\,, \tag{6.16}$$

where we put subscript ϵ to make explicit that the Wightman function in general has ϵ as UV regulator. We focus on Gaussian switching so we do not write $\chi(t)$ in place of the Gaussian.

Based on the previous section, it looks as if Method 4 (Juárez-Aubry's integral) should be the best; it involves a completely real-valued integral over the real line/plane, and no regulator that pushes things to the complex plane. It should, if anything, give uniquely correct result. The rest of the methods has to be parameterized by ϵ which may perform better or worse depending on situations. Unfortunately, in exchange for clarity and simplicity of our discussion, it turns out that Method 4 is only unambiguously the winner for inertial detectors in free space.

To see this, consider the derivative coupling Wightman function for $(1+1)$ dimensional

spacetime in the presence of a static mirror (cf. Chapter 5), given by

$$\mathcal{A}_\epsilon(t,T,d) := -\frac{1}{2\pi(t-T-i\epsilon)^2} + \frac{1}{4\pi(t-T+2d-i\epsilon)^2} + \frac{1}{4\pi(t-T-2d-i\epsilon)^2} \tag{6.17}$$

where d is the distance away from the mirror fixed at the origin $x = 0$. The first term corresponds to the free-space Wightman function for derivative coupling, but now we have additional two terms are contributions due to the mirror. Now if we multiply this by $1/(2\pi)$ so that the first term mimics the free-space case in $(3+1)$ dimensions, inserting $\mathcal{A}_0(u, u-v, d)$ (setting $\epsilon = 0$) in place of $\mathcal{W}(u, u-v)$ into I_4, the regular part of the integral becomes $(d > 0)$

$$I'_{4,\text{reg}} = 2\int_{\mathbb{R}} \mathrm{d}u \int_0^\infty \mathrm{d}s \chi(u)\chi(u-s)\mathrm{Re}\left(e^{-i\Omega s}\left(\frac{1}{8\pi^2(v-2d)^2} + \frac{1}{8\pi^2(v+2d)^2}\right)\right). \tag{6.18}$$

Notice that now we are in trouble: the integrand now contains second-order poles at $v = \pm 2d$ and as it is, this integral will diverge! The simplest way to solve this is to reinstate $i\epsilon$ on these mirror-dependent terms. This problem naturally persists for most Wightman functions that contain singularities that cannot be cancelled purely by the $1/s^2$ term in the regular part of the integral. One is then forced to reinstate the $i\epsilon$ prescription on these d-dependent terms to regulate the integral.

On the other hand, Method 2 (numerical contour integration) continues to apply verbatim. For the static mirror scenario, one simply has to break the integral into three parts: the free part which has poles at $t = T$ and two pieces from the mirror with poles at $t = T \pm 2d$. It can again be shown that for large range of ϵ parameterizing the size of the contour, the integral value does not change as required by the deformation theorem.

To make the comparison slightly more explicit, we show the results comparing Method 2, 3 and 4 (contour, Satz, and Juárez-Aubry respectively) for the static mirror above[10] in Figure 6.2. For each method, we plot 50 data points. We also tried to disable the SymbolicProcessing command in order to speed up calculation (essentially asking Mathematica not to try too hard to transform the integral into something nicer). To make comparison slightly fairer, we set MinRecursion to 3 and MaxRecursion to 20 (as one of the methods perform better in this). As it turns out, numerical contour integration in these settings took 70 seconds for all 50 data points, gives the correct result for all d, and largely independent of choice of ϵ (the smaller the ϵ, the integral is slightly slower). Juárez-Aubry integral took 63 seconds but fails near $d = 0$ (as seen from the dotted red curve). Satz integral

[10] Now we use a $(1+1)$ Wightman function so all the 2π factors from before are not needed anymore.

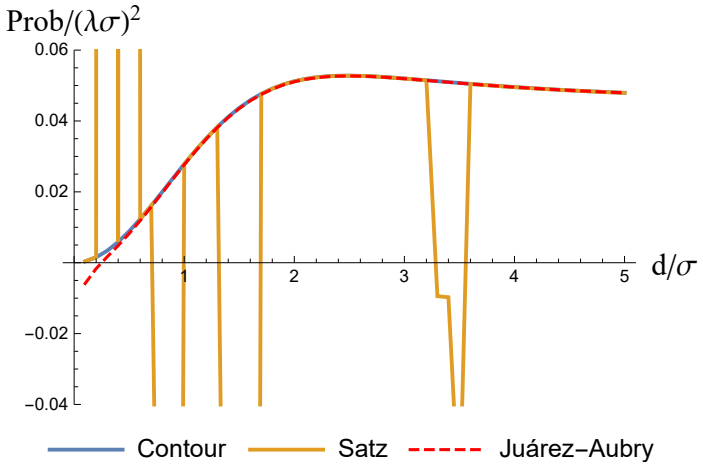

Figure 6.2: Comparing three methods for static mirror. For contour integral, we chose $\epsilon = 1/10$ since it is faster than smaller values (and the answer is constant). For Satz, we chose $\epsilon = 10^{-3}$ and for Juárez-Aubry, we chose $\epsilon = 10^{-2}$. It is clear that the contour integral gives the correct result for all d, while Juárez-Aubry integral fails near $d = 0$. Satz integral fluctuates at some places but remains correct otherwise; the fluctuations are purely numerical artefacts.

took 630 seconds in total, correctly giving the transition probability modulo numerical instabilities at several points; the points where it fluctuates change with ϵ, thus it is purely numerical artifact. Therefore, in this simple example alone, we see that contour integration is superior, and this superiority is not obvious when one considers inertial detector in free-space.

Of course, Method 1 (analytic expression) is no longer available in this case and Method 0, which is simply direct integration of the default expression in Eq. (6.5), remains the worst method to use without (significant) further efforts in controlling errors. The only main disadvantages, as far as the author is aware of, regarding numerical contour integration is that (1) for complicated Wightman functions, the integral does not always behave very well under domain truncation and when the poles are near the endpoints of the domain of integration; (2) if the Wightman functions are *logarithms* (hence no poles but branch cuts instead), then the method does not apply as it is; one may need to investigate specific contours (so-called "keyhole" contours, etc.) and how to implement them *easily*. How to deal with these is left for future investigation.

As a side remark, we have also checked that Method 2 works as well for computations of *transition rate* in the manner done e.g. in [67–69]. Therefore, investigations involving transition rate calculations will also benefit from this approach.

6.4 Summary and conclusion

In this chapter we briefly discuss the problem of evaluating certain double integrals that often appear in investigations involving the Unruh-DeWitt model. We compared several known methods and demonstrate, to the best of the author's knowledge, that numerical contour integration is a superior way of computing these integrals numerically. This is somewhat surprising because Mathematica's documentation does not make it obvious that integration along the imaginary axis (which Mathematica obviously can do) can be exploited to perform an actual contour integration[11]. This chapter therefore serves as both a demonstration and a summary of how this could be done for readers interested in exploiting this method.

Given the breadth and depth of numerical analysis, much improvements can be possibly attained with further investigations, but for our purposes we chose to keep the depth to a minimum. This is partially motivated by the fact that most physicists are not numerical

[11]This possibility was partially found in other problems e.g. in `mathematica.stackexchange.com` and more obscure sections of Mathematica's documentation.

analysts, and requiring one to know the back-end processes of symbolic/numerical integration softwares somewhat defeats the purpose of such a high-level language. At the level of our discussion, it is good enough to solve problems encountered in Chapter 5 when we encounter derivative coupling of moving mirrors. We wish to apply this method to one of the most problematic integrals — namely, in the context of $(1+1)$-dimensional Vaidja spacetime [128]. We should also mention that in the works such as [67–69, 128], despite the seemingly complicated Wightman function for collapsing spacetime, the question of *transition rate* reduces the integral to one-dimensional integral, and hence the difficulties we face do not occur there. Our method will be relevant, therefore, for studies involving entanglement dynamics between two detectors where these double integrals will be prevalent.

The short story one should at least take away from this chapter is that even with well-defined integrands and reasonably powerful symbolic integration methods, often the "plug-in-and-integrate" and choose settings that hopefully optimize the results may not help. In our case, the use numerical contour integration, while not a completely new method in itself, was inspired by the deformation theorem. We demonstrated the numerical stability for some of the relevant but manifestly difficult integrals in line with the theorem. The usual $i\epsilon$ prescription, while theoretically equivalent to contour integrals, turns out to be not the same when implemented numerically. Worse, optimal settings are found only by case-by-case basis: depending on the Wightman functions and other choices of parameters, settings may need to be changed and it is almost an art to find these things.

It is this gulf between theoretical, mathematical and numerical computations that form the core of this chapter. It is hoped that this chapter can serve as a guide for further investigations involving similar integrals, and more improvements can be found with more widespread use. In fact, the most recent MAPLE 2019 has implemented a new integration method using differentiation[12] and delta functions [129–131]. Whether these new methods would prove superior or even complement our proposed method will be of future interest.

[12] I thank Achim Kempf for bringing this to my attention.

Chapter 7

Final thoughts

The primary goal of this thesis was to present three modest results on the Unruh-DeWitt model applied to three different setups involving bosonic quantum field theory with non-trivial boundary conditions. The secondary goal was to discuss subtleties and difficulties and propose improved solutions in performing relevant integrals that appear in investigations involving Unruh-DeWitt model. Before concluding this thesis, it is perhaps a good time to briefly look back at what has been done and what could be pursued from now on.

Weak equivalence principle (WEP) has been at the centre stage of many attempts at formulating a quantum theory of gravity. It is not surprising that many believe this principle should be broken either at some scale or by some other processes in which quantum gravitational effects become important. There are several formulations of and tests of WEP, classical or otherwise, which have been proposed and tested (see e.g. [132–135]). At least within the regime when gravitational field is not quantized or treated non-classically, these tests suggest that WEP should be maintained. Our first result, somewhat different in spirit, by studying an atomic detector accelerating in a static cavity and vice versa, and checking the responses in various situations, complement these results. One message to take away is perhaps this: one should not expect violation of WEP in presence of any quantum test masses or probes, background fields, etc. unless it modifies the gravitational sector in some non-trivial way. This could be e.g. via non-minimal coupling, higher curvature gravity, direct quantization of gravitational field or quantum reference frames (see e.g. [136–138] for a discussion of quantum reference frames). How quantum reference frames can be applied to curved spacetimes is an interesting future pursuit.

The second result concerning the zero mode of a quantum field shows that there are operational implications when one attempts to ignore something that may appear harmless.

The zero mode, which has no Fock vacuum, seems to suggest that it should be discarded if one were to work with the massless field theory in two dimensions. We showed that this cannot be done if we wish to maintain relativistic causality, as the detector couples to that mode as well as other oscillatory modes of the field. It is also known that zero modes have led to problems in properly quantizing fields e.g. in de Sitter spacetimes [87, 90], and it is interesting to see if Unruh-DeWitt model sees something different. While our results do not solve the zero mode problem, our result shows at least that the Unruh-DeWitt model cares about the zero mode in order to respect some of the basic relativistic principles.

The third result concerning entanglement harvesting in moving mirror spacetimes fills a gap in the literature where most studies have involved some high degree of symmetry. In [43, 47, 50, 58, 62, 82], all of them have enough symmetry — at the very least time translation symmetry — which could render the computation of the density matrix manageable even in the presence of non-trivial curvature. The study of moving mirrors is attractive because they are known to be quite experimentally tenable (see e.g. [139, 140]). Lacking symmetries, Unruh and Hawking-like effects with moving mirrors were then studied in certain asymptotic limits where some degrees of symmetry is recovered. Here we take the problem head-on and evaluate the entanglement dynamics between two detectors coupled to the field with moving mirrors. We find that mirrors impact entanglement of the detectors in new ways, some of which closely resemble horizon effects in black hole spacetimes. Our result is more operational in contrast to the computations done e.g. in [141] or holographic calculations. A natural forward direction is to apply the model to holographic spacetimes or collapsing spacetime models such as Vaidja spacetimes.

Finally, our discussion on numerical schemes illustrate that some of the most common integrals in Unruh-DeWitt models are in fact difficult to integrate reliably, even if their expressions do not make it appear so. In facing these difficulties, we borrowed insights from complex analysis — the deformation theorem [127] — to modify the practical implementation from $i\epsilon$ to numerical contour integration. We make comparison with several known methods, and show that in a certain sense at least that this method is superior. This would be of interest for more complicated integrals e.g. in the context of QFT in Vaidja spacetime [128]. It would also be interesting to compare how these rather difficult integrals fare in the face of "integration by differentiation" recently developed in [129–131] and implemented in the latest MAPLE 2019 software, in contrast to Mathematica's methods.

The Unruh-DeWitt model has become central in the studies of quantum field theory in curved spacetimes and relativistic quantum information. It is mostly limited by perturbative calculations, which can be avoided with judicious setup and specific purposes, and the fact that it should couple semi-classically to the background field. It remains to be seen if the model can help us study beyond semi-classical limit, e.g. implementing it under quan-

tum reference frame settings, or using the model or its modification to quantized models of gravity, higher curvature gravity, spacetimes with holographic duals, interacting fields, etc. In many of these instances, even with perturbation theory certain numerical implementations may be needed which to the author's knowledge is not very well-developed due to the distributional nature of the two-point functions. Yet another interesting avenue is to see if there is a way to embed Unruh-DeWitt models to path-integral formalism: the reason is because interacting fields tend to admit nice treatments in terms of path integrals, e.g. as is done here [142]. Our results here are modest attempts to fill some gaps in the existing but already extensive literature of Unruh-DeWitt model applied to QFT in curved spacetimes.

References

[1] S. A. Fulling and J. H. Wilson, *The Equivalence Principle at Work in Radiation from Unaccelerated Atoms and Mirrors*, 1805.01013.

[2] A. Dragan, I. Fuentes and J. Louko, *Quantum accelerometer: Distinguishing inertial Bob from his accelerated twin Rob by a local measurement*, *Phys. Rev. D* **83** (2011) 085020.

[3] N. Birrell, N. Birrell and P. Davies, *Quantum Fields in Curved Space*, Cambridge Monographs on Mathematical Physics. Cambridge University Press, 1984.

[4] R. Wald, *General Relativity*. University of Chicago Press, 2010.

[5] R. A. Hennigar, E. Tjoa and R. B. Mann, *Thermodynamics of hairy black holes in Lovelock gravity*, *Journal of High Energy Physics* **2017** (2017) 70.

[6] R. A. Hennigar, R. B. Mann and E. Tjoa, *Superfluid black holes*, *Phys. Rev. Lett.* **118** (2017) 021301.

[7] M. A. Nielsen and I. L. Chuang, *Quantum Computation and Quantum Information: 10th Anniversary Edition*. Cambridge University Press, New York, NY, USA, 10th ed., 2011.

[8] S. W. Hawking, *Particle creation by black holes*, *Communications in Mathematical Physics* **43** (1975) 199.

[9] W. G. Unruh and R. M. Wald, *Information loss*, *Reports on Progress in Physics* **80** (2017) 092002.

[10] T. Jacobson and P. Nguyen, *Diffeomorphism invariance and the black hole information paradox*, 1904.04434.

[11] S. J. Summers and R. Werner, *The vacuum violates Bell's inequalities*, *Physics Letters A* **110** (1985) 257 .

[12] S. J. Summers and R. Werner, *Bell's inequalities and quantum field theory. I. General setting*, *Journal of Mathematical Physics* **28** (1987) 2440 [https://doi.org/10.1063/1.527733].

[13] S. J. Summers and R. Werner, *Maximal violation of bell's inequalities is generic in quantum field theory*, *Comm. Math. Phys.* **110** (1987) 247.

[14] E. Witten, *Aps medal for exceptional achievement in research: Invited article on entanglement properties of quantum field theory*, *Rev. Mod. Phys.* **90** (2018) 045003.

[15] S. Ryu and T. Takayanagi, *Holographic derivation of entanglement entropy from the anti–de sitter space/conformal field theory correspondence*, *Phys. Rev. Lett.* **96** (2006) 181602.

[16] T. Faulkner, F. M. Haehl, E. Hijano, O. Parrikar, C. Rabideau and M. Van Raamsdonk, *Nonlinear gravity from entanglement in conformal field theories*, *Journal of High Energy Physics* **2017** (2017) 57.

[17] D. Neuenfeld, K. Saraswat and M. Van Raamsdonk, *Positive gravitational subsystem energies from cft cone relative entropies*, *Journal of High Energy Physics* **2018** (2018) 50.

[18] B. Czech, J. L. Karczmarek, F. Nogueira and M. V. Raamsdonk, *Rindler quantum gravity*, *Classical and Quantum Gravity* **29** (2012) 235025.

[19] R. Sorkin, *Impossible Measurements on Quantum Fields*, vol. 2, pp. 293–305. Cambridge University Press, 1956. 10.1017/CBO9780511524653.024.

[20] W. G. Unruh, *Notes on black-hole evaporation*, *Phys. Rev. D* **14** (1976) 870.

[21] B. S. Dewitt, *Quantum gravity: the new synthesis.*, in *General Relativity: An Einstein centenary survey*, S. W. Hawking and W. Israel, eds., pp. 680–745, 1979.

[22] A. Valentini, *Non-local correlations in quantum electrodynamics*, *Physics Letters A* **153** (1991) 321 .

[23] B. Reznik, *Entanglement from the vacuum*, *Found. Phys.* **33** (2003) 167 [quant-ph/0212044].

[24] A. Peres and D. R. Terno, *Quantum information and relativity theory*, *Rev. Mod. Phys.* **76** (2004) 93.

[25] P. M. Alsing and G. J. Milburn, *Teleportation with a uniformly accelerated partner*, *Phys. Rev. Lett.* **91** (2003) 180404.

[26] P. M. Alsing and I. Fuentes, *Observer-dependent entanglement*, *Classical and Quantum Gravity* **29** (2012) 224001.

[27] A. G. S. Landulfo and G. E. A. Matsas, *Sudden death of entanglement and teleportation fidelity loss via the unruh effect*, *Phys. Rev. A* **80** (2009) 032315.

[28] A. G. S. Landulfo, *Nonperturbative approach to relativistic quantum communication channels*, *Phys. Rev. D* **93** (2016) 104019.

[29] I. Khavkine and V. Moretti, *Algebraic QFT in Curved Spacetime and Quasifree Hadamard States: An Introduction*, pp. 191–251. Springer International Publishing, Cham, 2015.

[30] M. Peskin and D. Schroeder, *An Introduction to Quantum Field Theory*, Advanced book classics. Avalon Publishing, 1995.

[31] T. Lancaster, S. Blundell and S. Blundell, *Quantum Field Theory for the Gifted Amateur*. OUP Oxford, 2014.

[32] R. Wald, *Quantum Field Theory in Curved Spacetime and Black Hole Thermodynamics*, Chicago Lectures in Physics. University of Chicago Press, 1994.

[33] Jürg Fröhlich, *On the triviality of $\lambda\phi^4_d$ theories and the approach to the critical point in $d_{(-)} > 4$ dimensions*, *Nuclear Physics B* **200** (1982) 281 .

[34] M. Aizenman, *Proof of the triviality of ϕ^4_d field theory and some mean-field features of ising models for $d > 4$*, *Phys. Rev. Lett.* **47** (1981) 1.

[35] T. Hattori, *A generalization of the proof of the triviality of scalar field theories*, *Journal of Mathematical Physics* **24** (1983) 2200 [https://doi.org/10.1063/1.525932].

[36] M. Schwartz, *Quantum Field Theory and the Standard Model*, Quantum Field Theory and the Standard Model. Cambridge University Press, 2014.

[37] R. Lopp, E. Martín-Martínez and D. N. Page, *Relativity and quantum optics: accelerated atoms in optical cavities*, *Classical and Quantum Gravity* **35** (2018) 224001.

[38] S.-Y. Lin, C.-H. Chou and B. L. Hu, *Quantum teleportation between moving detectors*, *Phys. Rev. D* **91** (2015) 084063.

[39] S.-Y. Lin, *Notes on nonlocal projective measurements in relativistic systems*, *Annals of Physics* **351** (2014) 773 .

[40] B. L. Hu, S.-Y. Lin and J. Louko, *Relativistic quantum information in detectors-field interactions*, *Classical and Quantum Gravity* **29** (2012) 224005.

[41] D. M. T. Benincasa, L. Borsten, M. Buck and F. Dowker, *Quantum information processing and relativistic quantum fields*, *Classical and Quantum Gravity* **31** (2014) 075007.

[42] E. Martín-Martínez and P. Rodriguez-Lopez, *Relativistic quantum optics: The relativistic invariance of the light-matter interaction models*, *Phys. Rev. D* **97** (2018) 105026.

[43] A. Pozas-Kerstjens and E. Martín-Martínez, *Harvesting correlations from the quantum vacuum*, *Phys. Rev. D* **92** (2015) 064042.

[44] S. Takagi, *Vacuum Noise and Stress Induced by Uniform Acceleration: Hawking-Unruh Effect in Rindler Manifold of Arbitrary Dimension*, *Progress of Theoretical Physics Supplement* **88** (1986) 1.

[45] L. C. B. Crispino, A. Higuchi and G. E. A. Matsas, *The Unruh effect and its applications*, *Rev. Mod. Phys.* **80** (2008) 787.

[46] C. J. Fewster and R. Verch, *Quantum fields and local measurements*, 1810.06512.

[47] P. Simidzija and E. Martín-Martínez, *Nonperturbative analysis of entanglement harvesting from coherent field states*, *Phys. Rev. D* **96** (2017) 065008.

[48] P. Simidzija, R. H. Jonsson and E. Martín-Martínez, *General no-go theorem for entanglement extraction*, *Phys. Rev. D* **97** (2018) 125002.

[49] J. de Ramón, L. J. Garay and E. Martín-Martínez, *Direct measurement of the two-point function in quantum fields*, *Phys. Rev. D* **98** (2018) 105011.

[50] A. Pozas-Kerstjens, J. Louko and E. Martín-Martínez, *Degenerate detectors are unable to harvest spacelike entanglement*, *Phys. Rev. D* **95** (2017) 105009.

[51] E. G. Brown, E. Martín-Martínez, N. C. Menicucci and R. B. Mann, *Detectors for probing relativistic quantum physics beyond perturbation theory*, *Phys. Rev. D* **87** (2013) 084062.

[52] S.-Y. Lin and B. L. Hu, *Backreaction and the Unruh effect: New insights from exact solutions of uniformly accelerated detectors*, *Phys. Rev. D* **76** (2007) 064008.

[53] P. R. Johnson and B. L. Hu, *Stochastic theory of relativistic particles moving in a quantum field: Scalar Abraham-Lorentz-Dirac-Langevin equation, radiation reaction, and vacuum fluctuations*, *Phys. Rev. D* **65** (2002) 065015.

[54] S.-Y. Lin, C.-H. Chou and B. L. Hu, *Entanglement dynamics of detectors in an Einstein cylinder*, *Journal of High Energy Physics* **2016** (2016) 47.

[55] E. Martín-Martínez, A. R. H. Smith and D. R. Terno, *Spacetime structure and vacuum entanglement*, *Phys. Rev. D* **93** (2016) 044001.

[56] A. Sachs, R. B. Mann and E. Martín-Martínez, *Entanglement harvesting and divergences in quadratic Unruh-DeWitt detector pairs*, *Phys. Rev. D* **96** (2017) 085012.

[57] E. Martín-Martínez, *Causality issues of particle detector models in QFT and quantum optics*, *Phys. Rev. D* **92** (2015) 104019.

[58] L. J. Henderson, R. A. Hennigar, R. B. Mann, A. R. H. Smith and J. Zhang, *Harvesting entanglement from the black hole vacuum*, *Classical and Quantum Gravity* **35** (2018) 21LT02.

[59] L. Hodgkinson, *Particle detectors in curved spacetime quantum field theory*, Ph.D. thesis, 2013.

[60] K. K. Ng, L. Hodgkinson, J. Louko, R. B. Mann and E. Martín-Martínez, *Unruh-DeWitt detector response along static and circular-geodesic trajectories for Schwarzschild–anti-de Sitter black holes*, *Phys. Rev. D* **90** (2014) 064003.

[61] K. K. Ng, R. B. Mann and E. Martín-Martínez, *Over the horizon: Distinguishing the Schwarzschild spacetime and the $\mathbb{RP}^3$ spacetime using an Unruh-DeWitt detector*, *Phys. Rev. D* **96** (2017) 085004.

[62] K. K. Ng, R. B. Mann and E. Martín-Martínez, *Unruh-DeWitt detectors and entanglement: The anti–de Sitter space*, *Phys. Rev. D* **98** (2018) 125005.

[63] A. Ahmadzadegan, R. B. Mann and E. Martin-Martinez, *Measuring motion through relativistic quantum effects*, *Phys. Rev. A* **90** (2014) 062107.

[64] E. Tjoa, R. B. Mann and E. Martín-Martínez, *Particle detectors, cavities, and the weak equivalence principle*, *Phys. Rev. D* **98** (2018) 085004.

[65] E. Tjoa and E. Martín-Martínez, *Zero mode suppression of superluminal signals in light-matter interactions*, *Phys. Rev. D* **99** (2019) 065005.

[66] W. Cong, E. Tjoa and R. B. Mann, *Entanglement Harvesting with Moving Mirrors*, 1810.07359.

[67] B. A. Juárez-Aubry and J. Louko, *Onset and decay of the 1+1 Hawking-Unruh effect: what the derivative-coupling detector saw*, *Classical and Quantum Gravity* **31** (2014) 245007.

[68] L. Hodgkinson and J. Louko, *How often does the Unruh-DeWitt detector click beyond four dimensions?*, *Journal of Mathematical Physics* **53** (2012) 082301.

[69] J. Louko and A. Satz, *Transition rate of the Unruh-DeWitt detector in curved spacetime*, *Class. Quant. Grav.* **25** (2008) 055012.

[70] A. Pozas-Kerstjens and E. Martín-Martínez, *Entanglement harvesting from the electromagnetic vacuum with hydrogenlike atoms*, *Phys. Rev. D* **94** (2016) 064074.

[71] A. Ahmadzadegan, E. Martin-Martinez and R. B. Mann, *Cavities in curved spacetimes: the response of particle detectors*, *Phys. Rev. D* **89** (2014) 024013.

[72] M. O. Scully, S. Fulling, D. M. Lee, D. N. Page, W. P. Schleich and A. A. Svidzinsky, *Quantum optics approach to radiation from atoms falling into a black hole*, *Proceedings of the National Academy of Sciences* **115** (2018) 8131.

[73] B. Schutz, *A First Course in General Relativity*. Cambridge University Press, 2009.

[74] G. Herglotz, *über den vom standpunkt des relativitätsprinzips aus als starr zu bezeichnenden körper*, *Ann. Phys. (Leipzig)* **31** (1910) 393.

[75] F. Noether, *Zur kinematik des starren körpers in der relativtheorie*, *Ann. Phys. (Leipzig)* **31** (1910) 919.

[76] R. J. Epp, R. B. Mann and P. L. McGrath, *Rigid motion revisited: Rigid quasilocal frames*, *Class. Quant. Grav.* **26** (2009) 035015.

[77] F. Kiałka, A. R. H. Smith, M. Ahmadi and A. Dragan, *Massive unruh particles cannot be directly observed*, *Phys. Rev. D* **97** (2018) 065010.

[78] L. Sriramkumar and T. Padmanabhan, *Finite-time response of inertial and uniformly accelerated Unruh-DeWitt detectors*, *Classical and Quantum Gravity* **13** (1996) 2061.

[79] H. Lass, *Accelerating frames of reference and the clock paradox*, *American Journal of Physics* **31** (1963) 274.

[80] "*NIST Digital Library of Mathematical Functions*." http://dlmf.nist.gov/, Release 1.0.18 of 2018-03-27.

[81] R. Haag and D. Kastler, *An algebraic approach to quantum field theory*, *Journal of Mathematical Physics* **5** (1964) 848.

[82] P. Simidzija and E. Martin-Martinez, *All coherent field states entangle equally*, *Phys. Rev. D* **96** (2017) 025020.

[83] E. Martín-Martínez and J. Louko, *Particle detectors and the zero mode of a quantum field*, *Phys. Rev. D* **90** (2014) 024015.

[84] P. Francesco, P. Mathieu and D. Senechal, *Conformal Field Theory*. Island Press, 1996.

[85] B. Allen and A. Folacci, *Massless minimally coupled scalar field in de sitter space*, *Phys. Rev. D* **35** (1987) 3771.

[86] K. Kirsten and J. Garriga, *Massless minimally coupled fields in de sitter space: O(4)-symmetric states versus de sitter–invariant vacuum*, *Phys. Rev. D* **48** (1993) 567.

[87] D. N. Page and X. Wu, *Massless scalar field vacuum in de sitter spacetime*, *Journal of Cosmology and Astroparticle Physics* **2012** (2012) 051.

[88] J. Bros, H. Epstein and U. Moschella, *Scalar tachyons in the de sitter universe*, *Letters in Mathematical Physics* **93** (2010) 203.

[89] J. Louko and V. Toussaint, *Unruh-DeWitt detector's response to fermions in flat spacetimes*, *Phys. Rev. D* **94** (2016) 064027.

[90] Y. K. Yazdi, *Zero modes and entanglement entropy*, *J. High Energ. Phys.* **2017** (2017) 140.

[91] S. Robles and J. Rodríguez-Laguna, *Local quantum thermometry using unruh-dewitt detectors*, *Journal of Statistical Mechanics: Theory and Experiment* **2017** (2017) 033105.

[92] E. G. Brown, *Thermal amplification of field-correlation harvesting*, *Phys. Rev. A* **88** (2013) 062336.

[93] W. Brenna, R. B. Mann and E. Martín-Martínez, *Anti-Unruh phenomena*, *Physics Letters B* **757** (2016) 307 .

[94] D. Hümmer, E. Martín-Martínez and A. Kempf, *Renormalized unruh-dewitt particle detector models for boson and fermion fields*, *Phys. Rev. D* **93** (2016) 024019.

[95] K. Lorek, D. Pecak, E. G. Brown and A. Dragan, *Extraction of genuine tripartite entanglement from the vacuum*, *Phys. Rev. A* **90** (2014) 032316.

[96] M. Cliche and A. Kempf, *Relativistic quantum channel of communication through field quanta*, *Phys. Rev. A* **81** (2010) 012330.

[97] R. H. Jonsson, E. Martín-Martínez and A. Kempf, *Information transmission without energy exchange*, *Phys. Rev. Lett.* **114** (2015) 110505.

[98] A. Pozas-Kerstjens, J. Louko and E. Martín-Martínez, *Degenerate detectors are unable to harvest spacelike entanglement*, *Phys. Rev. D* **95** (2017) 105009.

[99] G. Arfken, H. Weber and F. Harris, *Mathematical Methods for Physicists: A Comprehensive Guide*. Elsevier Science, 2011.

[100] A. Blasco, L. J. Garay, M. Martín-Benito and E. Martín-Martínez, *Violation of the Strong Huygen's Principle and Timelike Signals from the Early Universe*, *Phys. Rev. Lett.* **114** (2015) 141103.

[101] A. Blasco, L. J. Garay, M. Martín-Benito and E. Martín-Martínez, *Timelike information broadcasting in cosmology*, *Phys. Rev. D* **93** (2016) 024055.

[102] S. Sonego and V. Faraoni, *Huygens' principle and characteristic propagation property for waves in curved space-times*, *Journal of Mathematical Physics* **33** (1992) 625.

[103] V. Faraoni and E. Gunzig, *Tales of tails in cosmology*, *International Journal of Modern Physics D* **08** (1999) 177.

[104] S. Dubovsky, A. Nicolis, E. Trincherini and G. Villadoro, *Microcausality in curved space-time*, *Phys. Rev. D* **77** (2008) 084016.

[105] A. S. Wightman, *Cargèse Lectures in Theoretical Physics, 1964, edited by M, Lévy (New York, NY, 1967)* .

[106] N. Nakanishi, *Free massless scalar field in two-dimensional space-time*, *Progress of Theoretical Physics* **57** (1977) 269.

[107] G. Morchio, D. Pierotti and F. Strocchi, *Infrared and vacuum structure in two-dimensional local quantum field theory models. the massless scalar field*, *Journal of Mathematical Physics* **31** (1990) 1467.

[108] L. Bombelli, R. K. Koul, J. Lee and R. D. Sorkin, *Quantum source of entropy for black holes*, *Phys. Rev. D* **34** (1986) 373.

[109] M. Srednicki, *Entropy and area*, *Phys. Rev. Lett.* **71** (1993) 666.

[110] G. Salton, R. B. Mann and N. C. Menicucci, *Acceleration-assisted entanglement harvesting and rangefinding*, *New J. Phys.* **17** (2015) 035001.

[111] A. Pozas-Kerstjens and E. Martín-Martínez, *Harvesting correlations from the quantum vacuum*, *Phys. Rev. D* **92** (2015) 064042.

[112] G. V. Steeg and N. C. Menicucci, *Entangling power of an expanding universe*, *Phys. Rev. D* **79** (2009) 044027.

[113] C. M. Wilson, G. Johansson, A. Pourkabirian, M. Simoen, J. R. Johansson, D. T. et al., *Observation of the dynamical Casimir effect in a superconducting circuit*, *Nature* **479** (2011) 376.

[114] P. Lähteenmäki, G. S. Paraoanu, J. Hassel and P. J. Hakonen, *Dynamical Casimir effect in a Josephson metamaterial*, *Proceedings of the National Academy of Sciences* **110** (2013) 4234 [https://www.pnas.org/content/110/11/4234.full.pdf].

[115] N. Suzuki, *Accelerated detector nonlinearly coupled to a scalar field*, *Classical and Quantum Gravity* **14** (1997) 3149.

[116] P. C. W. Davies, Z. X. Liu and A. C. Ottewill, *Particle detectors in the presence of boundaries*, *Classical and Quantum Gravity* **6** (1989) 1041.

[117] R. D. Carlitz and R. S. Willey, *Reflections on moving mirrors*, *Phys. Rev. D* **36** (1987) 2327.

[118] M. R. R. Good, P. R. Anderson and C. R. Evans, *Time dependence of particle creation from accelerating mirrors*, *Phys. Rev. D* **88** (2013) 025023.

[119] M. R. R. Good, P. R. Anderson and C. R. Evans, *Mirror reflections of a black hole*, *Phys. Rev. D* **94** (2016) 065010.

[120] M. R. R. Good, K. Yelshibekov and Y. C. Ong, *On horizonless temperature with an accelerating mirror*, *Journal of High Energy Physics* **2017** (2017) 13.

[121] M. R. R. Good and E. V. Linder, *Eternal and evanescent black holes and accelerating mirror analogs*, *Phys. Rev. D* **97** (2018) 065006.

[122] L. J. Henderson, R. A. Hennigar, R. B. Mann, A. R. H. Smith and J. Zhang, *Entangling detectors in anti-de sitter space*, *Journal of High Energy Physics* **2019** (2019) 178.

[123] E. Martín-Martínez and J. Louko, $(1+1)D$ *Calculation Provides Evidence that Quantum Entanglement Survives a Firewall*, *Phys. Rev. Lett.* **115** (2015) 031301.

[124] R. M. Corless, G. H. Gonnet, D. E. G. Hare, D. J. Jeffrey and D. E. Knuth, *On the Lambert-W function*, *Advances in Computational Mathematics* **5** (1996) 329.

[125] P. R. Anderson, M. R. R. Good and C. R. Evans, *Black hole - moving mirror I: An exact correspondence*, pp. 1701–1704. $10.1142/9789813226609_0171$.

[126] M. R. R. Good, P. R. Anderson and C. R. Evans, *Black hole - moving mirror II: Particle creation*, pp. 1705–1708. 10.1142.

[127] J. Howie, *Complex Analysis*, Springer Undergraduate Mathematics Series. Springer London, 2003.

[128] B. A. Juárez-Aubry and J. Louko, *Quantum fields during black hole formation: how good an approximation is the Unruh state?*, *Journal of High Energy Physics* **2018** (2018) 140.

[129] A. Kempf, D. M. Jackson and A. H. Morales, *New dirac delta function based methods with applications to perturbative expansions in quantum field theory*, *Journal of Physics A: Mathematical and Theoretical* **47** (2014) 415204.

[130] A. Kempf, D. M. Jackson and A. H. Morales, *How to (path-) integrate by differentiating*, *Journal of Physics: Conference Series* **626** (2015) 012015.

[131] D. Jia, E. Tang and A. Kempf, *Integration by differentiation: new proofs, methods and examples*, *Journal of Physics A: Mathematical and Theoretical* **50** (2017) 235201.

[132] G. Rosi, G. D'Amico, L. Cacciapuoti, F. Sorrentino, M. Prevedelli, M. Zych et al., *Quantum test of the equivalence principle for atoms in superpositions of internal energy eigenstates*, *Nature Commun.* **8** (2017) 5529 [1704.02296].

[133] M. Zych and v. Brukner, *Quantum formulation of the Einstein Equivalence Principle*, *Nature Phys.* **14** (2018) 1027 [1502.00971].

[134] C. M. Will, *Violation of the weak equivalence principle in theories of gravity with a nonsymmetric metric*, *Phys. Rev. Lett.* **62** (1989) 369.

[135] J. Bergé, P. Brax, G. Métris, M. Pernot-Borràs, P. Touboul and J.-P. Uzan, *Microscope mission: First constraints on the violation of the weak equivalence principle by a light scalar dilaton*, *Phys. Rev. Lett.* **120** (2018) 141101.

[136] A. Vanrietvelde, P. A. Hoehn, F. Giacomini and E. Castro-Ruiz, *A change of perspective: switching quantum reference frames via a perspective-neutral framework*, 1809.00556.

[137] F. Giacomini, E. Castro-Ruiz and v. Brukner, *Quantum mechanics and the covariance of physical laws in quantum reference frames*, *Nature Commun.* **10** (2019) 494 [1712.07207].

[138] L. Hardy, *Implementation of the Quantum Equivalence Principle*, in *Progress and Visions in Quantum Theory in View of Gravity: Bridging foundations of physics and mathematics Leipzig, Germany, October 1-5, 2018*, 2019, 1903.01289.

[139] C. M. Wilson, G. Johansson, A. Pourkabirian, M. Simoen, J. R. Johansson, T. Duty et al., *Observation of the dynamical Casimir effect in a superconducting circuit*, *Nature* **479** (2011) 376 [1105.4714].

[140] P. Chen and G. Mourou, *Accelerating plasma mirrors to investigate the black hole information loss paradox*, *Phys. Rev. Lett.* **118** (2017) 045001.

[141] P. Chen and D.-h. Yeom, *Entropy evolution of moving mirrors and the information loss problem*, *Phys. Rev. D* **96** (2017) 025016.

[142] W. G. Unruh and N. Weiss, *Acceleration radiation in interacting field theories*, *Phys. Rev. D* **29** (1984) 1656.

[143] R. H. Jonsson, E. Martín-Martínez and A. Kempf, *Quantum signaling in cavity QED*, *Phys. Rev. A* **89** (2014) 022330.

[144] Smith, Alexander R. H., *Detectors, reference frames, and time*, 2017.

[145] M. Okumura and Y. Yamanaka, *Proper treatment of the zero mode in quantum field theory for trapped Bose-Einstein condensation*, *Phys. Rev. A* **68** (2003) 013609.

[146] K. Yagdjian, *Huygens' principle for the Klein-Gordon equation in the de Sitter spacetime*, *Journal of Mathematical Physics* **54** (2013) 091503 [https://doi.org/10.1063/1.4821115].

[147] A. J. Tolley and N. Turok, *Quantization of the massless minimally coupled scalar field and the dS/CFT correspondence*, hep-th/0108119.

[148] N. Friis, A. R. Lee and J. Louko, *Scalar, spinor, and photon fields under relativistic cavity motion*, *Phys. Rev. D* **88** (2013) 064028.

[149] D. E. Bruschi, I. Fuentes and J. Louko, *Voyage to alpha centauri: Entanglement degradation of cavity modes due to motion*, *Phys. Rev. D* **85** (2012) 061701.

[150] D. N. Page, *Hawking radiation and black hole thermodynamics*, *New J. Phys.* **7** (2005) 203.

[151] T. Ohta and R. B. Mann, *Canonical reduction of two-dimensional gravity for particle dynamics*, *Class. Quant. Grav.* **13** (1996) 2585 [gr-qc/9605004].

[152] R. B. Mann and S. F. Ross, *The $D \to 2$ limit of general relativity*, *Class. Quant. Grav.* **10** (1993) 1405 [gr-qc/9208004].

[153] S.-Y. Lin, C.-H. Chou and B. L. Hu, *Quantum teleportation between moving detectors*, *Phys. Rev. D* **91** (2015) 084063.

[154] L. Sriramkumar and T. Padmanabhan, *Finite-time response of inertial and uniformly accelerated unruh - dewitt detectors*, *Classical and Quantum Gravity* **13** (1996) 2061.

[155] E. G. Brown and J. Louko, *Smooth and sharp creation of a Dirichlet wall in 1+1 quantum field theory: how singular is the sharp creation limit?*, *JHEP* **08** (2015) 061 [1504.05269].

[156] C. Romero and F. Dahia, *Theories of gravity in 2 + 1 dimensions*, *International Journal of Theoretical Physics* **33** (1994) 2091.

[157] A. L. C. Rego, H. O. Silva, D. T. Alves and C. Farina, *New signatures of the dynamical casimir effect in a superconducting circuit*, *Phys. Rev. D* **90** (2014) 025003.

Appendix A

Unruh-DeWitt models

A.1 Dyson expansion

We follow the derivation in [36]. First, we start from the time-ordered exponential

$$\begin{aligned}\hat{U}(t,t_0) &= \mathcal{T}\exp\left(-i\int_{t_0}^{t}\mathrm{d}\tau\,\hat{H}_I(\tau)\right)\\ &= \mathcal{T}\left[\mathbb{1} - i\int_{t_0}^{t}\mathrm{d}\tau\,\hat{H}_I(\tau) - \frac{1}{2!}\int_{t_0}^{t}\mathrm{d}\tau\int_{t_0}^{t}\mathrm{d}\tau'\,\hat{H}_I(\tau)\hat{H}_I(\tau') + ...\right]\\ &= \mathbb{1} - i\int_{t_0}^{t}\mathrm{d}\tau\,\hat{H}_I(\tau) - \frac{1}{2!}\int_{t_0}^{t}\mathrm{d}\tau\int_{t_0}^{t}\mathrm{d}\tau'\,\mathcal{T}\left[\hat{H}_I(\tau)\hat{H}_I(\tau')\right] + ...\,,\end{aligned} \tag{A.1}$$

where the second order term needs to be time-ordered because the interaction Hamiltonian $\hat{H}_I$ may not commute at different times. The definition of time-ordering for bosonic operators are

$$\mathcal{T}[\hat{A}(\tau)\hat{B}(\tau')] = \Theta(\tau-\tau')\hat{A}(\tau)\hat{B}(\tau') + \Theta(\tau'-\tau)\hat{B}(\tau')\hat{A}(\tau)\,, \tag{A.2}$$

where $\Theta(\cdot)$ is the Heaviside step function.

Inserting this into the previous expression,

$$\begin{aligned}\hat{U}(t,t_0) &= \mathbb{1} - i\int_{t_0}^{t} \mathrm{d}\tau\, \hat{H}_I(\tau) \\ &\quad - \frac{1}{2!}\int_{t_0}^{t}\mathrm{d}\tau \int_{t_0}^{t}\mathrm{d}\tau' \left(\Theta(\tau-\tau')\hat{H}_I(\tau)\hat{H}_I(\tau') + \Theta(\tau'-\tau)\hat{H}_I(\tau')\hat{H}_I(\tau)\right) + ... \\ &= \mathbb{1} - i\int_{t_0}^{t} \mathrm{d}\tau\, \hat{H}_I(\tau) - \frac{1}{2!}\int_{t_0}^{t}\mathrm{d}\tau \int_{t_0}^{\tau}\mathrm{d}\tau'\, \hat{H}_I(\tau)\hat{H}_I(\tau') \\ &\qquad\qquad - \frac{1}{2!}\int_{t_0}^{t}\mathrm{d}\tau' \int_{t_0}^{\tau'}\mathrm{d}\tau\, \hat{H}_I(\tau')\hat{H}_I(\tau) + \dots . \end{aligned} \tag{A.3}$$

Notice that the double integrals are identical under relabelling $\tau \leftrightarrow \tau'$. Therefore, we get

$$\hat{U}(\tau,\tau_0) = \mathbb{1} - i\int_{t_0}^{t} \mathrm{d}\tau\, \hat{H}_I(\tau) - \int_{t_0}^{t}\mathrm{d}\tau \int_{t_0}^{\tau}\mathrm{d}\tau'\, \hat{H}_I(\tau)\hat{H}_I(\tau') + \dots . \tag{A.4}$$

This final expression is used in many literature texts and we see the disappearance of $1/2!$ prefactor. In this thesis, since the switching function governs the duration of interaction, we are really computing a quantity which is usually called the $\hat{S}$-operator (as in the $\hat{S}$-matrix) in standard QFT [31, 36]:

$$\hat{U} \coloneqq \hat{U}(\infty,-\infty) \equiv \hat{S}\,, \tag{A.5}$$

that is, by setting $t_0 = -\infty$ and $t = \infty$.

Appendix B

Particle detectors and weak equivalence principle

B.1 Massless Klein-Gordon equation without conformal transformation

In this section we solve for the solution for the massless Klein-Gordon field equation without invoking conformal transformation of any sort. We quote again the standard Rindler coordinates for convenience:

$$t = \xi \sinh \eta \,, \qquad x = \xi \cosh \eta \,.$$

From the general Klein-Gordon field equation (cf. Eq. (3.1)) in this coordinate system, which gives the modified Bessel differential equation for the spatial modes $v(\eta, \xi)$:

$$\xi^2 \frac{\mathrm{d}^2 v}{\mathrm{d}\xi^2} + \xi \frac{\mathrm{d}v}{\mathrm{d}\xi} + (\omega^2 - m^2 \xi^2) v = 0 \,. \tag{B.1}$$

The solution basis for $m \neq 0$ is given by $\mathrm{Re}(I_{i\omega})$ and $K_{i\omega}$ which are both real and linearly independent due to nontrivial Wronskian [80]. Now let us set $m = 0$ on Eq. (B.1). The eigenbasis[1] of the solution space is given by $\sin(\omega \log \xi)$ and $\cos(\omega \log \xi)$. Note that we

[1] This is not the ones used in e.g. [2, 148], but for our purposes either one will work. Roughly speaking, one can check from the series expansion at small m that this is analogous to the choice of writing solutions to harmonic oscillator equation in terms of cosine/sine functions or plane waves.

could also obtain this by doing a series expansion for small $m \to 0^+$ on the mode solutions in Eq. (3.27) which satisfies the Dirichlet boundary condition at $\xi = \xi_1$ [80]. Since η is dimensionless, so is ω here. If we let the boundary conditions to be at $\xi_1 = a^{-1}$ and $\xi_2 = a^{-1} + L$, we get

$$v_n \propto \sin(\omega_n \log \xi) - \tan\left(\omega_n \log \frac{1}{a}\right) \cos(\omega_n \log \xi) \ , \tag{B.2}$$

where ω_n is now a discrete spectrum due to the second boundary condition $\xi = \xi_2$. The normalization can be found by standard Klein-Gordon inner product [3]. Remarkably, even after imposing the second boundary condition, the spectrum is still exact, which reads

$$\omega_n = \frac{n\pi}{\log(1 + aL)} \ , \qquad n \in \mathbb{N} \, , \tag{B.3}$$

which is precisely what we got from the conformal transformation where we identify the denominator as aL', the conformally transformed length of the cavity multiplied by the kinematical parameter a. In some sense this is perhaps not surprising, since the same physical situation should be described by the same differential operator with the same set of spectrum (which is invariant under coordinate transformations).

Some representative plots of the modes for small and large accelerations are given in Figure B.1. Now it is very clear that the spatial modes approach Minkowski static cavity scenario very quickly for not too small $a \sim 0.01$, while for large acceleration (of the left wall) the modes are "deformed sine functions". These deformed modes are in fact very similar in form as the modes for massive case described in terms of modified Bessel functions of imaginary order $\mathrm{Re}(I_{i\omega})$ and $K_{i\omega}$.

This clearly demonstrates that the differential equation governing the form of the spatial modes is solvable directly even if the metric is not the one conformally equivalent to the Minkowski metric. In this standard Rindler coordinates, the Klein-Gordon equation would also not be conformally invariant under the change of coordinates. However, the standard Rindler coordinates and conformal Rindler coordinates both cover the Rindler wedge portion of Minkowski spacetime and each hypersurface of constant ξ in either coordinates describe the trajectory of uniformly accelerating test particles. One would not conclude that massless fields cannot distinguish the two scenarios on grounds of conformal invariance, while massive fields can; instead, one would conclude that both should have qualitatively similar behaviour up to some degradation factor due to mass of the field that enters the normalization constant and phase factor in the integral of transition probability.

Here we make a short remark on the distinction between conformal flatness and confor-

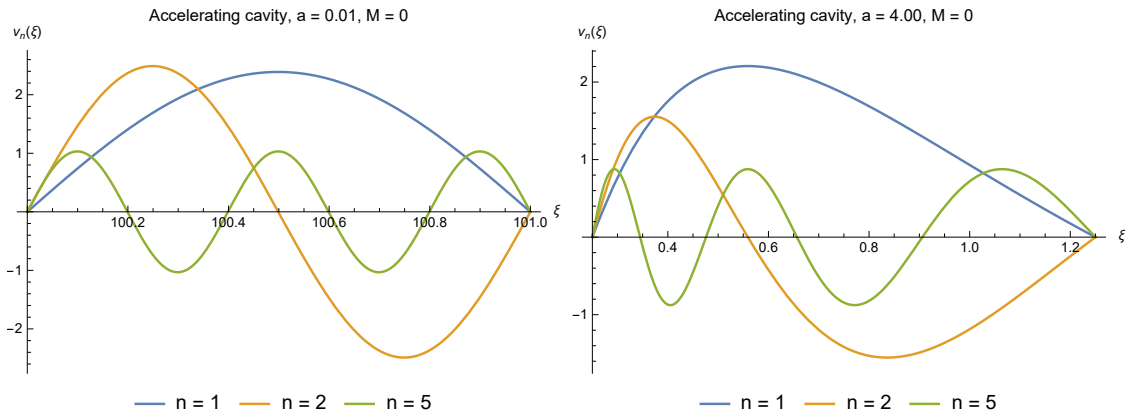

Figure B.1: Sample plots of mode functions for the second mode $n = 2$ for small and large accelerations. This makes clear that large acceleration limit is "Bessel-like", in that the mode function is a deformed sine function, squashed in the direction of acceleration. These plots are not normalized since we are concerned with their forms rather than their amplitudes.

mal invariance of field equations via a conformal transformation. A spacetime M is said to be conformally flat if *there exists* a coordinate system in which the metric can be rewritten as

$$g_{\mu\nu}(\mathsf{x}) = \Omega(\mathsf{x})^2 \eta_{\mu\nu} \,, \tag{B.4}$$

and in (1+1) dimensions all Lorentzian manifolds are conformally flat. The massless KG field is conformally invariant because under conformal transformation, the KG equation takes the same form as the wave equation in global Minkowski coordinates. However, performing conformal transformation is a calculational advantage that does not change the physics, since we could equally do physics using non-conformally equivalent metric that describes the same spacetime. Alternatively, we say that the physics is contained in $\Omega(\mathsf{x})$ and so the physics will still be different from static Minkowski spacetime [1]. A good example is the de Sitter expanding universe, which can be written in coordinates such that it is conformally flat — the mode functions inherit the form in flat space, but static detector in conformal vacuum of the de Sitter spacetime detects particles while a static detector in Minkowski vacuum does not.

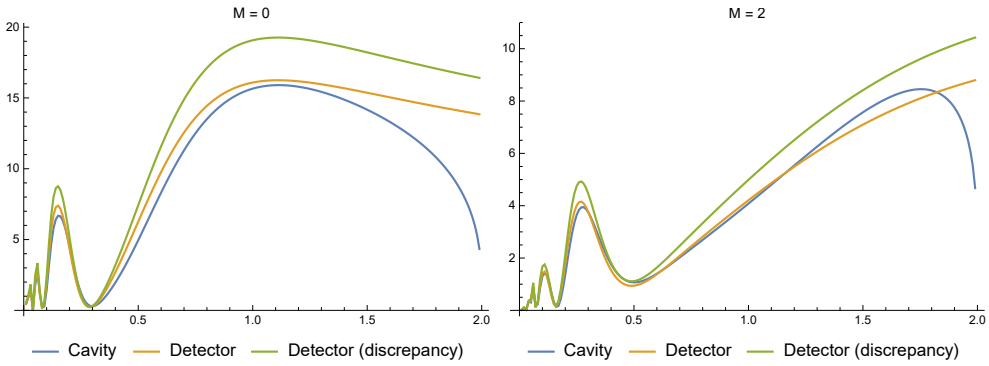

Figure B.2: The transition probability plot simulating the plots found in [2]. The discrepancy is possibly related to incorrect normalization for massive field-accelerating detector scenario (labelled 'discrepancy' here), thus producing the result that massive fields can better distinguish local acceleration.

B.2 Discrepancy with past results

Based on the argument above, there is a slight disparity in a result we obtained here and the results obtained in [2]. Since the exact parameters used previously [2] are unknown, we attempt to emulate the construction and the result is shown in Figure B.2. From what we can discern, this discrepancy arises from making the same (inappropriate) normalization choice for both the massive and massless cases. For a detector accelerating in a static cavity with a massive scalar field [2], this leads to the conclusion that (in the non-relativistic regime) massive fields can distinguish local acceleration whereas massless fields cannot.

Despite the discrepancy, the results here and in [2] nonetheless show that detector responses can indeed detect non-uniformity of accelerations in cavities, which lead to distinguishability between the two scenarios. Essentially, it boils down to the fact that in the accelerating cavity scenario, the static detector is only approximately uniformly accelerating from the perspective of the cavity frame, since the vertical worldlines cross hypersurfaces of constant but different ξ, which is approximately constant for very short cavity or very small accelerations. On the other hand, an accelerating detector is an *exactly* uniformly accelerating test body; thus the setup is not mathematically equivalent — hence "qualitative weak equivalence principle" [1].

To summarize, we first note that both accelerating cavity and accelerating detector setups are *kinematically inequivalent* for any nonzero aL, as illustrated in Section 3.3.2 and Appendix B.1. What conformal invariance in $(1+1)$ dimensions gives us is convenience, a

point made also in [1]. It boils down to the fact that in the rest frame of an accelerating cavity the detector does *not* undergo uniform acceleration. Therefore, for any value of aL, there exists a finite difference in transition probability $\Delta\,\mathrm{Pr} = |\mathrm{Pr}_{cav} - \mathrm{Pr}_{det}|$ between the two setups regardless of the mass of the field. This difference quickly vanishes as $aL \to 0$: in this 'quasilocal regime', we can approximate the whole cavity as accelerating with a single proper acceleration, recalling that the acceleration along the length of the cavity $a(x)$ is related to the acceleration of the rear wall a_1 by

$$a(x) = \frac{a_1}{1 + a_1(x - x_1)} \approx a_1 \tag{B.5}$$

if $a_1(x - x_1) < a_1 L \ll 1$. For this reason, $\Delta\,\mathrm{Pr}$ falls quickly as $a \to 0$, becoming exactly zero when $a = 0$ (entirely static detector and cavity setups). So long as $aL \neq 0$, in principle we can always distinguish local accelerations using nonlocal correlations of the field regardless of mass. Choosing the detector gap to be closer to the resonant frequency of the field (e.g. excited Fock state) will help in amplifying very small transition probabilities, noting that the resonant frequencies between massless and massive cases would be different.

B.3 Convergence of mode sums

We show some plots demonstrating how quickly the mode sums converge for certain choices of parameters. In Figure B.3 we plot the transition probabilities as a function of mode sum for the field initiated as vacuum state for two different accelerations a.

We see that the convergence is attained for relatively small $N \sim 100$, and even if we sum $N = 15$ (the smallest N in these plots), the values do not stray far from the converged value, thus for practical purposes we choose to perform calculations involving vacuum state for $N = 15$. Note that for fields initiated in excited states, the Wightman function has vacuum and excited state contributions but the latter does not occur as sums over modes and hence convergence issue does not appear.

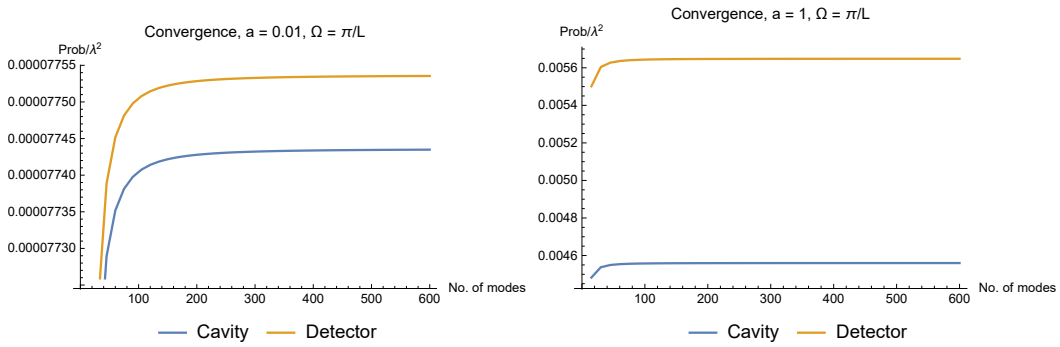

Figure B.3: Probability as a function of mode sum N for $a = 0.01$ and $a = 1.0$ with $M = 0$.

B.4 Transition rate

Computation of a transition probability — also known as a *response function* $F(\Omega)$ of a particle detector with energy gap Ω — as a detector traverses through a quantum field coupled to it has a physical interpretation: it provides an operational way of defining the particle content of the field without invoking a high degree of spacetime symmetry [20, 21]. However, the fact that it is a double integral may obscure information about the atom-field interaction. This prompts us to consider whether the *transition rate*, essentially the time-derivative of the response function along the detector trajectory, can provide further insights into the WEP.

To obtain the response rate, we need to rewrite the response function in such a way that it can be easily differentiated. This is done by changing variables [69]

$$F(\Omega) = 2\mathrm{Re}\int_{\tau_0}^{\tau} \mathrm{d}u \int_{0}^{u-\tau_0} \mathrm{d}s e^{-i\Omega s} W(u, u-s)\,, \tag{B.6}$$

where τ_0 denotes the time in which the detector is switched on. Instead of the usual response function which gives transition probability of exciting the atom from its ground state, we can now compute the *instantaneous transition rate* of a detector turned on at time τ_0 and read at time τ, given by [69]

$$\dot{F}(\Omega) = \frac{\mathrm{d}F(\Omega)}{\mathrm{d}\tau} = 2\mathrm{Re}\int_{0}^{\tau-\tau_0} \mathrm{d}s\, e^{-i\Omega s} W(\tau, \tau-s)\,. \tag{B.7}$$

Despite some subtleties in handling this observable for free space involving regularization, we expect that the cavity setup removes these difficulties since the field is compactly

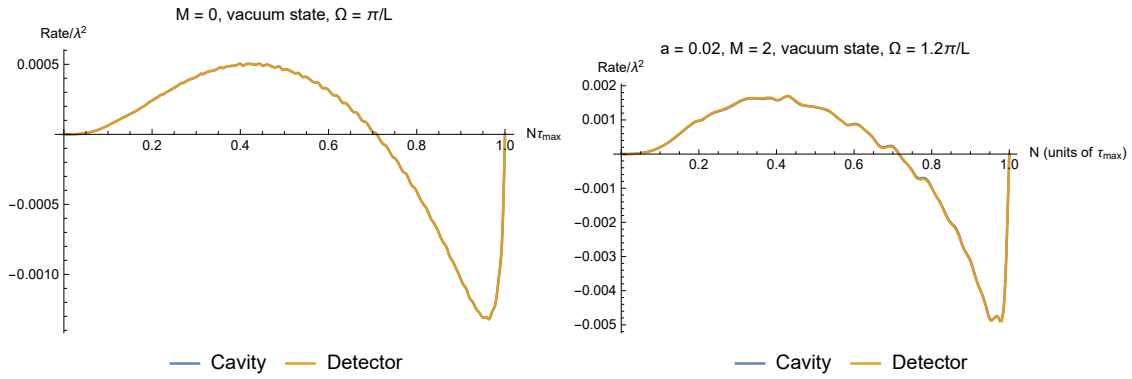

Figure B.4: Transition rate as a function of time τ. Note that in both cases the transition rates for accelerating cavity and accelerating detector scenarios are practically indistinguishable regardless of mass. We chose different parameters for variations.

supported and there is an infrared cutoff. In our scenario it is convenient to compute the case where $\tau_0 = 0$. If different field states have a chance of causing different responses to the detector, transition rate may be able to pick this up[2]. Conversely, if transition rate is identical, then the response of the detector should be the same under integration.

Since the response rate is linear in $W(\tau, \tau')$, we will split them into two parts:

$$\dot{F}(\Omega) = \dot{F}_0(\Omega) + \dot{F}_1(\Omega) \tag{B.8}$$

where $\dot{F}_0$ is the vacuum contribution and $\dot{F}_1$ is the remaining contribution due to the field in excited state. The vacuum state transition rate is shown in Figure B.4. The crucial thing to note here is that the vacuum contribution for both cases have negligible differences in transition rate — therefore the transition probability must be the same as well after integrating across the full trajectory. For computational time convenience, we chose $a = 0.02$ to represent the massive case and the same conclusion holds. This justifies our earlier results (also in [2]) that vacuum contributions are not sensitive to local accelerations.

Two examples for a highly populated first excited state ($k = 1, n_k = 100$) for the massless case are shown in Figure B.5. We see that while the rate appears qualitatively different at different read-out times, the *difference* between an accelerating cavity and an accelerating detector is very small (of course it is only exactly zero for a static setup). As far as differences go, massive fields generically do not perform better than massless ones,

[2]On the other hand, it is possible that response function washes out differential differences due to mean value theorem.

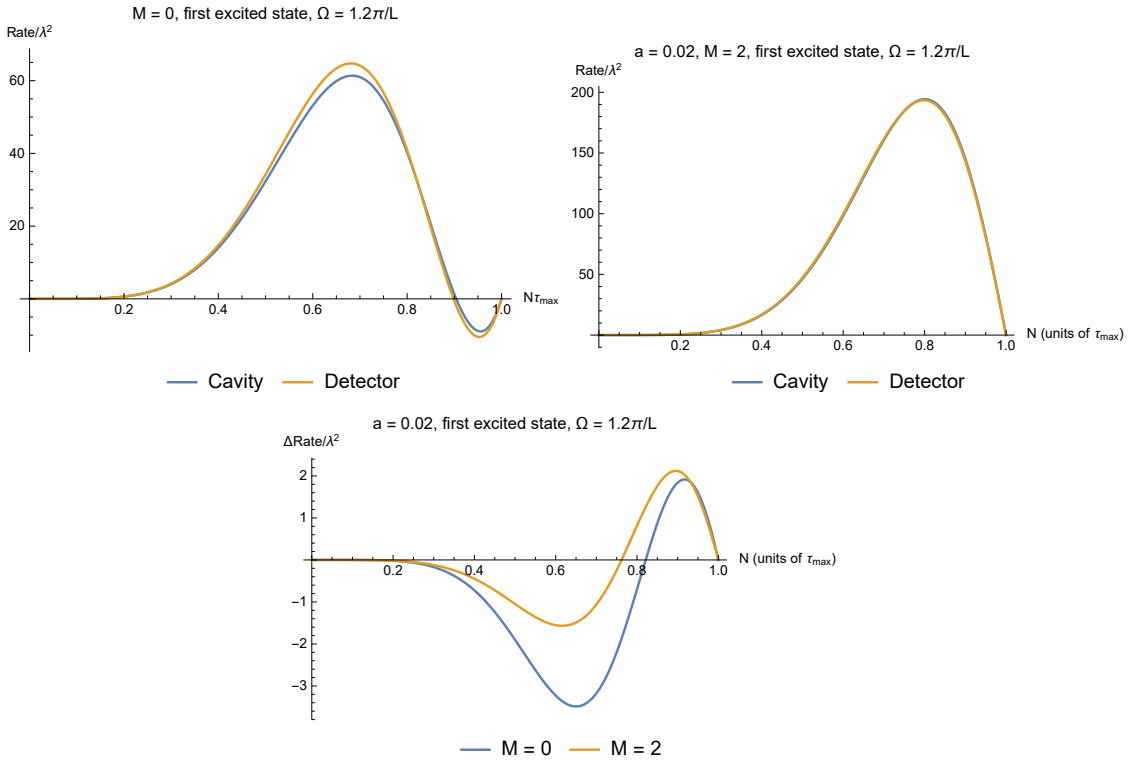

Figure B.5: Transition rate as a function of time τ for the first excited state of the field. **Top:** massless case. **Middle:** massive case. **Bottom:** Difference in transition rate for both scenarios. It appears that transition rate and hence transition amplitude is slightly more advantageous for massless case for a given acceleration. Here "ΔRate" is simply $\Delta\dot{F} = \dot{F}^D = \dot{F}^C$.

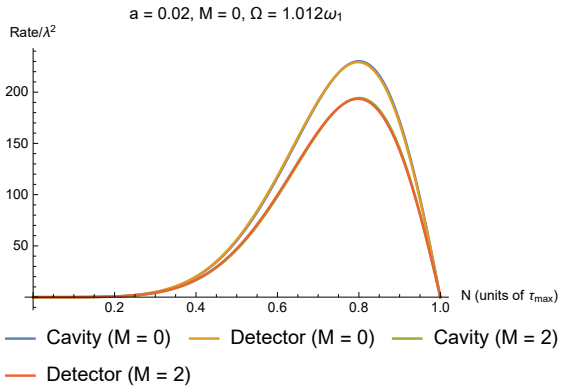

Figure B.6: Transition rate as a function of time τ for the first excited state of the field for massless and maassive case, close to resonance.

which is consistent with the idea that the role of mass tends to 'kill off' correlations at large distances and diminish the amplitudes.

From Figure B.5, one might be led to think that a massive field seems to have a *very large* response rate compared to a massless field, but this is not the right comparison. Note that the co-rotating frequency $\Omega - \omega_n$ determines quite directly the magnitude of these rates, and given the same gap Ω, one of the two fields will be closer to 'resonant frequency' than the other. In Figure B.6, we adjust the gap so that both massless and massive fields the atomic gap is $\Omega = 1.012\omega_1$, where ω_1 is the frequency of the first mode. As expected, the absolute value of the transition rate for massless fields dominate the massive case. The difference in response rates $\Delta\dot{F} = \dot{F}^D - \dot{F}^C$, where C, D denotes accelerating cavity and detector respectively, are of approximately the same order, as seen in Figure B.6.

Appendix C

Zero mode and superluminal signalling

C.1 Derivation of the oscillator part of the field commutator

Here will write derive the expressions for the commutators of the field in arbitrary dimensions when periodic boundary conditions and Neumann boundary conditions are imposed, or a combination of periodic and Neumann boundary conditions if spatial dimension is at least two. We first derive the most general expression and then illustrate in full detail the particular cases for various boundary conditions in $(1+1)$ and $(2+1)$ dimensions.

C.1.1 General expression in arbitrary dimensions

In $(n+1)$ dimensions, given an arbitrary state of the field $\hat{\rho}_{\hat{\phi}}$, the expectation value of the commutator with respect to the state $\hat{\rho}_{\hat{\phi}}$ is given by

$$\langle[\hat{\phi}_{\rm osc}(\mathsf{x}),\hat{\phi}_{\rm osc}(\mathsf{x}')]\rangle_{\hat{\rho}} = {\rm tr}\left(\hat{\rho}_{\hat{\phi}}[\hat{\phi}_{\rm osc}(\mathsf{x}),\hat{\phi}_{\rm osc}(\mathsf{x}')]\right) . \tag{C.1}$$

To reduce notational clutter, let us define I, J to be collective indices where n is the number of spatial dimensions. This will simplify the expression for the sum over modes in the commutators below. We define $\mathcal{A} := A_1, A_2, ..., A_n$ to be the collective indexing sets for

I, J which excludes the zero mode (if any). That is, $I \in \mathcal{A}$ means that every component i_l of the multi-index I takes values in the set A_l for each $l = 1, 2, ..., n$.

We can expand the field operator in terms of a complete set of orthonormal solutions to the Klein-Gordon equation $\{u_I, u_I^*\}$, that is,

$$\hat{\phi}(\mathsf{x}) = \sum_{I \in \mathcal{A}} \left(\hat{a}_I u_I(\mathsf{x}) + \hat{a}_I^\dagger u_I^*(\mathsf{x}) \right) . \tag{C.2}$$

Notice that the sum over the set of modes I can be a continuous sum (an integral) or a discrete sum depending on the boundary conditions imposed (by changing the indexing set $\mathcal{A}$). We can now evaluate then the expectation of the commutator as

$$\begin{aligned}
&\langle [\hat{\phi}_{\rm osc}(\mathsf{x}), \hat{\phi}_{\rm osc}(\mathsf{x}')] \rangle_{\hat{\rho}} \\
&= \sum_{I,J \in \mathcal{A}} \left(\langle [\hat{a}_I, \hat{a}_J] \rangle_{\hat{\rho}} \, u_I u'_J + \langle [\hat{a}_I^\dagger, \hat{a}_J^\dagger] \rangle_{\hat{\rho}} \, u_I^* {u'_J}^* + \langle [\hat{a}_I, \hat{a}_J^\dagger] \rangle_{\hat{\rho}} \, u_I {u'_J}^* + \langle [\hat{a}_I^\dagger, \hat{a}_J] \rangle_{\hat{\rho}} \, u_I^* u'_J \right) \\
&= \sum_{I,J \in \mathcal{A}} \left(\delta_{IJ} u_I {u'_J}^* - \delta_{JI} u_I^* u'_J \right) \\
&= \sum_{I \in \mathcal{A}} \left(u_I(\mathsf{x}) u_I^*(\mathsf{x}') - u_I^*(\mathsf{x}) u_I(\mathsf{x}') \right) \\
&\equiv \langle [\hat{\phi}_{\rm osc}(\mathsf{x}), \hat{\phi}_{\rm osc}(\mathsf{x}')] \rangle \ ,
\end{aligned} \tag{C.3}$$

where we have shortened notation by using $u'_I \equiv u_I(\mathsf{x}')$. We have also used the canonical commutation relations $[\hat{a}_I, \hat{a}_J^\dagger] = \delta_{IJ} \mathbb{1}$ to show explicitly the fact that the expectation value of the commutator is independent of the state of the field and drop the subscript $\hat{\rho}$ from the expectation value.

Eq. (C.3) above is the most general expression for the commutator of the oscillator part of the field. When different boundary conditions are imposed, we vary the choice of indexing set $\mathcal{A}$. For example, in the case of toroidal boundary conditions (periodic in all n spatial dimensions), the eigenfunctions are given by

$$u_I = N_I e^{-\mathrm{i}|\boldsymbol{k}_I| t + \mathrm{i} \boldsymbol{k}_I \cdot \boldsymbol{x}} \, , |\boldsymbol{k}_I| = \sqrt{\sum_{l=1}^{n} \left(\frac{2\pi i_l}{L} \right)^2} \, , \tag{C.4}$$

where the indices i_l are nonzero integers (hence excludes the zero mode), i.e., $A_l = \mathbb{Z} \setminus \{0\}$.

That is, the oscillator part of the commutator reads

$$\begin{aligned}
&\langle[\hat{\phi}_{\text{osc}}(\mathsf{x}),\hat{\phi}_{\text{osc}}(\mathsf{x}')]\rangle \\
&= \sum_{j_1\in\mathbb{Z}}\dots\sum_{j_{n-1}\in\mathbb{Z}}\sum_{j_n\neq 0} u_{j_1\dots j_n}(\mathsf{x})u^*_{j_1\dots j_n}(\mathsf{x}') - u_{j_1\dots j_n}(\mathsf{x}')u^*_{j_1\dots j_n}(\mathsf{x}) + \\
&\quad \sum_{j_1\in\mathbb{Z}}\dots\sum_{j_{n-2}\in\mathbb{Z}}\sum_{j_{n-1}\neq 0} u_{j_1\dots j_{n-1}0}(\mathsf{x})u^*_{j_1\dots j_{n-1}0}(\mathsf{x}') - u_{j_1\dots j_{n-1}0}(\mathsf{x}')u^*_{j_1\dots j_{n-1}0}(\mathsf{x}) + \\
&\quad \sum_{j_1\in\mathbb{Z}}\dots\sum_{j_{n-3}\in\mathbb{Z}}\sum_{j_{n-2}\neq 0} u_{j_1\dots j_{n-2}00}(\mathsf{x})u^*_{j_1\dots j_{n-2}00}(\mathsf{x}') - u_{j_1\dots j_{n-2}00}(\mathsf{x}')u^*_{j_1\dots j_{n-2}00}(\mathsf{x}) + \\
&\quad \sum_{j_1\neq 0} u_{j_100\dots 0}(\mathsf{x})u^*_{j_100\dots 0}(\mathsf{x}') - u_{j_100\dots 0}(\mathsf{x}')u^*_{j_100\dots 0}(\mathsf{x})\,.
\end{aligned} \tag{C.5}$$

For Neumann boundary conditions, the eigenfunctions are instead given by

$$u_I = N_I\prod_{l=1}^{n}\cos\frac{i_l\pi x_l}{L}\,e^{-\mathrm{i}|\boldsymbol{k}_I|t}\,,\,|\boldsymbol{k}_I| = \sqrt{\sum_{l=1}^{n}\left(\frac{i_l\pi}{L}\right)^2}\,, \tag{C.6}$$

and the indexing set is given by $A_l = \mathbb{N}\cup\{0\}$ in such a way that it excludes the zero mode, i.e. at least one of the summation is over $\mathbb{N}$. More concretely, we replace the summation for $j_k\in\mathbb{Z}$ with $j_k\in\mathbb{N}\cup\{0\}$ and the summation for $j_k\neq 0$ with $j_k\in\mathbb{N}$ in (C.3).

We will now use these results to write down the explicit expressions used in Chapter 4.

C.1.2 (1+1) periodic boundary conditions

For periodic boundary conditions, the eigenfunctions of the Klein-Gordon equation read

$$u_n(t,x) = \frac{1}{\sqrt{2\pi n}}e^{-\mathrm{i}|k_n|t+\mathrm{i}k_nx}\,,k_n = \frac{2\pi n}{L}\,,n\neq 0\,. \tag{C.7}$$

where the normalization constant $N_n = 1/\sqrt{2\pi n}$. The expectation of the commutator reads

$$\begin{aligned}
\langle[\hat{\phi}_{\text{osc}}(\mathsf{x})\hat{\phi}_{\text{osc}}(\mathsf{x}')]\rangle &= \sum_{n=1}^{\infty}\frac{1}{4\pi n}\left[e^{-\mathrm{i}k_n(\Delta u-\mathrm{i}\epsilon)} + e^{-\mathrm{i}k_n(\Delta v-\mathrm{i}\epsilon)} - e^{\mathrm{i}k_n(\Delta u-\mathrm{i}\epsilon)} - e^{\mathrm{i}k_n(\Delta v-\mathrm{i}\epsilon)}\right] \\
&= \sum_{n=1}^{\infty}\frac{\mathrm{i}}{2\pi n}\left[\sin\frac{2\pi n}{L}(\Delta u-\mathrm{i}\epsilon) + \sin\frac{2\pi n}{L}(\Delta v-\mathrm{i}\epsilon)\right]\,,
\end{aligned} \tag{C.8}$$

where $u = t - x$ and $v = t + x$ are the double null coordinates. Finally, we invoke the following identity

$$\sum_{n=1}^{\infty} \frac{\sin nx}{n} = \frac{1}{2}\left[\log\left(1 - e^{-\mathrm{i}x}\right) - \log\left(1 - e^{\mathrm{i}x}\right)\right] \tag{C.9}$$

and we obtain the commutator in Eq. (4.25).

C.1.3 (1+1)-dimensional Neumann boundary conditions

In the case of Neumann boundary conditions, the eigenfunctions of the Klein-Gordon equation take the form

$$u_n(t,x) = \frac{1}{\sqrt{n\pi}} \cos\frac{n\pi x}{L} e^{-\mathrm{i}|k_n|t}\,, k_n = \frac{n\pi}{L}\,, n \in \mathbb{N}\,, \tag{C.10}$$

where the normalization constant $N_n = 1/\sqrt{\pi n}$. The expectation of the commutator reads

$$\begin{aligned}\langle[\hat{\phi}_{\mathrm{osc}}(\mathsf{x})\hat{\phi}_{\mathrm{osc}}(\mathsf{x}')]\rangle &= \sum_{n=1}^{\infty} \frac{1}{\pi n}\left[\cos\frac{n\pi x}{L}\cos\frac{n\pi x'}{L} e^{-\mathrm{i}k_n(\Delta t - \mathrm{i}\epsilon)} - \cos\frac{n\pi x'}{L}\cos\frac{n\pi x}{L} e^{\mathrm{i}k_n(\Delta t - \mathrm{i}\epsilon)}\right] \\ &= \sum_{n=1}^{\infty} \frac{-2i}{\pi n}\left[\cos\frac{n\pi x}{L}\cos\frac{n\pi x'}{L}\sin\frac{n\pi \Delta t}{L}\right]\,,\end{aligned} \tag{C.11}$$

where $\Delta t = t - t'$. Notice that due to the form of the eigenfunction in Eq. (C.10), this commutator is no longer translation-invariant, unlike the case of periodic boundary conditions where the mode sums are purely functions of Δu and Δv. Still, this expression admits a closed-form expression, namely:

$$\begin{aligned}\langle[\hat{\phi}_{\mathrm{osc}}(\mathsf{x})\hat{\phi}_{\mathrm{osc}}(\mathsf{x}')]\rangle = \frac{1}{4\pi}\Bigg[&\log\left(1 - e^{\frac{\mathrm{i}\pi(\Delta u - \mathrm{i}\epsilon)}{L}}\right) + \log\left(1 - e^{\frac{\mathrm{i}\pi(\Delta v - \mathrm{i}\epsilon)}{L}}\right) \\ &+ \log\left(1 - e^{\frac{\mathrm{i}\pi(u - v' - \mathrm{i}\epsilon)}{L}}\right) + \log\left(1 - e^{\frac{\mathrm{i}\pi(v - u' - \mathrm{i}\epsilon)}{L}}\right) \\ &- \log\left(1 - e^{-\frac{i\pi(\Delta u - \mathrm{i}\epsilon)}{L}}\right) - \log\left(1 - e^{-\frac{i\pi(\Delta v - \mathrm{i}\epsilon)}{L}}\right) \\ &- \log\left(1 - e^{-\frac{i\pi(u - v' - \mathrm{i}\epsilon)}{L}}\right) - \log\left(1 - e^{-\frac{i\pi(v - u' - \mathrm{i}\epsilon)}{L}}\right)\Bigg]\,.\end{aligned} \tag{C.12}$$

C.1.4 (2+1)-dimensional periodic boundary conditions

In $(n+1)$ dimensions with $n \geq 2$, the mode sums do not have a closed form because the normalization constant N_I mixes contributions from different transverse momenta. As such, in practice, one would numerically impose a UV cutoff to evaluate these sums.

For simplicity let us impose the boundary condition across a length L in both transverse directions. This will simplify the expression for the normalization constant N_{mn}. The eigenfunctions for toroidal boundary condition (periodic boundary in both spatial directions) in $(2+1)$ dimensions read

$$\begin{aligned} u_{mn}(t,x,y) &= N_{mn} \exp\left[-\mathrm{i}|\boldsymbol{k}_{mn}|t + \mathrm{i}\frac{2\pi m}{L}x + \mathrm{i}\frac{2\pi n}{L}y\right], \\ \boldsymbol{k}_{mn} &= \sqrt{\left(\frac{2\pi m}{L}\right)^2 + \left(\frac{2\pi n}{L}\right)^2}. \end{aligned} \tag{C.13}$$

Recall that the normalization N_{mn} couples momenta from both transverse directions,

$$N_{mn} = \frac{1}{\sqrt{L\,|\boldsymbol{k}_{mn}|}}. \tag{C.14}$$

The expectation value of the commutator $\langle[\hat{\phi}_{\mathrm{osc}}(\mathsf{x})\hat{\phi}_{\mathrm{osc}}(\mathsf{x}')]\rangle$ is then given by the sum

$$\begin{aligned} \langle[\hat{\phi}_{\mathrm{osc}}(\mathsf{x})\hat{\phi}_{\mathrm{osc}}(\mathsf{x}')]\rangle = &\sum_{m=-\infty}^{\infty}\sum_{n\neq 0}\frac{1}{\sqrt{2L\,|\boldsymbol{k}_{mn}|}}\left(u_{mn}u'^{*}_{mn} - u'_{mn}u^{*}_{mn}\right) + \\ &\sum_{m\neq 0}\frac{1}{\sqrt{2L\,|\boldsymbol{k}_{m0}|}}\left(u_{m0}u'^{*}_{m0} - u'_{m0}u^{*}_{m0}\right). \end{aligned} \tag{C.15}$$

These two sums only exclude the $|\boldsymbol{k}_{00}|$ term corresponding to the zero mode. This expression generalizes easily to higher dimensions, essentially including all sums which excludes the "zero frequency" part containing $|\boldsymbol{k}_{00\ldots0}|$.

C.1.5 (2+1)-dimensional Neumann boundary conditions

For the Neumann boundary conditions on both transverse directions, we get

$$\begin{aligned} u_{mn}(t,x,y) &= N_{mn}\cos\frac{m\pi x}{L}\cos\frac{n\pi y}{L}e^{-\mathrm{i}|\boldsymbol{k}_{mn}|t}\,, \\ \boldsymbol{k}_{mn} &= \sqrt{\left(\frac{\pi m}{L}\right)^2+\left(\frac{\pi n}{L}\right)^2}\,. \end{aligned} \tag{C.16}$$

According to Eq. (C.3), the expectation of the commutator will now read

$$\begin{aligned} \langle[\hat{\phi}_{\mathrm{osc}}(\mathsf{x})\hat{\phi}_{\mathrm{osc}}(\mathsf{x}')]\rangle = &\sum_{m=0}^{\infty}\sum_{n=1}^{\infty}\frac{1}{\sqrt{2L\,|\boldsymbol{k}_{mn}|}}\left(u_{mn}u'^{*}_{mn}-u'_{mn}u^{*}_{mn}\right)+ \\ &\sum_{m=1}^{\infty}\frac{1}{\sqrt{2L\,|\boldsymbol{k}_{m0}|}}\left(u_{m0}u'^{*}_{m0}-u'_{m0}u^{*}_{m0}\right)\,. \end{aligned} \tag{C.17}$$

In fact, this suggests the possibility of using periodic *and* Neumann boundary conditions on different transverse dimensions. If we impose Neumann boundary along x-direction and periodic boundary across y-direction, the eigenfunctions would be

$$\begin{aligned} u_{mn}(t,x,y) &= N_{mn}\cos\frac{m\pi x}{L}\exp\left[-\mathrm{i}|\boldsymbol{k}_{mn}|t+\mathrm{i}\frac{2\pi n y}{L}\right]\,, \\ \boldsymbol{k}_{mn} &= \sqrt{\left(\frac{\pi m}{L}\right)^2+\left(\frac{2\pi n}{L}\right)^2}\,, \end{aligned} \tag{C.18}$$

where $m\in\mathbb{N}\cup\{0\}$ and $n\in\mathbb{Z}$. The expected value of the commutator will now read

$$\begin{aligned} \langle[\hat{\phi}_{\mathrm{osc}}(\mathsf{x})\hat{\phi}_{\mathrm{osc}}(\mathsf{x}')]\rangle = &\sum_{m=0}^{\infty}\sum_{n\neq 0}\frac{1}{\sqrt{2L\,|\boldsymbol{k}_{mn}|}}\left(u_{mn}u'^{*}_{mn}-u'_{mn}u^{*}_{mn}\right)+ \\ &\sum_{m=1}^{\infty}\frac{1}{\sqrt{2L\,|\boldsymbol{k}_{m0}|}}\left(u_{m0}u'^{*}_{m0}-u'_{m0}u^{*}_{m0}\right)\,. \end{aligned} \tag{C.19}$$

C.2 (n+1)-dimensional Einstein cylinder

In the case of the $(n+1)$ Einstein cylinder, the result is analogous to the toroidal case except replacing the sum over $\mathbb{Z}$ with an integral over momentum along the non-compact

spatial direction (see Eq. (4.45) for the $(2+1)$ case). In our multi-index notation, this is basically setting $A_l = \mathbb{R}$ for non-compact transverse dimensions and integrating over momentum instead of summing over discrete momentum. However, since the spectrum is continuous, the commutator of the oscillator modes computed in this manner is in fact the full field commutator (or rather, the zero mode does not contribute since it is a point of measure zero in momentum space). Therefore, effectively there is no zero mode relevant physics in the Einstein cylinder when $n \geq 2$.

C.3 Derivation of the zero mode commutator

Here we derive the fact that the zero mode commutator scales polynomially with the length of the "cavity" where the boundary conditions are imposed, i.e.

$$\langle [\hat{\phi}_{\mathrm{zm}}(\mathsf{x}), \hat{\phi}_{\mathrm{zm}}(\mathsf{x}')] \rangle = -\mathrm{i}\frac{\Delta t}{L^n} \tag{C.20}$$

where n is the number of spatial dimensions. Thus, in some sense, the zero mode contribution is (polynomially) weaker in higher dimensions.

To prove this, it is simplest to start from the Lagrangian of the field theory. In $(n+1)$ dimensions, the Lagrangian is given by

$$\mathcal{L} = -\frac{1}{2}\int \mathrm{d}^n \boldsymbol{x}\, \partial_\mu \phi(t,\boldsymbol{x}) \partial^\mu \phi(t,\boldsymbol{x}) = \frac{1}{2}\int \mathrm{d}^n \boldsymbol{x} \left[\left(\frac{\partial \phi}{\partial t}\right)^2 - (\nabla \phi)^2 \right] . \tag{C.21}$$

The boundary conditions which will produce zero modes need to have discrete spectrum. Hence, the field can be expanded as a Fourier series

$$\phi(t,\boldsymbol{x}) = \sum_{I \in \mathcal{A}} \varphi_{_I}(t) e^{\mathrm{i}\boldsymbol{k}_I \cdot \boldsymbol{x}} \tag{C.22}$$

where we have used the notation I for collective indices for summation as defined in Appendix C.1. Here we denote the Fourier coefficients as $\{\varphi_I(t)\}$.

The first in term in Eq. (C.21) reads

$$\int \mathrm{d}^n \boldsymbol{x} \left(\frac{\partial \phi}{\partial t}\right)^2 = \int \mathrm{d}^n \boldsymbol{x} \sum_{I \in \mathcal{A}} \sum_{J \in \mathcal{A}} \dot{\varphi}_{_I}(t) \dot{\varphi}_{_J}(t) e^{\mathrm{i}(\boldsymbol{k}_I + \boldsymbol{k}_J)\cdot \boldsymbol{x}} . \tag{C.23}$$

When we have periodic/Neumann boundary conditions across distance L (in all spatial dimensions), the expression becomes

$$\int \mathrm{d}^n\boldsymbol{x}\left(\frac{\partial\phi}{\partial t}\right)^2 = \int_{[0,L]^n}\mathrm{d}^n\boldsymbol{x}\sum_{I,J\in\mathcal{A}}\dot{\varphi}_I\dot{\varphi}_J e^{\mathrm{i}(\boldsymbol{k}_I+\boldsymbol{k}_J)\cdot\boldsymbol{x}} = L^n\sum_{I\in\mathcal{A}}\dot{\varphi}_I\dot{\varphi}_{-I}\,. \tag{C.24}$$

The second term reads

$$\int_{[0,L]^n}\mathrm{d}^n\boldsymbol{x}\,(\nabla\phi)^2 = -|\boldsymbol{k}_I|^2L^n\sum_{I\in\mathcal{A}}\varphi_I\varphi_{-I}\,. \tag{C.25}$$

The full Lagrangian is therefore given by

$$\mathcal{L} = \frac{L^n}{2}\sum_{I\in\mathcal{A}}\left[\dot{\varphi}_I\dot{\varphi}_{-I} + |\boldsymbol{k}_I|^2\varphi_I\varphi_{-I}\right]. \tag{C.26}$$

From this expression, we can read off the zero mode Lagrangian (which corresponds to $|\boldsymbol{k}_I| = 0$ with $I = j_1j_2...j_n = 00...0$), namely

$$\mathcal{L}_{\mathrm{zm}} = \frac{L^n}{2}\dot{\varphi}^2_{0...0} \equiv \frac{L^n}{2}\dot{Q}^2\,. \tag{C.27}$$

The case for $n = 1$ is given in [83, 84]. The momentum conjugate to φ_I is given by

$$\pi_{_I} = \frac{\partial\mathcal{L}}{\partial(\dot{\varphi}_{_I})} = L^n\dot{\varphi}_{-I}\,, \tag{C.28}$$

hence the Hamiltonian is given by

$$H = \left[\sum_{I\in\mathcal{A}}\frac{\pi_{_I}\pi_{-I}}{2L^n} - \frac{|\boldsymbol{k}_I|^2}{2}\sum_{I\in\mathcal{A}}\varphi_{_I}\varphi_{-I}\right]. \tag{C.29}$$

Canonical quantization converts π_I, φ_I into operators $\hat{\pi}_I, \hat{\varphi}_I$, thus we have the zero mode Hamiltonian in $(n+1)$ dimensions:

$$\hat{H}_{\mathrm{zm}} = \frac{\hat{P}^2_{0...0}}{2L^n} \equiv \frac{\hat{P}^2}{2L^n}\,. \tag{C.30}$$

So, for n dimensions, the procedure that lead Eq. (4.26) is exactly the same replacing L by L^n in (4.21). Consequently, the commutator of the zero mode in $(n+1)$ dimension is

obtained by replacing L with L^n, namely

$$\langle[\hat{\phi}_{\rm zm}(\mathsf{x}),\hat{\phi}_{\rm zm}(\mathsf{x}')]\rangle = -\frac{\mathrm{i}\Delta t}{L^n}\,, \qquad \Delta t = t - t'\,, \tag{C.31}$$

as claimed.

Appendix D

Entanglement harvesting with moving mirrors

D.1 Derivation of the joint detector density matrix

Here we explicitly derive the time-evolved joint detector density matrix of the two detectors. This is partially motivated by the fact that in the literature there are many versions which may not be manifestly clear how they are the same. Once and for all we rectify and expound clearly the derivation by calculating very explicitly the density matrix.

Recall that the Dyson expansion reads

$$\begin{aligned} \hat{U} &= \mathbb{1} + \hat{U}^{(1)} + \hat{U}^{(2)} + O(\lambda^3)\,, \\ \hat{U}^{(1)} &= -i\int_{\mathbb{R}} \mathrm{d}t \hat{H}_I(t)\,, \qquad \text{(D.1)} \\ \hat{U}^{(2)} &= -\int_{\mathbb{R}} \mathrm{d}t \int_{-\infty}^{t} \mathrm{d}t' \hat{H}_I(t)\hat{H}_I(t') + O(\lambda^3)\,. \qquad \text{(D.2)} \end{aligned}$$

The evolved density matrix reads

$$\hat{\rho} = \hat{U}\hat{\rho}\hat{U}^\dagger = \hat{\rho}_0 + \hat{\rho}^{(1)} + \hat{\rho}^{(2)}\,, \qquad \text{(D.3)}$$

where $\hat{\rho}^{(j)}$ refers to terms of order λ^j. We derive this term by term. First of all, notice that for $\mathrm{tr}_\phi\, \hat{\rho}^{(1)} = 0$ if the field is in ground state. To see this, we just have to look at the term $\mathrm{tr}_\phi\, \hat{U}^{(1)}\hat{\rho}$ (and its Hermitian conjugate) since these are the only two terms of order

$O(\lambda)$. It is clear that they both depend on one-point function of the field $\langle 0|\hat{\phi}(\mathsf{x}_j(t))|0\rangle$ because there is only one copy of $\hat{H}_I$ acting on $\hat{\rho}_0$, and hence only one copy of $\hat{\phi}(\mathsf{x}(t))$ acting on the field vacuum $|0\rangle\langle 0|$. The one-point function is *always zero* for Fock states because schematically

$$\langle n|\hat{\phi}|n\rangle \sim \langle n|\hat{a}+a^\dagger|n\rangle \sim \langle n+1|n\rangle + \langle n|n+1\rangle \equiv 0 \tag{D.4}$$

by orthonormality of the Fock basis, no matter which momentum mode $\boldsymbol{k}$ the excitation is in. We conclude therefore that in our time-dependent perturbative calculation, the density matrix does not have any $O(\lambda)$ contribution and the leading order contribution is $O(\lambda^2)$.

It remains to compute the second-order contributions. Since in this case we have

$$\hat{H}_I = \hat{H}_I^A + \hat{H}_I^B\,, \tag{D.5}$$

the second-order operator $U^{(2)}$ can be broken into four parts:

$$\hat{U}^{(2)} = [AB] + [BA] + [AA] + [BB]\,, \tag{D.6}$$

$$[ij] \coloneqq -\int_{\mathbb{R}} \mathrm{d}t \int_{-\infty}^{t} \mathrm{d}t' H_I^i(t) H_I^j(t')\,, \quad j = A, B\,. \tag{D.7}$$

Let us now compute them. We use the shorthand $\mathsf{x}_j \equiv \mathsf{x}_j(t)$ and $\mathsf{x}'_j = \mathsf{x}_j(t')$. Let us compute the [AA] term:

$$\begin{aligned}
\mathrm{tr}_\phi[AA]\hat{\rho}_0 &= -\int_{\mathbb{R}} \mathrm{d}t \int_{-\infty}^{t} \mathrm{d}t' H_I^A(t) H_I^A(t') \,|g_A g_B\rangle\langle g_A g_B| \otimes |0\rangle\langle 0| \\
&= -\lambda_A^2 \int_{\mathbb{R}} \mathrm{d}t \int_{-\infty}^{t} \mathrm{d}t' \chi_A(t)\chi_A(t') \left(\hat{\sigma}_A^+ e^{i\Omega_A t} + \hat{\sigma}_A^- e^{-i\Omega_A t}\right)\left(\hat{\sigma}_A^+ e^{i\Omega_A t'} + \hat{\sigma}_A^- e^{-i\Omega_A t'}\right) \times \\
&\qquad\qquad |g_A g_B\rangle\langle g_A g_B| \,\mathrm{tr}_\phi\left[\hat{\phi}(\mathsf{x}_A(t))\hat{\phi}(\mathsf{x}_A(t'))\,|0\rangle\langle 0|\right] \\
&= -\lambda_A^2 \int_{\mathbb{R}} \mathrm{d}t \int_{-\infty}^{t} \mathrm{d}t' \chi_A(t)\chi_A(t') e^{i\Omega_A t'} \left(\hat{\sigma}_A^+ e^{i\Omega_A t} + \hat{\sigma}_A^- e^{-i\Omega_A t}\right) \times \\
&\qquad\qquad |e_A g_B\rangle\langle g_A g_B| \,\mathrm{tr}_\phi\left[\hat{\phi}(\mathsf{x}_A(t))\hat{\phi}(\mathsf{x}_A(t'))\,|0\rangle\langle 0|\right] \\
&= -\lambda_A^2 \int_{\mathbb{R}} \mathrm{d}t \int_{-\infty}^{t} \mathrm{d}t' \chi_A(t)\chi_A(t') e^{i\Omega_A t'} e^{-i\Omega_A t} \,|g_A g_B\rangle\langle g_A g_B| \,\langle 0|\hat{\phi}(\mathsf{x}_A(t))\hat{\phi}(\mathsf{x}_A(t'))|0\rangle \\
&\equiv -\frac{1}{2}\lambda_A^2 \int_{\mathbb{R}} \mathrm{d}t \int_{\mathbb{R}} \mathrm{d}t' \chi_A(t)\chi_A(t') e^{-i\Omega_A(t-t')} W(\mathsf{x}_A, \mathsf{x}'_A) \,|g_A g_B\rangle\langle g_A g_B| \\
&\equiv -\frac{1}{2} P_A \,|g_A g_B\rangle\langle g_A g_B|\,.
\end{aligned} \tag{D.8}$$

The case for $[BB]$ is obtained by simply replacing $A \leftrightarrow B$ in the integral (but not the ket and bra) and the ladder operators $\sigma_B^{\pm}$ acting on detector B's Hilbert space instead of detector A's Hilbert space. This integral is half the full transition probability because the domain of integration is an infinite triangle, i.e. subset of $\mathbb{R}^2$ given by $t' < t$. If we compute the Hermitian conjugate part $\mathrm{tr}_\phi\, \hat{\rho}_0[jj]^\dagger$, this will give the other half of the triangle as a domain of integration and they can be combined to give the full double integral over $\mathbb{R}^2$. Therefore, together they give the $1 - P_A - P_B$ term (i.e. the $|g_A g_B\rangle\langle g_A g_B|$ entry) in the density matrix.

Next, we have

$$\begin{aligned}
\mathrm{tr}_\phi[AB]\hat{\rho}_0 &= -\int_{\mathbb{R}} \mathrm{d}t \int_{-\infty}^{t} \mathrm{d}t' H_I^A(t) H_I^B(t') \, |g_A g_B\rangle\langle g_A g_B| \, |0\rangle\langle 0| \\
&= -\lambda_A \lambda_B \int_{\mathbb{R}} \mathrm{d}t \int_{-\infty}^{t} \mathrm{d}t' \chi_A(t)\chi_B(t') \left(\hat{\sigma}_A^+ e^{i\Omega_A t} + \hat{\sigma}_A^- e^{-i\Omega_A t}\right)\left(\hat{\sigma}_B^+ e^{i\Omega_B t'} + \hat{\sigma}_B^- e^{-i\Omega_B t'}\right) \times \\
&\qquad\qquad |g_A g_B\rangle\langle g_A g_B| \, \mathrm{tr}_\phi\left[\hat{\phi}(\mathsf{x}_A(t))\hat{\phi}(\mathsf{x}_B(t')) \, |0\rangle\langle 0|\right] \\
&= -\lambda_A \lambda_B \int_{\mathbb{R}} \mathrm{d}t \int_{-\infty}^{t} \mathrm{d}t' \chi_A(t)\chi_B(t') e^{i\Omega_B t'} \left(\hat{\sigma}_A^+ e^{i\Omega_A t} + \hat{\sigma}_A^- e^{-i\Omega_A t}\right) \times \\
&\qquad\qquad |g_A e_B\rangle\langle g_A g_B| \, \mathrm{tr}_\phi\left[\hat{\phi}(\mathsf{x}_A(t))\hat{\phi}(\mathsf{x}_B(t')) \, |0\rangle\langle 0|\right] \\
&= -\lambda_A \lambda_B \int_{\mathbb{R}} \mathrm{d}t \int_{-\infty}^{t} \mathrm{d}t' \chi_A(t)\chi_B(t') e^{i\Omega_B t'} e^{i\Omega_A t} \, |e_A e_B\rangle\langle g_A g_B| \, \langle 0|\hat{\phi}(\mathsf{x}_A(t))\hat{\phi}(\mathsf{x}_B(t'))|0\rangle \\
&\equiv -\lambda_A \lambda_B \int_{\mathbb{R}} \mathrm{d}t \int_{-\infty}^{t} \mathrm{d}t' \chi_A(t)\chi_B(t') e^{i\Omega_A t + i\Omega_B t'} W(\mathsf{x}_A, \mathsf{x}'_B) \, |e_A e_B\rangle\langle g_A g_B| \, . \qquad \text{(D.9)}
\end{aligned}$$

The case for $[BA]$ is obtained by relabelling $A \leftrightarrow B$. This reads

$$\mathrm{tr}_\phi[BA]\hat{\rho}_0 = -\lambda_A \lambda_B \int_{\mathbb{R}} \mathrm{d}t \int_{-\infty}^{t} \mathrm{d}t' \chi_B(t)\chi_A(t') e^{i\Omega_B t + i\Omega_A t'} W(\mathsf{x}_B, \mathsf{x}'_A) \, |e_A e_B\rangle\langle g_A g_B| \, . \quad \text{(D.10)}$$

Together, $[AB] + [BA]$ contribution gives the entry X in the density matrix. To see this, we relabel $t \leftrightarrow t'$ in $[BA]$ and we get

$$\begin{aligned}
\mathrm{tr}_\phi([AB] + [BA])\hat{\rho}_0 = &-\lambda_A \lambda_B \int_{\mathbb{R}} \mathrm{d}t \int_{-\infty}^{t} \mathrm{d}t' \chi_A(t)\chi_B(t') e^{i\Omega_A t + i\Omega_B t'} W(\mathsf{x}_A, \mathsf{x}'_B) \, |e_A e_B\rangle\langle g_A g_B| \\
&- \lambda_A \lambda_B \int_{\mathbb{R}} \mathrm{d}t' \int_{-\infty}^{t'} \mathrm{d}t \chi_A(t)\chi_B(t') e^{i\Omega_A t + i\Omega_B t'} W(\mathsf{x}'_B, \mathsf{x}_A) \, |e_A e_B\rangle\langle g_A g_B| \, . \qquad \text{(D.11)}
\end{aligned}$$

Finally, using the fact that for an integrable function $F(t,t')$ we can write

$$\int_{\mathbb{R}} \mathrm{d}t \int_{-\infty}^{t} \mathrm{d}t'\, F(t,t') = \int_{\mathbb{R}} \mathrm{d}t \int_{\mathbb{R}} \mathrm{d}t' \Theta(t-t') F(t,t')\,, \tag{D.12}$$

we can combine both integrals to give

$$\begin{aligned}
&\mathrm{tr}_\phi([AB]+[BA])\hat{\rho}_0 \\
&= -\lambda_A\lambda_B \left|e_A e_B\right\rangle\!\left\langle g_A g_B\right| \\
&\quad \int_{\mathbb{R}} \mathrm{d}t' \int_{\mathbb{R}} \mathrm{d}t\, \chi_A(t)\chi_B(t') e^{i\Omega_A t + i\Omega_B t'} \left[\Theta(t-t')W(\mathsf{x}_A,\mathsf{x}'_B) + \Theta(t'-t)W(\mathsf{x}'_B,\mathsf{x}_A)\right] .
\end{aligned} \tag{D.13}$$

The expression in Chapter 5 is obtained once we set $\lambda_j = \lambda, \Omega_j = \Omega$, giving

$$\begin{aligned}
&\mathrm{tr}_\phi([AB]+[BA])\hat{\rho}_0 \\
&= -\lambda^2 \left|e_A e_B\right\rangle\!\left\langle g_A g_B\right| \\
&\quad \int_{\mathbb{R}} \mathrm{d}t' \int_{\mathbb{R}} \mathrm{d}t\, \chi_A(t)\chi_B(t') e^{i\Omega(t+t')} \left[\Theta(t-t')W(\mathsf{x}_A,\mathsf{x}'_B) + \Theta(t'-t)W(\mathsf{x}'_B,\mathsf{x}_A)\right] \\
&\equiv X \left|e_A e_B\right\rangle\!\left\langle g_A g_B\right| .
\end{aligned} \tag{D.14}$$

This can be simplified even further if we choose the same switching $\chi_j(t) = \chi(t)$. The Hermitian conjugate contribution $\hat{\rho}_0([AB]+[BA])^\dagger$ will give X^* contribution (i.e. $|g_A g_B\rangle\langle e_A e_b|$ entry) in the density matrix. Notice that this expression for X is different from [58, 122], and to our knowledge the expression in [58, 122] is in fact X^*.

An alternative expression that does not involve the Heaviside step function is obtained simply by adding Eq. (D.9) and Eq. (D.10), and if we set $\chi_j(t) = \chi(t)$, $\lambda_j = \lambda$ and $\Omega_j = \Omega$, then this simplifies to

$$\begin{aligned}
&\mathrm{tr}_\phi([AB]+[BA])\hat{\rho}_0 \\
&= -\lambda^2 \int_{\mathbb{R}} \mathrm{d}t \int_{-\infty}^{t} \mathrm{d}t' \chi(t)\chi(t') e^{i\Omega(t+t')} \left[W(\mathsf{x}_A,\mathsf{x}'_B) + W(\mathsf{x}_B,\mathsf{x}'_A)\right] \left|e_A e_B\right\rangle\!\left\langle g_A g_B\right| .
\end{aligned} \tag{D.15}$$

This expression agrees with the first equality of Eq. (4) of [112] but not the second, since it is not clear that the symmetry of the Wightman function in [112] holds in general. This also agrees with Eq. (A20) of [55], Eq. (32) of [70] (after using pointlike limit) and the middle term of Eq. (31) in [47]. However, oddly enough this does not match with Eq. (3.40) or Eq. (4.39c) of [144] despite the matching with [55], and to our knowledge this is because the expression flips X and X^*.

If we do the exact same computation but for $\hat{U}^{(1)}\hat{\rho}_0\hat{U}^{(1)\dagger}$, we will again be able to break the computation into four parts, which we can again label as $[AA], [BB], [AB], [BA]$ depending on which Hamiltonian product appears:

$$[ij] := -\int_{\mathbb{R}} \mathrm{d}t \int_{-\infty}^{t} \mathrm{d}t' \hat{H}_I^i(t) \, |g_A g_B\rangle\langle g_A g_B| \otimes |0\rangle\langle 0| \, \hat{H}_I^j(t') \tag{D.16}$$

The contribution due to the $[AB]$ and $[BA]$ parts will give the entries with values C, C^*, while $[AA]$ and $[BB]$ will give the diagonal elements whose values are P_A and P_B respectively.

D.2 IR cut-off in free-space and unbounded transition probability in mirror spacetimes

One peculiarity we found in this work is that for a linearly coupled detector in $(1+1)$ dimensions, there seems to be a slow but unbounded growth of the transition probability $P(\Omega)$ as a function of distance from the boundary, which we denote by d. In particular, this means that in $(1+1)$ dimensions the static mirror does not smoothly recover the free space limit as $d \to \infty$, which is in contrast to the expectation that a detector does not sense nonlocal differences and in particular whether there is a boundary far away. This may influence the reliability of entanglement measures that inherently depend on $|X|$ and $P(\Omega)$. Although the problem of particle detectors in half-space has been previously considered [115, 116, 155], the growth of $P(\Omega)$ as a function of d was not clarified. We will compare two scenarios for static Dirichlet boundary conditions in (1+1) and (3+1) dimensions. We will show that the peculiarity is dimension dependent and not generically true in the presence of a boundary.

In $(3+1)$ dimensions, the Wightman function for a Dirichlet boundary on the yz-plane such that a detector is located at $(d, 0, 0)$ where $d > 0$ is given by the image sum

$$W(\mathsf{x}, \mathsf{x}') = \frac{-1}{4\pi^2}\left[\frac{1}{(\Delta\tau - i\epsilon)^2} - \frac{1}{(\Delta\tau - i\epsilon)^2 - 4d^2}\right] \tag{D.17}$$

where the second term is the image term that gives the distance dependence d. Evaluating the expression for $P(\Omega)$ in Eq. (5.6) for this Wightman function and the usual Gaussian switching in Eq. (5.7), we will get two contributions to the integral:

$$P(\Omega) = P_{\text{free}}(\Omega) + P_{\text{image}}(\Omega) \tag{D.18}$$

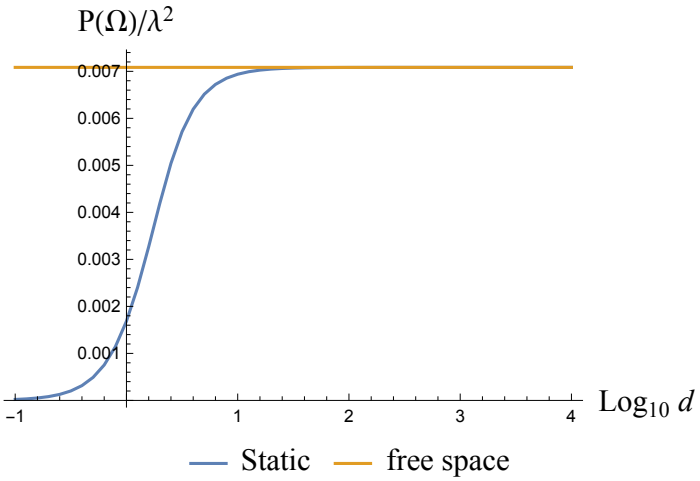

Figure D.1: Transition probability for Gaussian switching $\sigma = 1$ and $\Omega = 1$ ($\Omega\sigma = 1$) in $(3+1)D$. Near the mirror $P(\Omega)$ decays quickly, and far from the mirror the contribution from the image term vanishes quickly. In this figure the asymptotic behaviour is reached at $d/\sigma \sim 10^2$.

where

$$\begin{aligned} P_{\text{free}}(\Omega) &= -\frac{\sigma}{\sqrt{16\pi^3}} \int_{-\infty}^{\infty} \mathrm{d}y \frac{e^{-\frac{y^2}{4\sigma^2}} e^{-i\Omega y}}{(y - i\epsilon)^2}\,, \\ P_{\text{image}}(\Omega) &= \frac{\sigma}{\sqrt{16\pi^3}} \int_{-\infty}^{\infty} \mathrm{d}y \frac{e^{-\frac{y^2}{4\sigma^2}} e^{-i\Omega y}}{(y - i\epsilon)^2 - 4d^2}\,. \end{aligned} \tag{D.19}$$

The first term is just the finite-time response of a detector in free space and hence is independent of d. The image term [78] is known to be finite even in free space for finite width $\sigma > 0$. We are interested in the behaviour of the integral of the image term as d increases, which we show in Figure D.1. This is in fact not hard to see from the form of the Wightman function: as $d \to \infty$, the image term becomes more and more negligible because the finite width Gaussian window suppresses contributions at large u. Hence, in (3+1) dimensions the phenomenology of inertial (static) detectors in Minkowski half-space has the expected free-space limit as $d \to \infty$.

This, however, is not true in (1+1) dimensions because the Wightman function has a logarithmic instead of power law dependence on d. For a static mirror, the expression is

instead

$$
\begin{aligned}
P_{\text{free}}(\Omega) &= -\frac{\sigma}{\sqrt{16\pi}} \int_{-\infty}^{\infty} \mathrm{d}y\, e^{-i\Omega y} e^{-\frac{y^2}{4\sigma^2}} \log\left[\Lambda^2(\epsilon+iy)^2\right] , \\
P_{\text{image}}(\Omega) &= -\frac{\sigma}{\sqrt{16\pi}} \int_{-\infty}^{\infty} \mathrm{d}y\, e^{-i\Omega y} e^{-\frac{y^2}{4\sigma^2}} \log\left[\frac{1}{\Lambda^2\left((\epsilon+iy)^2+4d^2\right)}\right] , \\
\implies P(\Omega) &= -\frac{\sigma}{\sqrt{16\pi}} \int_{-\infty}^{\infty} \mathrm{d}y\, e^{-i\Omega y} e^{-\frac{y^2}{4\sigma^2}} \log\left[\frac{(\epsilon+iy)^2}{(\epsilon+iy)^2+4d^2}\right] ,
\end{aligned}
\tag{D.20}
$$

where we have made the free-space IR cutoff Λ explicit for comparison. The branch of the logarithm is chosen to match that of Eq. (5.10). Recall that in (1+1) dimensions, the free-space Wightman function is infrared (IR) divergent. The common regularisation scheme employed in the literature is the addition of an IR cutoff, which can be thought of (for example) as the length scale of an optical fibre [111, 123]. Numerical results have been shown to be reliable as long as Λ is chosen to be significantly smaller than the lowest frequency scale in the problem (i.e. the sensitivity to the choice of cutoff is very small). In the mirror spacetime, we note that the computation of $P(\Omega)$ does not require an IR cut-off as we see from the last expression in Eq. (D.20). However, the growth in the image term as d increases causes $P(\Omega)$ to eventually overtake the free-space result instead of asymptotic to it. The comparison is shown in Figure D.2. We also note that this growth is strictly a finite-time effect, i.e. not in the long interaction regime (cf. [66]). To see this, note that the total probability in Eq. (D.20) can be re-expressed as *total probability per unit time* $P(\Omega)/\sigma$ and in the limit $\sigma \to \infty$ we get

$$
\lim_{\sigma\to\infty} \frac{P(\Omega)}{\sigma} = -\frac{\sqrt{\pi}\Theta(-\Omega)}{\Omega} e^{2\Omega\epsilon} \left(1-\cos(2\Omega d)\right) , \tag{D.21}
$$

which is in fact oscillatory for excited detector ($\Omega < 0$), as one may expect from e.g. [59]. However, the transition probability itself diverges (though the *rate* does not), so in this sense the large-d growth of $P(\Omega)$ is similar to large-σ growth, as one may have guessed from relativistic considerations, which put space and time on equal footing.

What this highlights is that within perturbation theory, one should take extra care in distinguishing what is due to the physics of the boundary and what is an artifact of the dimensionality of spacetime. An effect strictly confined to $(1+1)$ dimensions will not necessarily provide guidance to our understanding of $(3+1)$ dimensional physics. In particular the observable $P(\Omega)$ in the presence of a mirror is generically an ill-behaved quantity in (1+1) dimensions, even without the IR ambiguity associated with the free-space counterpart.

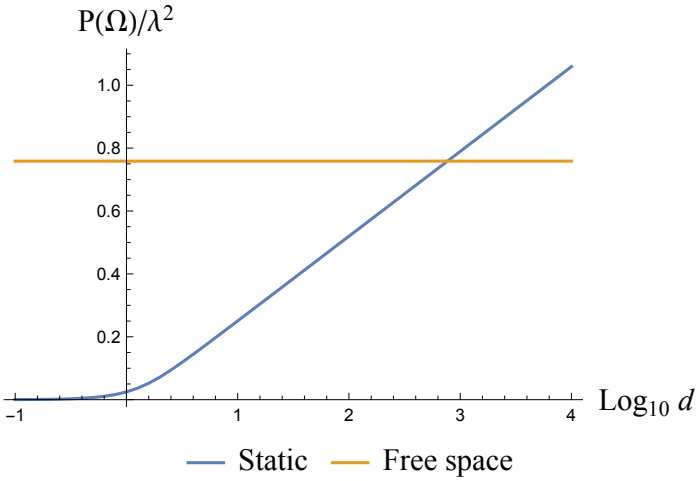

Figure D.2: Transition probability for Gaussian switching $\sigma = 1$ and $\Omega = 1$ ($\Omega\sigma = 1$) in $(1+1)$ dimensions. Near the mirror $P(\Omega)$ still decays quickly, but far from the mirror the contribution from the image term dominates and will exceed the free space case for any choice of IR cutoff Λ.

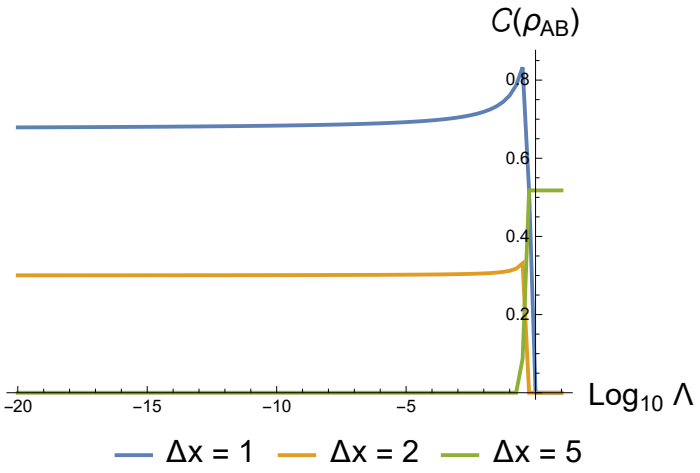

Figure D.3: The concurrence in free space as a function of IR cutoff (in logarithmic scale), for $\Omega = 1$ and $\sigma = 1$ in natural units (i.e. $\Omega\sigma = 1$ is dimensionless).

However, not all is lost. As we saw earlier, the concurrence is a quantity based on the *difference* $|X| - \sqrt{P_A P_B}$. Roughly speaking, we can understand this by noting that for static mirror we have a $\log[(\Delta\tau - i\epsilon)^2 - 4d_A^2]$ dependence due to the form of the Wightman $W(\mathsf{x}_A, \mathsf{x}'_A)$. Very roughly, for $|X|$ we will have a contribution of the form

$$\begin{aligned} &W(\mathsf{x}_A, \mathsf{x}'_B) \\ &\quad \sim \log\left[\left((\Delta\tau - i\epsilon) - (2d_A - \Delta x_{AB})^2\right)\right] \end{aligned} \tag{D.22}$$

which can be seen to scale the same way as $\sqrt{P_A P_B}$ for any fixed x_{AB}. From this, we expect that concurrence $\mathcal{C}$ is in some sense 'dimension-independent': it removes the part of the Wightman function that depends on the *absolute distance* d_A, d_B away from the mirror. What remains is the *relative distance* dependence Δx_{AB} of $\mathcal{C}(\rho_{AB})$ which leads to the usual decay of correlations as we make the detectors have larger spacelike separation. Effectively, $\mathcal{C}(\rho_{AB})$ 'regulates' the ill-behaved part of $|X|$ and $P(\Omega)$ somewhat analogous to adding counterterms in QFT. This provides strong evidence that we can rely on concurrence calculations in $(1+1)$ dimensions even if we cannot separately trust the entries in the evolved density matrix ρ_{AB} as $d \to \infty$ due to the divergent behavior at large mirror distance.

With some thought, this growth of P with distance from the mirror d may not be as surprising at it seems: it is already known in classical gravity that the Newtonian gravitational potential in one-dimensional space also grows linearly with separation between masses [151, 152] unlike the $1/r$ power law in the three-dimensional context [156]. We should also remark that since this is an inherent problem associated with the long-distance behaviour of the Wightman function, the issue will not disappear for general choices of ray-tracing functions. We can check this numerically for the three ray tracing functions in this paper – we find that indeed $\mathcal{C}(\rho_{AB})$ seems to provide proper regularization in $(1+1)$ dimensions: that is, for each ray tracing function we find similar divergences in both the nonlocal term $|X|$ and probability P, but not in $\mathcal{C}(\rho_{AB})$.

As a consequence of this "regularization", the concurrence $\mathcal{C}(\rho_{AB})$ also does not suffer from an IR ambiguity even in free space. For the same reason as why the divergences in the $d_A \to \infty$ limit is subtracted off by the definition of $\mathcal{C}(\rho_{AB})$, the IR ambiguity is also subtracted off. We can thus think of $\mathcal{C}(\rho_{AB})$ as having an IR regulator *by definition*. This is the reason why the free space limit of the concurrence in the presence of mirrors is well-defined (cf. Figure 5.2). Since concurrence is IR-regular, it can be reverse-engineered to induce a natural IR cutoff for the free-space Wightman function. This is shown in Figure D.3. We see that the concurrence approaches an approximately constant value once Λ is reasonably small, which we can take to be at least $\Lambda \lesssim 10^{-3}$. In [111] and [123]

the value $\Lambda = 10^{-3}$ was adopted arbitrarily due to the ambiguity argument: this value is arguably small enough for their purposes, though choosing a smaller value allowed by the numerical precision used during computation is preferable. We verified this for up to $\Lambda \sim 10^{-100}$ and the IR ambiguity does not seem to play a role in computation of $\mathcal{C}(\rho_{AB})$.

In short, we see that concurrence $\mathcal{C}(\rho_{AB})$ is an IR-safe quantity for the Unruh-DeWitt detector coupled linearly to a massless scalar field in any dimensions. That is, as the IR cutoff $\Lambda \to 0$, the concurrence converges quickly to a fixed value. We propose that this can be used to choose an appropriate IR cutoff Λ for computation of the density matrix $\hat{\rho}_{AB}$ in perturbation theory despite the IR ambiguity of massless scalar field in $(1+1)$ dimensional Minkowski space.